Size Effects in Thermoelectric Cobaltate Heterostructures

Peter Brinks

Size Effects in Thermoelectric Cobaltate Heterostructures

Peter Brinks

Cover: The cover image shows a X-Ray photoelectron diffraction measurement of an epitaxially grown Na_xCoO_2 thin film on an Al_2O_3 substrate. The colorscale and the level of detail of the image are manipulated.

Ph.D. Committee

Chairman and Secretary

Prof. dr. J.F.J. Engbersen (University of Twente)

Promotor

Prof. dr. ing. A.J.H.M. Rijnders (University of Twente)

Assistant-promotor

Dr. ir. M. Huijben (University of Twente)

Members

Prof. dr. ir. A. Brinkman (University of Twente)

Prof. dr. ir. H. Hilgenkamp (University of Twente)

Dr. A. Maignan (Crismat Laboratory (CNRS/ENSICAEN))

Prof. dr. G. Mul (University of Twente)

Prof dr. T.T.M. Palstra (University of Groningen)

The research described in this thesis was carried out within the Inorganic Materials Science group, Department of Science and Technology and the MESA$^+$ institute for Nanotechnology at the University of Twente. This work is financially supported by the strategic research orientation "Nanomaterials for Energy" of the MESA$^+$ Institute for Nanotechnology.

Ph.D. thesis, University of Twente, Enschede, The Netherlands

Printed by CPI Royal Wöhrmann, Zutphen, The Netherlands

ISBN: 978-90-365-3710-0

DOI: 10.3990/1.9789036537100

Size Effects in Thermoelectric Cobaltate Heterostructures

Proefschrift

Ter verkrijging van
de graad van doctor aan de Universiteit Twente,
op gezag van de rector magnificus,
Prof. dr. H. Brinksma,
volgens besluit van het College voor Promoties
in het openbaar te verdedigen
op 10 september 2014 om 12.45 uur

door

Petrus Brinks
Geboren op 20-01-1986
te Hellendoorn

Dit proefschrift is goedgekeurd door de promotor

Prof. dr. ing. A.J.H.M. Rijnders

en de assistent promotor

Dr. ir. M. Huijben

Contents

Chapter 1

Introduction into Oxide Thermoelectrics

1.1 Introduction

In view of the increasing global population and a rapidly changing climate, our global energy sources have to be used more efficiently. Currently, most of the energy of the resources that we use is being discharged as waste heat into the environment, even up to 60% as published by the Lawrence Livermore National Laboratory. [1] This waste heat can potentially be partly recovered through the application of thermoelectric devices. These thermoelectric devices are lightweight, small, inexpensive and only minimal susceptible to failure, due to the absence of moving parts or liquids/gases. However, the use of thermoelectric devices is still very limited, because of their low conversion efficiencies at this moment.

The rather low efficiencies of these thermoelectric energy converters are mainly limited by the performance of the applied thermoelectric materials. The challenge for achieving improved performance of thermoelectric materials is to obtain separate control over the electronic and the thermal properties of the materials. So far, the most promising approaches to enhance the thermoelectric performance make use of nanostructured samples. By engineering thermoelectric materials on various length scales, ranging from macroscopic length down to the atomic scale, enhanced thermoelectric performance can be achieved. This involvement of nanoscience has led to renewed interest for thermoelectrics. [2–5]

This thesis will focus on the ability to control oxide thermoelectric materials in confined heterostructures, ranging down to the nanometer scale, and study their

Parts of this chapter were used in chapter 24 of the book: Epitaxial Growth of Complex Metal Oxides, to be published by Woodhead Publishing

potential for thermoelectric applications. The class of oxide materials is interesting for thermoelectric applications because of their good thermal and chemical stability, their non-toxicity and the use of abundant elements. Additionally, confinement of oxides into thin films or superlattices has been previously used to obtain new and unexpected interface phenomena, such as ferroelectric, electrical or magnetic interface properties. [6] This demonstrates the potential to engineer the properties of oxide heterostructures and also that a control of the structural properties on the atomic level can be achieved in these materials. Similar effects could be expected in thermoelectric heterostructures. In this thesis, thin films and superlattice structures are fabricated to obtain nanoscale confinement. These heterostructures are used to engineer the thermoelectric properties of these oxide thermoelectric materials.

1.1.1 Discovery of thermoelectrics

Thomas Johann Seebeck observed for the first time in 1821 that a magnet is deflected if the two junctions of an electrical circuit with two different metals, are held at a different temperature. Quickly afterwards it was understood that an electrical current is induced if the circuit is exposed to a temperature gradient. The effect is called the Seebeck effect, named after its discoverer.

The Seebeck effect can also be described as the direct conversion of a temperature gradient into an electrical potential difference inside a (thermoelectric) material. The potential difference originates from the enhanced thermal drift of the electronic charge carriers at the warmer side of the material, causing a charge buildup at the colder side. The charge buildup at the colder side is causing an opposite flow of charge carriers, because of the electrostatic repulsion of the charge carriers. These two processes form an equilibrium and the resulting potential buildup increases linearly as a function of the temperature gradient. The corresponding proportionality constant is called the Seebeck coefficient, often also referred to as the thermopower or thermoelectric power. The Seebeck coefficient is defined as follows

$$S = -\frac{\Delta V}{\Delta T} \tag{1.1}$$

with S the Seebeck coefficient, ΔT the temperature difference between the ends of the material, and ΔV the potential difference. The SI units of the Seebeck coefficient are V/K, but more commonly used is μV/K.

In analogy to the Seebeck effect, the inverse effect can also occur, which means that a current which is passed through an electrical circuit with two different materials, leads to heating or cooling at the junction of these two materials. This effect was first observed and reported in 1836 by the French scientist Jean Charles Athanase Peltier and is called the Peltier effect. In 1838 the observations were confirmed by Lenz, who also demonstrated for the first time the practical use of the Peltier effect. He used a bismuth-antimony junction to freeze water by passing

an electrical current through the junction and also demonstrated that the ice could be melted again by reversing the direction of the electrical current. In analogy to the Seebeck effect, the strength of the Peltier effect depends linearly on the electrical current passing through the junction and the proportionality constant is called the Peltier coefficient.

William Thomson, often also referred to as Lord Kelvin, predicted and observed the last thermoelectric effect in 1851. The Thomson effect is the generation of reversible heat when an electrical current is send through a conducting material that is subjected to a temperature gradient. This effect is typically much smaller than the Seebeck effect and Peltier effect and is often not taken into account in studies focusing on applications of thermoelectrics.

1.1.2 Thermoelectric generation and the figure of merit

The most widespread application of thermoelectrics is its use in thermocouples, which are used as temperature sensors. Typical areas of application are for example temperature monitoring in industrial processes and household ovens. A thermocouple is build up from two wires of different materials, where the temperature difference between the junction of the two materials and the other end of the wires is measured. Even though a thermocouple only measures a temperature difference, the absolute temperature can be determined if a reference junction is used. Most thermocouples use two different metallic wires, where the most important material property is the Seebeck coefficient, which should be different for the two materials to obtain a potential difference in response to a temperature gradient.

More complicated applications of thermoelectrics are its use for thermoelectric cooling or thermoelectric energy conversion. In the case of a thermoelectric cooler a p- and n-type thermoelectric material are combined in such way that they are electrically connected in series, whereas thermally connected in parallel. If an electrical current is send through the device, one side of the device is heated and the other side of the device is cooled, as a consequence of the Peltier effect. This is schematically shown in Fig. 1.1. For a thermoelectric energy converter, a similar device is used, where now a temperature gradient is applied across the device. Because of the Seebeck effect, this temperature gradient results in a potential difference, which can be used to generate an electrical power output. This is also shown in Fig. 1.1. In addition to the Seebeck coefficient of the applied materials, the electrical as well as thermal conductivity of the thermoelectric materials play a determining role for the conversion efficiency or power output of the device. Therefore, a more thorough understanding of the thermoelectric materials as well as the device design is required to maximize the actual power output of such a device.

The conversion efficiency of a thermoelectric generator is determined by the

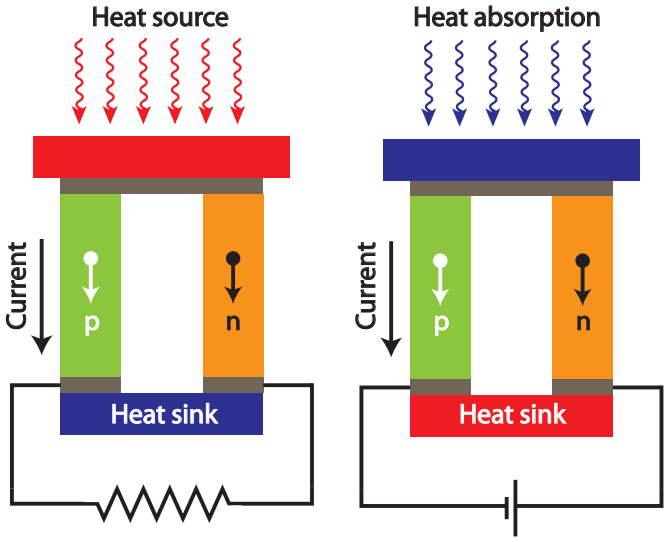

Figure 1.1: Thermoelectric generator (left) and thermoelectric refrigerator (right). Both devices use a similar setup with a p- and n-type thermoelectric material combined as schematically shown. For the thermoelectric refrigerator an electrical current is send through the device which is used to generate a temperature gradient. For the thermoelectric generator the temperature difference between hot and cold side is converted into electrical energy.

electronic and thermal properties of the thermoelectric materials that are used. Making the assumptions that the relevant thermoelectric properties are constant within the temperature range and that both thermoelectric materials have the same thermoelectric properties, the maximum efficiency of a thermoelectric generator is given by

$$\phi_{max} = \frac{T_H - T_C}{T_H} \frac{\sqrt{1+Z\bar{T}}-1}{\sqrt{1+Z\bar{T}}+\frac{T_C}{T_H}}, \text{with} \tag{1.2}$$

$$\bar{T} = \frac{T_H + T_C}{2}, \text{and} \tag{1.3}$$

$$Z = \frac{S^2\sigma}{\lambda} \tag{1.4}$$

in which T_H and T_C are the temperature at respectively the hot and the cold side and S, σ and λ are respectively the Seebeck coefficient, electrical conductivity and thermal conductivity of the thermoelectric material. The maximum efficiency of a thermoelectric generator is proportional to Z and therefore this parameter is called the figure of merit. Because of convenience to compare the figure of merit of different materials at different temperatures, the dimensionless figure of merit ZT

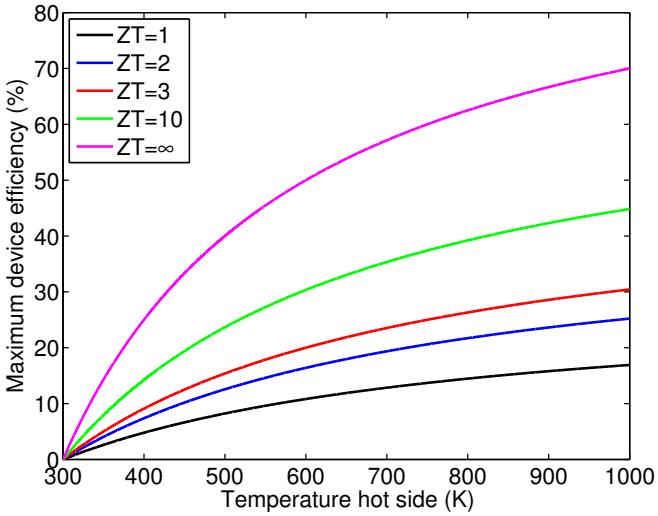

Figure 1.2: Maximum device efficiency of a thermoelectric energy generator as a function of the temperature of the hot side, with a fixed cold side temperature of 300K. The different colours represent different values for the dimensionless figure of merit (ZT value). For an infinitely large ZT value the efficiency reaches the theoretical limit of the Carnot efficiency.

is more often used as a performance indicator and this is obtained by multiplying the figure of merit with the absolute temperature.

$$ZT = \frac{S^2\sigma}{\lambda}T \tag{1.5}$$

To improve the efficiency of thermoelectric generators, or equivalently thermoelectric refrigerators, the dimensionless figure of merit, ZT, should be maximized and a treshold value of about 3 is typically considered for large scale applications. [7] A thermoelectric generator with a ZT value of 3 and a temperature difference of about 200K will result in a thermoelectric generator with a maximum efficiency of about 15%, as shown in Fig. 1.2. To obtain a maximum efficiency of about 25% with the same temperature difference, it can be seen that a ZT value of about 10 is required. The theoretical limit is the Carnot efficiency, which is reached for an infinitely large ZT value. It should however be noted that in addition to efficiency, also fabrication costs will play a determining role for large scale applications. If at a low cost about 10% of the waste heat can be recovered in industrial applications where a large temperature gradient can be used, thermoelectric energy generators could already be economically feasible and lead to a more efficient energy usage.

1.1.3 Thermoelectric materials

The development and improvement of thermoelectric materials mainly aims at maximizing the ZT value of thermoelectric materials. Increasing the ZT value can either be achieved by increasing the Seebeck coefficient and/or the electrical conductivity or by suppression of the thermal conductivity. These three parameters, the Seebeck coefficient, the electrical conductivity and the thermal conductivity are all dependent on the carrier concentration of the material. As shown in Fig. 1.3 the Seebeck coefficient is decreasing, whereas the electrical and thermal conductivity are increasing as a function of carrier concentration. As a consequence of these interdependent relations on the carrier concentration, the ZT value is peaked at a specific carrier concentration after which it is very difficult to obtain further improvement.

By changing the carrier concentration of thermoelectric materials, mostly done by adding various dopants, ZT values up to about one were achieved, after which it was found to be very difficult to obtain further improvement. The most promising materials showing this high figure of merit were based on Bi_2Te_3, which was considered as a good thermoelectric candidate material already in the 1950's. [8–10]. This material has been studied intensively and Bi_2Te_3-based materials remained the best performing thermoelectric materials until the 1990's, with a ZT value of about 1. [11–14]

Improvements of the ZT value between the first report of Bi_2Te_3 as a thermoelectric material and the 1990's have only been very incremental. As a consequence of this, the potential to use thermoelectrics for large scale energy conversion could not be realized and interest in thermoelectrics dropped. However, interest in thermoelectrics increased again in 1993, when new approaches were proposed to improve the performance of thermoelectric materials. [15, 16] It was realized that in addition to the carrier density of a material, which influences all three relevant material properties, the thermal conductivity consists of an electronic and a phononic contribution. This phonon contribution is not influenced by the carrier density and could therefore be used to independently change the thermal conductivity, without changing the Seebeck coefficient and the electrical conductivity. [2, 14, 17] Even though this was already realized by Ioffe in the 1950's, in 1993 Hicks and Dresselhaus predicted that by nanoscale confinement an additional improvement could be achieved for the electronic properties. [15, 16]

These reports predicted that if thermoelectric materials are confined into thin films and superlattice structures [15] or nanowires, [16] a significant enhancement of the thermoelectric properties would be obtained, because of the increased density of states at the Fermi level, leading to an enhancement of the Seebeck coefficient. The prediction of an enhanced Seebeck coefficient in samples with nanoscale dimensions originates from the linear relation between the density of states at the Fermi level and the Seebeck coefficient, which is valid for metals and degener-

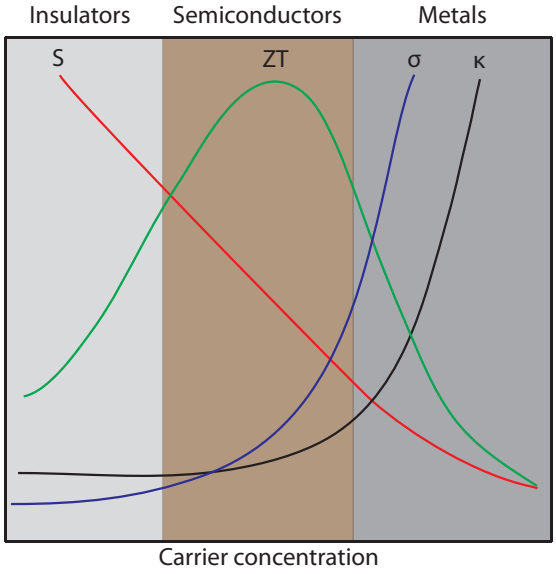

Figure 1.3: Dependency of the Seebeck coefficient S, the electrical conductivity σ and the thermal conductivity κ on the carrier concentration in a typical thermoelectric material. The resulting ZT value shows a maximum as a function of carrier concentration, as indicated by the green line. Adapted from Snyder et al. [14]

ately doped semiconductors. The predictions have been experimentally verified for PbTe-based superlattices [18] as well as Bi_2Te_3-based superlattices. [19–21] In these material systems, enhanced Seebeck coefficients were observed in combination with a significant suppression of the thermal conductivity, leading to ZT values up to 2.4. [20] Even tough these studies clearly show the thermoelectric potential of nanostructured samples, it's use for large scale applications remains limited because of the complex and expensive fabrication process as well as the limited thermal stability of these materials. However, these studies have been important for understanding the underlying phenomena and also for identifying new approaches to obtain enhanced thermoelectric performance of existing and new thermoelectric materials.

Around the same time as the early work of confinement of thermoelectrics in nanostructured materials, Slack proposed the concept of '*phonon-glass electron-crystal*' type of materials. [22] This presents the ideal combination of electrons which behave similar as in a crystal, whereas phonons behave like in a glass. This would exhibit the ideal combination of good electronic properties (as in typical thermoelectric materials) and a very low phonon thermal conductivity (as in a glass). The idea is relatively comparable to the superlattice approach, however now the nanostructuring occurs on the unit cell level. New compounds were identified as thermoelectric candidates, such as the clathrates [23,24], skutterudites [4]

and the Zintl phases. [25] These materials indeed benefit from a low phonon thermal conductivity because of disorder and complexity in the structure, for example by filling the cage-like crystal structure inside the clathrate structures. Because the lower phonon thermal conductivity of these materials is intrinsic, there is no need for confinement into small scale structures. This enables large scale fabrication, making them very suitable for applications. Relatively high ZT values up to 1.7 were obtained for these type of materials [26], but a similar thermoelectric performance as the previously mentioned thermoelectric superlattices was not achieved.

The two different approaches to obtain enhanced phonon scattering are recently also combined by introducing nanostructuring on various length scales, ranging from the nanoscale to the mesoscale. [27] Here, the advantage of bulk materials, enabling large scale fabrication is combined with the effect of nanostructured samples. The precise manipulation which is required for the fabrication of superlattices is not necessary, because the nanostructures are randomly distributed throughout the material and form a disordered system. By careful sample preparation it is shown that the electronic properties can be preserved, while the nanostructures effectively scatter the phonons, thereby reducing the thermal conductivity and enhancing the overall thermoelectric performance. The new approach is that a range of length scales is used, resulting in an '*all-scale hierarchical architecture*'. [27] Comparing this with PbTe bulk materials where atomic control, or substitution, has led to a maximum ZT value of 1.1, which could be increased to 1.7 by the inclusion of nanoprecipitates of endotaxial SrTe nanocrystals. [28] These precipitated nanocrystals scatter short wavelength phonons and only influence the electronic properties to a minimum. Now this approach is even extended to the mesoscale by engineering the grain boundaries, and using them to obtain also scattering of phonons with a larger wavelength, leading to an enhancement of the ZT value up to 2.2. [27] This demonstrates the importance of control of the structural properties on various length scales to engineer the materials in a specific way and emphasizes the importance of combining different approaches, such as bulk materials and nanostructured materials, to obtain improved thermoelectric performance.

Recently, other new compounds, such as SnSe, are also identified as promising thermoelectric materials. [29] This material has a layered structure and thereby forms an intrinsic nanostructured material, with a correspondingly low thermal conductivity. For single crystals ZT values up to 2.6 were measured around 900K, supporting the approach to use nanostructured materials.

1.2 Thermoelectric oxides

Until the discovery of Na_xCoO_2 as a good thermoelectric material in 1997, [30,31] oxide materials have not been considered as thermoelectric materials, because of their limited thermoelectric performance. These first reports of Na_xCoO_2 demonstrated a high Seebeck coefficient of 100 μV/K in combination with a low resistivity of 0.2 mΩcm. [30, 31] These initial studies led to increased interest for oxides as thermoelectric materials, which is supported by the promising advantages of oxide materials for thermoelectric applications. Many of the oxides are non-toxic and have a good thermal and chemical stability, in contrast to the telluride-based materials, making them very suitable for high temperature thermoelectric applications. Additionally, many oxides only contain relatively abundant elements, making them also suitable for large scale fabrication and applications.

After those first reports of Na_xCoO_2, related compounds, such as $Ca_3Co_4O_9$, were also identified as good thermoelectric materials. [32,33] These cobaltate materials show a similar high Seebeck coefficient together with a good electrical conductivity. Within the oxides, these cobaltates are the most promising thermoelectric materials and ZT values up to 1.2 have been reported. [34] This class of materials will be introduced in more detail in the next section, as the research described in this thesis is focussed on these oxide materials.

Even though the layered cobaltates are promising oxide thermoelectric materials, they are only p-type materials and n-type cobaltates have not yet been reported. Because of the necessity of both p- and n-type thermoelectric materials for applications, also other oxides have been studied to obtain similar thermoelectric performance for n-type oxide thermoelectrics. The main candidates as n-type thermoelectric oxides are ZnO and $SrTiO_3$. [3, 35–39]

The electronic properties of Al-doped ZnO are very promising and thermoelectric power factors of 20 $\mu W/K^2cm$, comparable to conventional thermoelectric materials can be obtained, however the challenge is to reduce it's high thermal conductivity of 40 W/mK. [40] By doping of Al and Ga to $Zn_{0.96}Al_{0.02}Ga_{0.02}O$, a maximum ZT value of 0.6 was achieved at 1273K. [41]

By doping with Nb or La, the electronic properties of $SrTiO_3$ can be tuned from insulating to metallic, giving rise to the possibility to optimize the electronic properties for thermoelectric applications. For bulk samples, Nb and La doping can be used to obtain ZT values of about 0.4 at 1000K. [42,43] One of the approaches to improve the thermoelectric performance of $SrTiO_3$ is to use Ruddlesden-Popper phases ($SrO[SrTiO_3]_m$ with m an integer), which is a layered structure consisting of $SrTiO_3$ with layers of SrO in between, forming a natural superlattice. It is shown that these Ruddlesden-Popper phases can lead to a reduction of the thermal conductivity by a factor of 2, however this also leads to a deterioration of the electronic properties. [44]

1.2.1 Cobaltates

The observation of a high thermopower and a low resistivity in Na_xCoO_2 single crystals [30, 31] opened up the interest as a promising thermoelectric candidate material [34, 45–48] and ZT values exceeding unity have already been achieved. Thermoelectric power factor ($S^2\sigma$) values up to 50 $\mu W/K^2cm$, which is comparable for Bi_2Te_3 crystals [49] are reported, demonstrating that the electronic properties are comparable with traditional thermoelectric materials. However, currently the thermoelectric performance of Na_xCoO_2 single crystals is limited due to the relatively high thermal conductivity (8-19 W/mK) [50–52], which is significantly higher than for Bi_2Te_3 crystals (1 W/mK) [49]. In addition to Na_xCoO_2, also other cobaltates, such as $Ca_3Co_4O_9$ and $Bi_2Sr_2Co_2O_y$, with related crystal structures, were studied for their thermoelectric properties and they also show similarly interesting thermoelectric properties. [32, 33]

1.2.1.1 Cobaltate structural properties

The class of cobaltate materials consist of a stacking of CoO_2 sheets and various different layers in between these CoO_2 sheets. The most simple structure of these cobaltates is observed for Na_xCoO_2, where the interlayers are formed by sodium ions, as shown in Fig. 1.4a. Two of the other cobaltate materials that are frequently studied are $Ca_3Co_4O_9$ and $Bi_2Sr_2Co_2O_y$ and are shown in Fig. 1.4 (b and c). For these materials the interlayers are formed by square lattices of respectively Ca_2CoO_3 and $Bi_2Sr_2O_4$. [53] The crystal structure of these cobaltates is very comparable, because of the same triangular CoO_2 layers that are used, giving rise to similar in-plane (a and b) lattice parameters. The CoO_2 layers are arranged in a CdI_2-type structure, forming a triangular lattice.

Even though Na_xCoO_2 seems to have the simplest crystallographic structure of these cobaltates, it has the unique property that the composition of the interlayers (sodium ions) can be varied, leading to significant changes in crystal structure as well as functional properties. [46, 47, 55–57] The interesting stoichiometry of this material as a thermoelectric candidate is between 0.5 and 1, leading therefore to compositions in the range of $Na_{0.5}CoO_2$ to $NaCoO_2$. In this range four different phases are identified, β ($0.55 \leq x \leq 0.6$), α' phase (x=0.75) and α phase ($0.9 \leq x \leq 1$). [47, 55, 56] Within this range of composition, different structures have been reported, depending on the position of the oxygen atoms in the subsequent CoO_2 layers. The most common structure consists of similar CoO_2 layers and is referred to as the two-layer structure. However, in some cases a more complex stacking is observed, where the subsequent CoO_2 layers are differently stacked, resulting in an enlarged unit cell which contains three layers of CoO_2, this structure is therefore referred to as the three-layer structure. [57] Because the two-layer structure shows the best thermoelectric properties, the three-layer structure will not be discussed here in more detail.

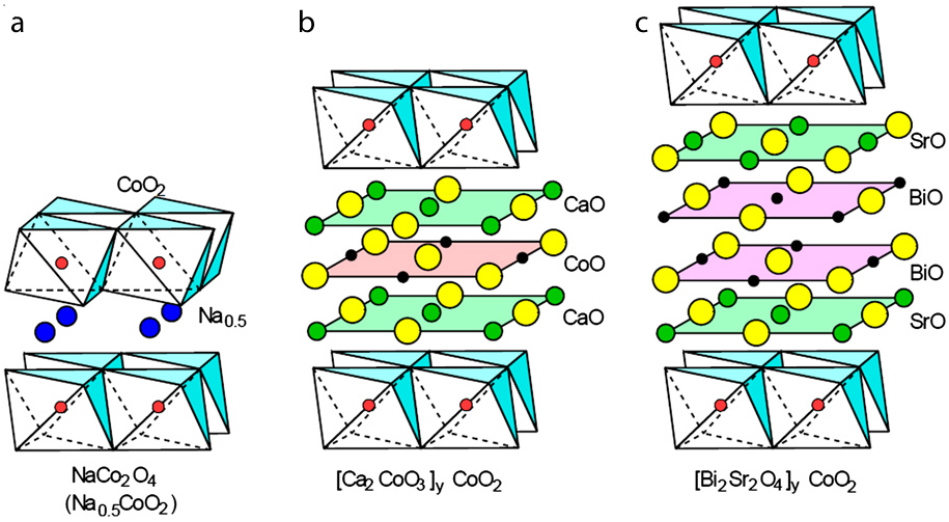

Figure 1.4: Crystal structure of Na_xCoO_2 (a) $Ca_3Co_4O_9$ (b) and $Bi_2Sr_2Co_2O_y$ (c). The common feature of these cobaltates is their CoO_2 layers, leading to similar in-plane crystal structure (a and b lattice parameters). [54]

These different compositions lead to significant differences in the crystal structure. The a-axis lattice parameter changes from 0.281 nm to 0.288 nm when the composition is changed from $Na_{0.5}CoO_2$ to $NaCoO_2$. For the c-axis lattice parameter even more significant changes from 1.11 nm to 1.05 nm are observed within the same range of compositions. In addition to the changes in lattice parameter also several structural transitions are observed for this range of compositions. [57–59]

Because the c-axis lattice parameter is most significantly changing with sodium composition, this lattice parameter has been of interest in several studies to determine the relation between the c-axis lattice parameter and the exact composition of Na_xCoO_2 samples. Even though several studies report the similar behavior of a decreasing c-axis lattice parameter upon an increase of the sodium to cobalt ratio, there is no exact agreement about the actual corresponding compositions and lattice parameters. [57, 58, 60–62]

The CdI_2 type CoO_2 layers in $Ca_3Co_4O_9$ are similar as in the Na_xCoO_2 structure, and in this structure the sodium atoms are replaced by layers of Ca_2CoO_3, as shown in Fig. 1.4b. These Ca_2CoO_3 layers are arranged in a distorted rocksalt structure with different lattice parameters, thereby forming the misfit structure. The lattice parameters a (0.4834 nm), c (1.084 nm) and β (98.14°) are shared for the two sublattice systems, in contrast to the b-axis lattice parameter, which are 0.2824 nm and 0.4558 nm for respectively the CoO_2 and the Ca_2CoO_3 sublattices. [53,63] From these two substructures the correct notation $[Ca_2CoO_3]_q[CoO_2]$, can be easily derived, with q approximately 0.6, being the ratio between the

two b-axis lattice parameters. The more commonly used notations, $Ca_3Co_4O_9$ or $Ca_3Co_4O_{9+\delta}$, are abbreviations for this compound with the approximate stoichiometries. In contrast to Na_xCoO_2, the ratio between calcium and cobalt cannot be easily changed to influence the carrier concentration. It is however possible to change the carrier concentration of the conducting CoO_2 layers by controlling the oxygen content of the Ca_2CoO_3 layers or by cation substitution. [64–66]

1.2.1.2 Cobaltate Thermoelectric properties

For Na_xCoO_2 single crystals power factor ($S^2\sigma$) values of 50 μW/K^{2}cm have been obtained [30], which is comparable to values for Bi_2Te_3 crystals [49]. This remarkable high thermoelectric power factor at 300K is obtained, because of a simultaneous high Seebeck coefficient of 100 μV/K and low resistivity of 0.2 mΩcm. In contrast to traditional thermoelectric materials, Na_xCoO_2 shows metallic behavior and has a rather low electron mobility (estimated at 13 cm^2/Vs at 4K). [30] Even though the initial reports could not explain this remarkable combination, a strong anisotropy of the resistivity was observed. For the in-plane direction (perpendicular to the c-axis) a much lower resistivity was observed in comparison with the out-of-plane direction (parallel to the c-axis). The ratio of the resistivity between these two different directions increases from about 30 to 200 between 300K and 4K. The results were compared with the layered high-temperature superconductors and it was suggested that the electronic states can be regarded as quasi-2D, stating the importance of the CoO_2 layers. [30]

It was realized that Na_xCoO_2 is a strongly correlated material, thereby exhibiting strong electron-electron interactions. [67] Such a strongly correlated electron system is typically described by the Hubbard model. In this model the electron transport is described in terms of a hopping parameter t and the on-site repulsion U, which are the energies involved for respectively hopping to a nearest neighbour site and double occupancy of a specific site. Using this model, the thermoelectric properties of Na_xCoO_2 as a function of doping (sodium content) were calculated, assuming that the onsite repulsion is much larger than the thermal energy (Heikes limit). [68, 69]

In the relevant regime for thermoelectrics (x between 0.5 and 1) these calculations show a sharp increase of the Seebeck coefficient for an increasing amount of sodium [69], which is in good agreement with experimental observations. [48, 52] From these calculations a maximum for the thermoelectric power factor is determined at a composition of $Na_{0.88}CoO_2$, also leading to a maximum of the ZT value at the same composition. For different phonon thermal conductivities, the resulting ZT value is calculated, showing that if the phonon thermal conductivity can be suppressed to 1 W/mK, a maximum ZT value of about 1.2 can be obtained at room temperature for the composition of $Na_{0.88}CoO_2$. Even though the absolute values are showing some differences, the trends of both the theoretical as

well as the experimental work suggest that the best thermoelectric performance is expected for a composition of approximately $Na_{0.9}CoO_2$. [48, 69]

As previously mentioned, the electronic properties of Na_xCoO_2 single crystals at room temperature are comparable to that of Bi_2Te_3 crystals. However, currently the ZT value of Na_xCoO_2 crystals is limited due to the relatively high thermal conductivity (8-19 W/mK) [50–52], which is significantly higher than for Bi_2Te_3 crystals (∼1 W/mK) [49]. For single crystals, ZT values of about 0.03 at 300K are obtained, which increases to 1.2 at 800K, showing the high-temperature potential of oxide thermoelectrics. [45]

Because of the large anisotropy observed in the resistivity for the different crystallographic orientations, polycrystalline samples of Na_xCoO_2 are not performing as good as single crystals, due to the increased resistivity by about a factor of 10. The ZT value of polycrystalline Na_xCoO_2 is limited to about 0.3 at 800K. [45] In addition to changing the sodium content and thereby influencing the carrier concentration, attempts have been made to substitute sodium, however this has been very difficult and did not result in significant improvements of the thermoelectric performance. [70]

Relatively comparable thermoelectric performance as for Na_xCoO_2 is obtained for $Ca_3Co_4O_9$ single crystals. The resistivity is higher, but also the Seebeck coefficient is higher, resulting in ZT values exceeding unity around 900K. [34, 71] Because of enhanced chemical and thermal stability compared to Na_xCoO_2 and the possibility to add dopants, more effort has been put into the fabrication of polycrystalline samples of $Ca_3Co_4O_9$. It is shown that textured samples, which can take advantage of the anisotropic transport properties, can be obtained by for example spark plasma sintering. [72] By controlling the oxygen content incremental improvements for the thermoelectric performance have been achieved. [73] Most promising improvements can be obtained by adding various dopants, such as Ga or Ag, to polycrystalline $Ca_3Co_4O_9$ samples. [72, 74–77] For the best polycrystalline samples, a ZT value of 0.6 at 1100K is obtained, which is however still significantly lower than that observed for single crystals of $Ca_3Co_4O_9$. [72]

1.2.2 Oxide thin films and superlattices

As described in Section 1.1.3, a promising approach to improve the thermoelectric performance is to enhance the Seebeck coefficient by electron confinement into thin layers and simultaneously suppress the thermal conductivity. This approach was aimed for in $SrTiO_3$-based thin films and superlattices. [35, 38, 78–80] By fabricating superlattices of $SrTiO_3$ and $SrTi_{0.8}Nb_{0.2}O_3$ with various thicknesses of the $SrTi_{0.8}Nb_{0.2}O_3$ layers, the effect of electron confinement on the Seebeck coefficient was studied, and a significant improvement was indeed obtained. To obtain even stronger confinement, a 2 dimensional electron gas (2DEG) was fabricated at the interface between the single crystal $SrTiO_3$ substrate and an epitaxially

grown TiO_2 thin film, leading to an even stronger enhancement by a factor of 5 (up to 1050 μV/K) for the Seebeck coefficient at room temperature. [78] For these superlattices, ZT values up to 2.4 were achieved at room temperature. Even though it should be noted that for these ZT values only the 2DEG layer was taken into account, still a significant enhancement is remaining after correction for the volume of the deposited thin film. After correction, the ZT value reduces to 0.24 at room temperature, which is still a factor of three larger than values obtained in bulk $SrTiO_3$ at room temperature.

The studies on thin films and superlattices of $SrTiO_3$ clearly demonstrate the potential of superlattices of oxide thermoelectrics, however still the obtained thermoelectric performance is limited. A similar approach could be used for the layered cobaltate materials, however no detailed studies have been reported so far. For thin films of Na_xCoO_2 several studies are reported, however most of these studies focus on the structural properties. [61, 62, 81–91] It was also observed that these Na_xCoO_2 thin films are not stable in air, complicating thermoelectric characterization. [86] If the stability issues could be solved, a systematic study focusing on the structural and thermoelectric properties of Na_xCoO_2 thin films is required to understand their thermoelectric potential.

In addition to the reported studies on Na_xCoO_2 thin films, a limited number of studies on $Ca_3Co_4O_9$ thin films were reported. [92–101] Some of these studies focus on a combination of the structural and thermoelectric properties, but no systematic studies that relate the structural and thermoelectric properties of these thin films have been reported. The most promising thermoelectric properties are expected at elevated temperatures, in analogy to the single crystal and polycrystalline samples, but very limited studies measuring the high-temperature properties of these cobaltate thin films are reported.

In analogy to the studies on thin films and superlattices of $SrTiO_3$-based materials, the layered cobaltates are also promising candidates for enhancement of the thermoelectric properties by nanoscale confinement. The similarities of these different cobaltate materials make this class of materials very suitable for thin films and possibly superlattices. A layered structure of conducting layers (CoO_2 sheets) and insulating layers is already part of the structure of the material itself, making it an intrinsic nano-layered material. In addition to this, because the electronically active part of the materials (the CoO_2 sheets) is the same for all cobaltates, the properties can be further engineered by changing the composition of the layers in between, which could lead to enhanced control over the electronic as well as thermal properties.

1.3 Thesis Outline

In this thesis, a study of thin films and superlattices of thermoelectric cobaltates is presented. As explained in the previous sections, oxide materials, especially the layered cobaltates. are very promising for thermoelectric applications. However, knowledge about thin films of these cobaltates is currently very limited. The main focus of the work described in this thesis is to understand size effects in thermoelectric cobaltate heterostructures. This is done by studying the relation between structural and thermoelectric properties of cobaltates, which are confined down to the nanometer scale into thin films and superlattices.

In Chapter 2 the growth of Na_xCoO_2 thin films by pulsed laser deposition is studied. It is shown that epitaxial thin films can be deposited on different single-crystal substrates, without the presence of impurity phases. A significant increase of the resistivity by more than one order of magnitude was observed when the thin films are exposed to air for several days. The main topic of this chapter is to understand the underlying mechanisms of the observed sample degradation and to use this knowledge to overcome these stability issues. It is realized that sodium carbonate is forming, by reactions between sodium from the thin film and moisture and carbon dioxide from the air. These stability issues were overcome by the *in-situ* deposition of an AlO_x capping layer, which results in chemically stable Na_xCoO_2 thin films. The intrinsic properties of Na_xCoO_2 thin films are for the first time analyzed and these samples show comparable thermoelectric properties as Na_xCoO_2 single crystals.

Using these chemically stable thin films, the relation between the structural properties and their thermoelectric properties is studied in Chapter 3. The aim of this study is to identify possibilities for structural engineering of these Na_xCoO_2 thin films and to understand the effect on the thermoelectric properties. By X-Ray Photoelectron Diffraction and X-Ray diffraction measurements the epitaxial relation between several cubic as well as hexagonal single-crystal substrates and the deposited Na_xCoO_2 thin films is determined. By changing the (cubic) substrate material, the grain size in these Na_xCoO_2 thin films can be reduced, leading to a significant enhancement of the thermoelectric power factor. Additionally, the thermal conductivity of several Na_xCoO_2 thin films is significantly suppressed in these thin films, compared to Na_xCoO_2 single crystals, clearly demonstrating that these structurally engineered thin films show very promising thermoelectric properties.

The effect of confinement of Na_xCoO_2 into thin films is studied in Chapter 4. This study focusses on understanding the effect of nanoscale confinement on the electronic properties, thereby identifying the thermoelectric potential of ultra-thin Na_xCoO_2 thin films. The structural as well as thermoelectric properties of Na_xCoO_2 thin films with thicknesses between 5 and 250 nm are shown. It is shown that for a thickness above approximately 10 nm misfit dislocations start

to form, because of the difference in lattice parameter as well as crystal structure (symmetry). In agreement with theoretical models, the resistivity shows a sharp increase for samples with a thickness below 60 nm. However, the Seebeck coefficient does not show a clear trend as a function of the layer thickness, in contrast to the models which predict a suppression of the Seebeck coefficient for very thin films. The observed behavior is promising for the use of these cobaltate thin films in superlattice structures, because the thermoelectric properties can be preserved for ultra-thin layers.

The high temperature stability and thermoelectric properties of cobaltate thin films are studied in Chapter 5. The thermal stability of Na_xCoO_2 and $Ca_3Co_4O_9$ thin films is studied using high-temperature X-ray diffraction. These measurements are combined with high temperature measurements of the electrical resistivity and the Seebeck coefficient. By comparing the temperature dependent X-ray diffraction data with the electronic measurements, it is shown that temperature dependent electronic measurements are a much more sensitive tool to study the thermal stability of these cobaltate thin films. The measurements are performed in different atmospheres, to understand the influence of the partial oxygen pressure on the stability of thermoelectric cobaltate thin films. By systematic cycling to increasingly high temperatures and also performing measurements during the cooling of the samples, it is shown that the thermal stability is strongly enhanced when the samples are heated in an oxygen-rich environment. At elevated temperatures a significant improvement compared to bulk samples is achieved for these thin films.

In Chapter 6 superlattices based on thermoelectric cobaltates are studied. The aim of such superlattices is to suppress the thermal conductivity through enhanced phonon scattering at the introduced interfaces within the superlatttice. A simultaneous preservation of the electronic properties in these superlattices is required to achieve enhanced thermoelectric performance. Combining the previous studies of structural engineering and size effects in Na_xCoO_2 thin films, these thin films are used as basic building blocks in thermoelectric superlattices. Firstly Na_xCoO_2 is combined with insulating materials ($LaAlO_3$ and Al_2O_3) into superlattices structures. Because of limitations to the deposition process caused by the volatile nature of the sodium, the crystallinity of these superlattices is very limited. As a consequence of this limited crystallinity, the electrical properties could not be preserved in such superlattices. Secondly, Na_xCoO_2 is combined with the related material $Ca_3Co_4O_9$ into a superlattice. Because two thermoelectric materials are combined into a superlattice, this new approach does not require the use of an insulating barrier material. It is shown that when started with Na_xCoO_2, such superlattices can be fabricated with a high degree of crystalline ordering, leading to a preservation of the electronic properties, compared to thin films of both materials. Even though the results described in this chapter are preliminary and additional characterization, mostly focusing on the thermal properties of such superlattices,

is required, these thermoelectric superlattices form a promising pathway towards enhanced thermoelectric performance of oxide thermoelectrics.

Bibliography

[1] Energy Flow Chart of the United States of America 2013, Published by Lawrence Livermore National Laboratory, work performed under the auspices of the Department of Energy of the United States of America.

[2] F. J. DiSalvo, "Thermoelectric Cooling and Power Generation," *Science*, vol. 285, pp. 703–706, 1999.

[3] J. R. Sootsman, D. Y. Chung, and M. G. Kanatzidis, "New and Old Concepts in Thermoelectric Materials," *Angewandte Chemie International Edition*, vol. 48, pp. 8616–8639, 2009.

[4] B. C. Sales, D. Mandrus, and K. Williams, "Filled Skutterudite Antimonides: A New Class of Thermoelectric Materials," *Science*, vol. 272, pp. 1325–1328, 1996.

[5] J. P. Heremans, M. S. Dresselhaus, L. E. Bell, and D. T. Morelli, "When Thermoelectrics Reached the Nanoscale," *Nature Nanotechnology*, vol. 8, pp. 471–473, 2013.

[6] F. Miletto, G. Koster, and G. Rijnders, "Functional Oxide Interfaces," *MRS Bulletin*, vol. 38, pp. 1017–1023, 2013.

[7] A. Majumdar, "Thermoelectricity in Semiconductor Nanostructures," *Science*, vol. 303, pp. 777–778, 2004.

[8] H. J. Goldsmid and R. W. Douglas, "The Use of Semiconductors in Thermoelectric Refrigeration," *British Journal of Applied Physics*, vol. 5, pp. 386–390, 1954.

[9] F. D. Rosi, E. F. Hockings, and N. E. Lindenblad, "Semiconducting Materials for Thermoelectric Power Generation," *RCA Review*, vol. 22, pp. 28–121, 1961.

[10] F. D. Rosi, "Thermoelectricity and Thermoelectric Power Generation," *Solid-State Electronics*, vol. 11, pp. 833–848, 1968.

[11] C. Wood, "Materials for Thermoelectric Energy Conversion," *Reports on Progress in Physics*, vol. 51, pp. 459–539, 1988.

[12] H. Scherrer and S. Scherrer, *Thermoelectrics Handbook Macro to Nano, Ch. 27.* CRC Press, 2 ed., 2006.

[13] V. A. Kutasov, L. N. Lukyanova, and M. V. Vedernikov, *Thermoelectrics Handbook Macro to Nano, Ch. 37.* CRC Press, 2 ed., 2006.

[14] J. G. Snyder and E. S. Toberer, "Complex Thermoelectric Materials," *Nature Materials*, vol. 7, pp. 105–114, 2008.

[15] L. D. Hicks and M. S. Dresselhaus, "Effect of Quantum-Well Structures on the Thermoelectric Figure of Merit," *Physical Review B*, vol. 47, pp. 12727–12731, 1993.

[16] L. Hicks and M. Dresselhaus, "Thermoelectric Figure of Merit of a One-Dimensional Conductor," *Physical Review B*, vol. 47, p. 16631, 1993.

[17] M. S. Dresselhaus, G. Chen, M. Y. Tang, R. Yang, H. Lee, D. Wang, Z. Ren, J. P. Fleurial, and P. Gogna, "New Directions for Low-Dimensional Thermoelectric Materials," *Advanced Materials*, vol. 19, pp. 1043–1053, 2007.

[18] L. Hicks, T. Harman, X. Sun, and M. Dresselhaus, "Experimental Study of the Effect of Quantum-Well Structures on the Thermoelectric Figure of Merit," *Physical Review B*, vol. 53, p. 10493, 1996.

[19] R. Venkatasubramanian, T. Colitts, E. Watko, M. Lamvik, and N. El-Masry, "MOCVD of Bi_2Te_3, Sb_2Te_3 and their superlattice structures for thin-film thermoelectric applications," *Journal of Crystal Growth*, vol. 170, pp. 817–821, 1997.

[20] R. Venkatasubramanian, E. Siivola, T. Colpitts, and B. O'Quinn, "Thin-Film Thermoelectric Devices with High Room-Temperature Figures of Merit," *Nature*, vol. 413, pp. 597–602, 2001.

[21] R. Venkatasubramaniam, "Lattice Thermal Conductivity Reduction and Phonon Localizationlike Behavior in Superlattice Strucures," *Physical Review B*, vol. 61, p. 3091, 2000.

[22] G. A. Slack, *Handbook of Thermoelectrics.* CRC Press, 1 ed., 1995.

[23] H. Kleinke, "New bulk Materials for Thermoelectric Power Generation: Clathrates and Complex Antimonides," *Chemistry of Materials*, vol. 22, pp. 604–611, 2010.

[24] T. Takabatake, K. Suekuni, T. Nakayama, and F. Kaneshita, "Phonon-Glass Electron-Crystal Thermoelectric Clathrates: Experiments and Theory," *Reviews of Modern Physics*, vol. 86, pp. 669–716, 2014.

[25] S. M. Kauzlarich, S. R. Brown, and J. G. Snyder, "Zintl Phases for Thermoelectric Devices," *Dalton Transactions*, vol. 21, pp. 2099–2107, 2007.

[26] X. Hi, J. Yang, J. R. Salvador, M. Chi, J. Y. Cho, H. Wang, S. Bai, J. Yang, W. Zhang, and L. Chen, "Multiple-Filled Skutterudites: High Thermoelectric Figure of Merit through Separately Optimizing Electrical and Thermal Transports," *Journal of the American Chemical Society*, vol. 133, pp. 7837–7846, 2011.

[27] K. Biswas, J. He, I. D. Blum, C.-I. Wu, T. P. Hogan, D. N. Seidman, V. P. Dravid, and M. G. Kanatzidis, "High-Performance Bulk Thermoelectrics with All-Scale Hierarchical Architectures," *Nature*, vol. 489, pp. 414–418, 2012.

[28] K. Biswas, J. He, Q. Zhang, G. Wang, C. Uher, V. P. Dravid, and M. G. Kanatzidis, "Strained Endotaxial Nanostructures with High Thermoelectric Figure of Merit," *Nature Chemistry*, vol. 3, pp. 160–166, 2011.

[29] L.-D. Zhao, S.-H. Lo, Y. Zhang, H. Sun, G. Tan, C. Uher, C. Wolverton, V. P. Dravid, and M. G. Kanatzidis, "Ultralow Thermal Conductivity and High Thermoelectric Figure of Merit in SnSe crystals," *Nature*, vol. 508, pp. 373–377, 2014.

[30] I. Terasaki, Y. Sasago, and K. Uchinokura, "Large Thermoelectric Power in $NaCo_2O_4$ Single Crystals," *Physical Review B*, vol. 56, pp. R12685–R12687, 1997.

[31] H. Yakabe, K. Kikuchi, I. Terasaki, Y. Sasago, and K. Uchinokura, "Thermoelectric Properties of Transition-Metal Oxide $NaCo_2O_4$ System," *Proceedings of the 16th International Conference on Thermoelectrics*, pp. 523–527, 1997.

[32] W. Shin and N. Murayama, "Thermoelectric Properties of (Bi,Pb)-Sr-Co-O Oxide," *Journal of Materials Research*, vol. 15, pp. 382–386, 2011.

[33] Y. Miyazaki, K. Kudo, M. Akoshima, Y. Ono, Y. Koike, and T. Kajitani, "Low-Temperature Thermoelectric Properties of the Composite Crystal $[Ca_2CoO_{3.34}]_{0.614}[CoO_2]$," *Japanese Journal of Applied Physics*, vol. 39, pp. 531–533, 2000.

[34] R. Funahashi, I. Matsubara, H. Ikuta, T. Takeuchi, U. Mizutani, and S. Sodeoka, "An Oxide Single Crystal with High Thermoelectric Performance in Air," *Japanese Journal of Applied Physics*, vol. 39, pp. L1127–L1129, 2000.

[35] H. Ohta, "Thermoelectrics Based on Strontium Titanate," *Materials Today*, vol. 10, pp. 44–49, 2007.

[36] J. He, Y. Liu, and R. Funahashi, "Oxide thermoelectrics: The challenges, progress, and outlook," *Journal of Materials Research*, vol. 26, pp. 1762–1772, 2011.

[37] M. Ohtaki, "Recent Aspects of Oxide Thermoelectric Materials for Power Generation from Mid-to-High Temperature Heat Source," *Journal of the Ceramic Society of Japan*, vol. 119, pp. 770–775, 2011.

[38] H. Ohta, K. Sugiura, and K. Koumoto, "Recent Progress in Oxide Thermoelectric Materials: p-Type $Ca_3Co_4O_9$ and n-Type $SrTiO_3$," *Inorganic Chemistry*, vol. 47, pp. 8429–8436, 2008.

[39] J. W. Fergus, "Oxide Materials for High Temperature Thermoelectric Energy Conversion," *Journal of the European Ceramic Society*, vol. 32, pp. 252–540, 2012.

[40] T. Tsubota, M. Ohtaki, K. Eguchi, and H. Arai, "Thermoelectric Properties of Al-Doped ZnO as a Promising Oxide Material for High-Temperature Thermoelectric Conversion," *Journal of Materials Chemistry*, vol. 7, pp. 85–90, 1997.

[41] M. Ohtaki, K. Araki, and K. Yamamoto, "High Thermoelectric Performance of Dually Doped ZnO Ceramics," *Journal of Electronic Materials*, vol. 38, pp. 1234–1238, 2009.

[42] S. Ohta, T. Nomura, H. Ohta, and K. Koumoto, "High-Temperature Carrier Transport and Thermoelectric Properties of Heavily La- or Nb-Doped $SrTiO_3$ Single Crystals," *Journal of Applied Physics*, vol. 97, p. 034106, 2005.

[43] S. Ohta, H. Ohta, and K. Koumoto, "Grain Size Dependence of Thermoelectric Performance of Nb-Doped $SrTiO_3$ Polycrystals," *Journal of the Ceramic Society of Japan*, vol. 114, pp. 102–105, 2006.

[44] Y. Wang, K. H. Lee, H. Ohta, and K. Koumoto, "Thermoelectric Properties of Electron Doped $SrO(SrTiO_3)_n$ (n=1,2) Ceramics," *Journal of Applied Physics*, vol. 105, p. 103701, 2009.

[45] K. Fujita, T. Mochida, and K. Nakamura, "High-Temperature Thermoelectric Properties of $Na_xCoO_{2-\delta}$ Single Crystals," *Japanese Journal of Applied Physics*, vol. 40, pp. 4644–4647, 2001.

[46] T. Motohashi, E. Naujalis, R. Ueda, K. Isawa, M. Karppinen, and H. Yamauchi, "Simultaneously Enhanced Thermoelectric Power and Reduced Resistivity of Na_xCoO_2 by Controlling Na Nonstoichiometry," *Applied Physics Letters*, vol. 79, pp. 1480–1482, 2001.

[47] M. Mikami, M. Yoshimura, Y. Mori, T. Sasaki, R. Funahashi, and M. Shikano, "Thermoelectric Properties of Two Na_xCoO_2 Crystallographic Phases," *Japanese Journal of Applied Physics*, vol. 42, pp. 7383–7386, 2003.

[48] M. Lee, L. Viciu, L. Li, Y. Wang, M. L. Foo, S. Watauchi, R. A. Pascal Jr., R. J. Cava, and N. P. Ong, "Large Enhancement of the Thermopower in Na_xCoO_2 at high Na doping," *Nature Materials*, vol. 5, pp. 537–540, 2006.

[49] T. Caillat, M. Carle, P. Pierrat, and S. Scherrer, "Thermoelectric Properties of $(Bi_xSb_{1-x})_2Te_3$ Single Crystal Solid Solutions Grown by the T.H.M. Method," *Journal of Physics and Chemistry of Solids*, vol. 53, pp. 1121–1129, 1992.

[50] B. C. Sales, R. Jin, K. A. Affholter, P. Khalifah, G. M. Veith, and D. Mandrus, "Magnetic, Thermodynamic, and Transport Characterization of $Na_{0.75}CoO_2$ Single Crystals," *Physical Review B*, vol. 70, p. 174419, 2004.

[51] X. Tang and T. M. Tritt, "Overview of Thermoelectric Sodium Cobaltite: $Na_xCo_2O_4$," *Journal of the South Carolina Academy of Science*, vol. 6, pp. 10–13, 2008.

[52] M. Lee, L. Viciu, L. Li, Y. Wang, M. L. Foo, S. Watauchi, R. A. Pascal Jr., R. J. Cava, and N. P. Ong, "Enhancement of the Thermopower in Na_xCoO_2 in the large x regime ($x \geq 0.75$)," *Physica B*, vol. 403, pp. 1564–1568, 2008.

[53] Y. Miyazaki, "Crystal Structure and Thermoelectric Properties of the Misfit-Layered Cobalt Oxides," *Solid State Ionics*, vol. 172, pp. 463–467, 2004.

[54] K. Koumoto, I. Terasaki, and R. Funahashi, "Complex Oxide Materials for Potential Thermoelectric Applications," *MRS Bulletin*, vol. 31, pp. 206–210, 2006.

[55] C. Fouassier, G. Matejka, and J. M. Reau, "Sur de nouveaux bronzes oxygénés de formule Na_xCoO_2 ($x \leq 1$). Le système cobalt-oxygène-sodium," *Journal of Solid State Chemistry*, pp. 532–537, 1973.

[56] Y. Ono, R. Ishikawa, Y. Miyazaki, Y. Ishii, Y. Morii, and T. Kajitani, "Crystal Structure, Electric and Magnetic Properties of Layered Cobaltite β-Na_xCoO_2," *Journal of Solid State Chemistry*, vol. 166, pp. 177–181, 2002.

[57] L. Viciu, J. W. G. Bos, H. W. Zandbergen, Q. Huang, M. L. Foo, S. Ishiwata, A. P. Ramirez, M. Lee, N. P. Ong, and R. J. Cava, "Crystal Structure and Elementary Properties of Na_xCoO_2 (x=0.32, 0.51, 0.6, 0.75, and 0.92) in the Three-Layer $NaCoO_2$ Family," *Physical Review B*, vol. 73, p. 174104, 2006.

[58] Q. Huang, M. L. Foo, R. A. Pascal, J. W. Lynn, B. H. Toby, T. He, H. W. Zandbergen, and R. J. Cava, "Coupling between electronic and structural degrees of freedom in the triangular lattice conductor Na_xCoO_2," *Physical Review B*, p. 184110, 2004.

[59] Q. Huang, B. Khaykovich, F. Chou, J. Cho, J. Lynn, and Y. Lee, "Structural Transition in Na_xCoO_2 with x near 0.75 due to Na Rearrangement," *Physical Review B*, vol. 70, p. 134115, 2004.

[60] R. Berthelot, D. Carlier, and C. Delmas, "Electrochemical Investigation of the P2-Na_xCoO_2 Phase Diagram," *Nature Materials*, vol. 10, pp. 74–80, 2011.

[61] Y. Krockenberger, I. Fritsch, G. Christiani, H. U. Habermeier, L. Yu, C. Bernhard, B. Keimer, and L. Alff, "Superconductivity in Epitaxial Thin Films of $Na_xCoO_2{\cdot}yD_2O$," *Applied Physics Letters*, vol. 88, p. 162501, 2006.

[62] X. P. Zhang, Y. S. Xiao, H. Zhou, B. T. Xie, C. X. Yang, and Y. G. Zhao, "Surface Morphology, Structure and Transport Property of Na_xCoO_2 Thin Films Grown by Pulsed Laser Deposition," *Materials Science Forum*, vol. 3807, pp. 475–479, 2005.

[63] T. Paulauskas and R. F. Klie, "Observations of Co^{4+} in a Higher Spin State and the Increase in the Seebeck Coefficient of Thermoelectric $Ca_3Co_4O_9$," *Journal of Undergraduate Research*, vol. 5, p. 196601, 2011.

[64] Y. Morita, J. Poulse, K. Sakai, T. Motohashi, T. Fujii, I. Terasaki, H. Yamauchi, and M. Karppinen, "Oxygen Nonstoichiometry and Cobalt Valence in Misfit-Layered Cobalt Oxides," *Journal of Solid State Chemistry*, vol. 177, pp. 3149–3155, 2004.

[65] Y. Tanaka, T. Fujii, M. Nakanishi, Y. Kusano, H. Hashimoto, Y. Ikeda, and J. Takada, "Systematic Study on Synthesis and Structural, Electrical Transport and Magnetic Properties of Pb-Substituted Bi-Ca-Co-O Misfit-Layer Cobaltites," *Solid State Communications*, vol. 141, pp. 122–126, 2007.

[66] J.-i. Shimoyama, S. Horii, K. Otzschi, M. Sano, and K. Kishio, "Oxygen Nonstoichiometry in Layered Cobaltite $Ca_3Co_4O_y$," *Japanese Journal of Applied Physics*, vol. 42, pp. 194–197, 2003.

[67] Y. Wang, N. S. Rogado, R. J. Cava, and N. P. Ong, "Spin Entropy as the Likely Source of Enhanced Thermopower in $Na_xCo_2O_4$," *Nature*, vol. 423, pp. 425–428, 2003.

[68] S. Mukerjee, "Thermopower of the Hubbard Model: Effects of Multiple Orbitals and Magnetic Fields in the Atomic Limit," *Physical Review B*, vol. 72, p. 195109, 2005.

[69] S. Mukerjee and J. E. Moore, "Doping Dependence of Thermopower and Thermoelectricity in Strongly Correlated Materials," *Applied Physics Letters*, vol. 90, p. 112107, 2007.

[70] T. Kawata, Y. Iguchi, T. Itoh, K. Takahata, and I. Terasaki, "Na-Site Substitution Effects on the Thermoelectric Properties of $NaCo_2O_4$," *Physical Review B*, vol. 60, p. 10584, 1999.

[71] M. Shikano and R. Funahashi, "Electrical and Thermal Properties of Single-Crystalline $(Ca_2CoO_3)_{0.7}CoO_2$ with a $Ca_3Co_4O_9$ Structure," *Applied Physics Letters*, vol. 82, pp. 1851–1853, 2003.

[72] N. Van Nong, N. Pryds, S. Linderoth, and M. Ohtaki, "Enhancement of the Thermoelectric Performance of p-Type Layered Oxide $Ca_3Co_4O_{9+\delta}$ Through Heavy Doping and Metallic Nanoinclusions," *Advanced Materials*, vol. 23, pp. 2484–2490, 2011.

[73] D. Moser, L. Karvonen, S. Populoh, M. Trottmann, and A. Weidenkaff, "Influence of the Oxygen Content on Thermoelectric Properties of $Ca_{3-x}Bi_xCo_4O_{9+\delta}$ System," *Solid State Sciences*, vol. 13, pp. 2160–2164, 2011.

[74] Y. Wang, Y. Sui, J. Cheng, X. Wang, and W. Su, "Comparison of the High Temperature Thermoelectric Properties for Ag-Doped and Ag-Added $Ca_3Co_4O_9$," *Journal of Alloys and Compounds*, vol. 477, pp. 817–821, 2009.

[75] N. V. Nong, C.-J. Liu, and M. Ohtaki, "Improvement on the High Temperature Thermoelectric Performance of Ga-Doped Misfit-Layered $Ca_3Co_{4-x}Ga_xO_{9+\delta}$ (x=0, 0.05, 0.1, and 0.2)," *Journal of Alloys and Compounds*, vol. 491, pp. 53–56, 2010.

[76] N. V. Nong, S. Yanagiya, S. Monica, N. Pryds, and M. Ohtaki, "High-Temperature Thermoelectric and Microstructural Characteristics of Cobalt-Based Oxides with Ga Substituted on the Co-Site," *Journal of Electronic Materials*, vol. 40, pp. 716–722, 2011.

[77] N. V. Nong, C.-J. Liu, and M. Ohtaki, "High-temperature Thermoelectric Properties of Late Rare Earth-Doped $Ca_3Co_4O_{9+\delta}$," *Journal of Alloys and Compounds*, vol. 509, pp. 977–981, 2011.

[78] H. Ohta, S. Kim, Y. Mune, T. Mizoguchi, K. Nomura, S. Ohta, T. Nomura, Y. Nakanishi, Y. Ikuhara, M. Hirano, H. Hosono, and K. Koumoto, "Giant Thermoelectric Seebeck Coefficient of a Two-Dimensional Electron Gas in $SrTiO_3$," *Nature Materials*, vol. 6, pp. 129–134, 2007.

[79] Y. Mune, H. Ohta, K. Koumoto, T. Mizoguchi, and Y. Ikuhara, "Enhanced Seebeck Coefficient of Quantum-Confined Electrons in $SrTiO_3/SrTi_{0.8}Nb_{0.2}O_3$ Superlattices," *Applied Physics Letters*, vol. 91, p. 192105, 2007.

[80] H. Ohta, "Two-dimensional Thermoelectric Seebeck Coefficient of $SrTiO_3$-based Superlattices," *Physica Status Solidi (b)*, vol. 245, pp. 2363–2368, 2008.

[81] S. Hildebrandt, P. Komissinskiy, M. Major, W. Donner, and L. Alff, "Epitaxial Growth and Control of the Sodium Content in Na_xCoO_2 Thin Films," *Thin Solid Films*, vol. 545, pp. 291–295, 2013.

[82] L. Yu, L. Gu, Y. Wang, P. X. Zhang, and H. U. Habermeier, "Epitaxial Layered Cobaltite Na_xCoO_2 Thin Films Grown on Planar and Vicinal Cut Substrates," *Journal of Crystal Growth*, vol. 328, pp. 34–38, 2011.

[83] J. Y. Son, Y. H. Shin, and C. S. Park, "Fabrication and Optical Conductivities of Strained Epitaxial Na_xCoO_2 Thin Films: x=0.5, 0.7," *Journal of Solid State Chemistry*, vol. 181, pp. 2020–2023, 2008.

[84] J. Y. Son, "Epitaxial Layered Cobaltite Na_xCoO_2 Thin Films: x= 0.5, 0.7," *Journal of Physics D: Applied Physics*, vol. 41, p. 095405, 2008.

[85] J. Y. Son, H. B. R. Lee, and J. H. Cho, "Stress Dependence of Growth Mode Change of Epitaxial Layered Cobaltite γ-$Na_{0.7}CoO_2$," *Applied Surface Science*, vol. 254, pp. 436–440, 2007.

[86] H. Zhou, X. P. Zhang, B. T. Xie, Y. S. Xiao, C. X. Yang, Y. J. He, and Y. G. Zhao, "Fabrication of Na_xCoO_2 Thin Films by Pulsed Laser Deposition," *Thin Solid Films*, vol. 497, pp. 338–340, 2006.

[87] Y. Krockenberger, I. Fritsch, G. Cristiani, A. Matveev, L. Alff, H. U. Habermeier, and B. Keimer, "Epitaxial Growth of Na_xCoO_2 Thin Films by Pulsed-Laser Deposition," *Applied Physics Letters*, vol. 86, p. 191913, 2005.

[88] J. Y. Son, B. G. Kim, and J. H. Cho, "Kinetically Controlled Thin-Film Growth of Layered β- and γ-Na_xCoO_2 Cobaltate," *Applied Physics Letters*, vol. 86, p. 221918, 2005.

[89] K. Sugiura, H. Ohta, K. Nomura, M. Hirano, and H. Hosono, "Fabrication and Thermoelectric Properties of Layered Cobaltite, γ-$Sr_{0.32}Na_{0.21}CoO_2$ Epitaxial Films," *Applied Physics Letters*, vol. 88, p. 082109, 2006.

[90] L. Yu, Y. Krockenberger, I. Fritsch, and H. U. Habermeier, "Substrate-Induced Anisotropy of c-Axis Textured Na_xCoO_2 Thin Films," *Progress in Solid State Chemistry*, vol. 35, pp. 545–551, 2007.

[91] A. Venimadhav, A. Soukiassian, D. A. Tenne, Q. Li, X. X. Xi, D. G. Schlom, R. Arroyave, Z. K. Liu, H. P. Sun, X. Pan, M. Lee, and N. P. Ong, "Structural and Transport Properties of Epitaxial Na_xCoO_2 Thin Films," *Applied Physics Letters*, vol. 87, p. 172104, 2005.

[92] M. G. Kang, K. H. Cho, S. M. Oh, J. S. Kim, C. Y. Kang, S. Nahm, and S. J. Yoon, "High-Temperature Thermoelectric Properties of Nanostructured $Ca_3Co_4O_9$ Thin Films," *Applied Physics Letters*, vol. 98, p. 142102, 2011.

[93] T. Sun, H. H. Hng, Q. Yan, and J. Ma, "Effects of Pulsed Laser Deposition Conditions on the Microstructure of $Ca_3Co_4O_9$ Thin Films," *Journal of Electronic Materials*, vol. 39, pp. 1611–1615, 2010.

[94] R. Moubah, S. Colis, C. Ulhaq-Bouillet, and A. Dinia, "Defects Analysis at the Nanometric Scale in $Ca_3Co_4O_9$ Thin Films," *Applied Physics Letters*, vol. 96, p. 041902, 2010.

[95] K. Sugiura, H. Ohta, K. Nomura, M. Hirano, H. Hosono, and K. Koumoto, "High Electrical Conductivity of Layered Cobalt Oxide $Ca_3Co_4O_9$ Epitaxial Films Grown by Topotactic Ion-Exchange Method," *Applied Physics Letters*, vol. 89, p. 032111, 2006.

[96] A. Sakai, T. Kanno, S. Yotsuhashi, A. Odagawa, and H. Adachi, "Control of Epitaxial Growth Orientation and Anisotropic Thermoelectric Properties of Misfit-Type $Ca_3Co_4O_9$ Thin Films," *Japanese Journal of Applied Physics*, vol. 44, pp. 966–969, 2005.

[97] H. W. Eng, W. Prellier, S. Hébert, D. Grebille, L. Méchin, and B. Mercey, "Influence of Pulsed Laser Deposition Growth Conditions on the Thermoelectric Properties of $Ca_3Co_4O_9$ Thin Films," *Journal of Applied Physics*, vol. 97, p. 013706, 2005.

[98] Y. F. Hu, W. D. Si, E. Sutter, and Q. Li, "In Situ Growth of c-Axis-Oriented $Ca_3Co_4O_9$ Thin Films on Si (100)," *Applied Physics Letters*, vol. 86, p. 082103, 2005.

[99] Y. F. Hu, E. Sutter, W. D. Si, and Q. Li, "Thermoelectric Properties and Microstructure of c-Axis-Oriented $Ca_3Co_4O_9$ Thin Films on Glass Substrates," *Applied Physics Letters*, vol. 87, p. 171912, 2005.

[100] Y. Zhou, "Effect of Grain Size on Electric Resistivity and Thermopower of $(Ca_{2.6}Bi_{0.4})Co_4O_9$ Thin Films," *Journal of Applied Physics*, vol. 95, pp. 625–628, 2004.

[101] Q. Qiao, A. Gulex, T. Paulauskas, S. Kolesnik, B. Dabrowski, M. Ozdemir, C. Boyrax, D. Mazumdar, A. Gupta, and R. F. Klie, "Effect of Substrate on the Atomic Structure and Physical Properties of Thermoelectric $Ca_3Co_4O_9$ Thin Films," *Journal of Physics: Condensed Matter*, vol. 23, p. 305005, 2011.

Chapter 2

Chemical Stability of Na_xCoO_2 Thin Films

Abstract

The growth of Na_xCoO_2 thin films by pulsed laser deposition is studied in this chapter. Epitaxial growth was achieved on single-crystal substrates of Al_2O_3, without the formation of impurity phases. The deposited thin films were not stable when exposed to air, resulting in an increase of the electrical resistivity by more than one order of magnitude over a period of several days. These stability issues are studied in this chapter, and found to be caused by the reactive nature of the sodium, forming sodium carbonate with moisture and carbon dioxide from air. By the *in-situ* deposition of an amorphous AlO_x capping layer, the stability issues were overcome. Na_xCoO_2 thin films with this capping layer show chemically stable behavior when exposed to air and the intrinsic properties of these Na_xCoO_2 thin films are analysed for the first time. These Na_xCoO_2 thin films show comparable thermoelectric properties at room temperature as Na_xCoO_2 single crystals.

Part of the work discussed in this chapter is published in: P. Brinks, H. Heijmerikx, T.A. Hendriks, G. Rijnders, M. Huijben, "Achieving Chemical Stability in Thermoelectric Na_xCoO_2 Thin Films", RSC Advances **2**, 6023-6027 (2012)

2.1 Introduction

Since the first observation of a high thermopower and low electrical resisitivity in Na_xCoO_2 single crystals [1], this material was studied as a promising thermoelectric candidate. [2–6] Thin films of Na_xCoO_2 have also been investigated in previous studies, with a strong focus on the structural properties. [7–12] These previous reports mostly describe thin films deposited on Al_2O_3, $LaAlO_3$ and $SrTiO_3$, where in all studies these films are c-axis oriented and in some cases also epitaxial. [9–12] The focus of these reports is to study the stoichiometry through the relation between the c-axis lattice parameter and the sodium to cobalt ratio and comparing this with single crystals. [13–15] A strong dependence between the deposition parameters (most significantly temperature) as well as the annealing procedure, and the c-axis lattice parameter (and therewith the sodium to cobalt ratio) is found. The film thickness used for these studies was relatively comparable, ranging from 100 to 300 nm, and was not systemically varied to study the relation between film thickness and structural properties.

No detailed analysis of the thermoelectric properties of these Na_xCoO_2 thin films has been performed to date, due to chemical instability of the thin films at ambient conditions, which hampers characterization of the intrinsic material properties. [7] This lack of chemical stability is observed through an increase of the (room temperature) electrical resistivity with time, when the samples are exposed to ambient conditions. The observed increase could be fitted well with an exponential curve and showed an increase of more than one order of magnitude within 24 hours. In addition to the reported increase of the room temperature resistivity, after one day of exposure to ambient conditions, the temperature dependence of the resistivity showed a transition from the initial metallic behavior to semiconducting or insulating behavior.

This lack of chemical stability has also been observed in single crystals [16] of Na_xCoO_2 and is caused by the reactivity of the sodium with moisture and carbon dioxide from air, which results in the formation of sodium carbonate. Because of these stability issues, research focusing on Na_xCoO_2 has been limited during the past several years. However, if these stability issues can be overcome, the intrinsic properties of Na_xCoO_2 can be studied and this could reveal the full thermoelectric potential of Na_xCoO_2.

In this chapter a study on the growth of Na_xCoO_2 thin films by pulsed laser deposition and their chemical stability in air is presented. The aim of this study is to suppress the reactivity of Na_xCoO_2 thin films and thereby improve the chemical stability of these thin films, which would enable a study of the intrinsic properties of these thin films. The first part of this chapter focuses on the growth of Na_xCoO_2 thin films and a study of the structural properties. The chemical stability is studied in the second part of this chapter where it is also shown that by preventing direct contact between the Na_xCoO_2 layer, CO_2 and moisture (from

air), chemically stable thin films can be obtained. This is achieved by the addition of an *in situ* amorphous AlO_x capping layer. In the final part of this chapter the thermoelectric properties of these chemically stable thin films are presented, which show comparable values at room temperature as their single crystal analogues.

2.2 Growth and Structural Properties of Na_xCoO_2 Thin Films

2.2.1 Growth

Thin film samples of Na_xCoO_2 were fabricated by pulsed laser deposition (PLD). This technique is used because of its versatility, which enables depositions of a variety of complex oxide materials and the stoichiometric transfer from target to substrate that can be achieved for many materials. [17–19] Another advantage of PLD is that by tuning the deposition parameters, the structural properties of the deposited thin films can be engineered, providing a direct tool to consequently also control the functional properties. Additionally, with PLD it is also possible to stack various different materials, enabling the fabrication of superlattices or the addition of capping layers.

Na_xCoO_2 thin films were deposited with a laser fluence of 4 J/cm^2, a spotsize of 1.1 mm^2 and a repetition rate of 1 Hz. A KrF excimer laser with a wavelength of 248 nm was used (Lambda Physik LPX 210). These laser settings resulted in single-phase thin films, whereas for higher laser repetition rates impurity phases were formed. During growth the oxygen environment was kept at 0.4 mbar. After the growth the samples were slowly cooled to room temperature in 1 atm. of oxygen at a rate of 10°C/min to optimize the oxidation level.

As substrate material, single crystal (001)-oriented Al_2O_3 and (001)-oriented $LaAlO_3$ were chosen, because these were previously used to obtain single-phase and c-axis oriented or epitaxial thin films. [7,8,10–12]. Before deposition, the substrates were annealed for 1 hour at 1050°C (Al_2O_3) and at 950°C with an oxygen flow of 150 ml/min ($LaAlO_3$), exhibiting smooth surfaces with clear unit-cell-height steps in atomic force microscopy (AFM). The low level of surface roughness after annealing can be seen in Fig. 2.1a and Fig. 2.1b for respectively a typical annealed Al_2O_3 and $LaAlO_3$ substrate. A sintered target with the composition $Na_{0.9}CoO_2$ was used, because this composition is expected to show the best thermoelectric properties, as explained in Chapter 1.

2.2.2 Structural Properties

The structural properties of the thin films were determined by X-ray diffraction. A typical $2\theta/\omega$ scan for a 60 nm thin Na_xCoO_2 film, deposited at 430°C, is shown in Fig. 2.2 when grown on an Al_2O_3 and a $LaAlO_3$ substrate. Both thin films exhibit

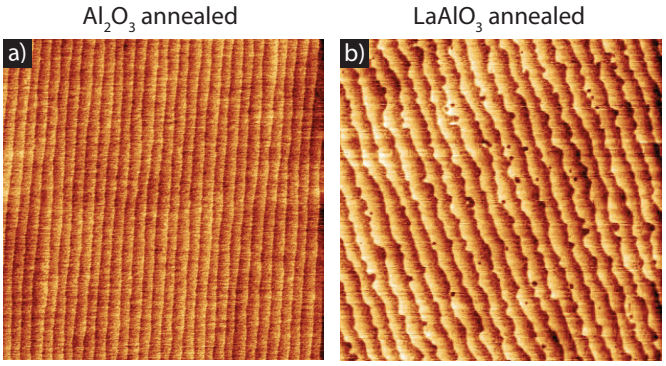

Figure 2.1: Atomic force microscopy images (3×3 μm^2) of (001) oriented Al_2O_3 and $LaAlO_3$ single crystal substrates (a and b), after annealing for 60 minutes at respectively 1050°C and 950°C.

only (00l) peaks of Na_xCoO_2 indicating a preferred growth orientation with the c-axis of the thin film and the substrate aligned parallel to each other. The c-axis lattice parameters are 10.95±0.05 Å and 11.05±0.05 Å for samples deposited on respectively Al_2O_3 and $LaAlO_3$ substrates. Since no impurity peaks are observed it is concluded that the films are single-phase.

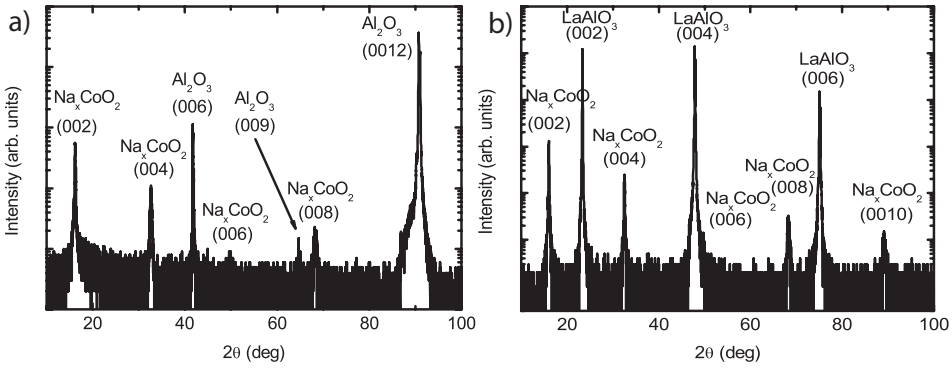

Figure 2.2: X-ray diffraction spectrum for 60 nm Na_xCoO_2 thin films deposited on single crystal Al_2O_3 (a) and $LaAlO_3$ (b) substrates. Only (00l) peaks of the thin films are observed, indicating that the films are single phase and exhibit a preferred growth orientation.

Even though the growth orientation is similar for the thin films grown on these two different substrates, for the in-plane direction clear differences are observed. For thin films grown on Al_2O_3 substrates an in-plane epitaxial relationship is found between the substrate and the thin film. The hexagonal structure of the Na_xCoO_2 is rotated by 30° with respect to that of the substrate. This is demonstrated in

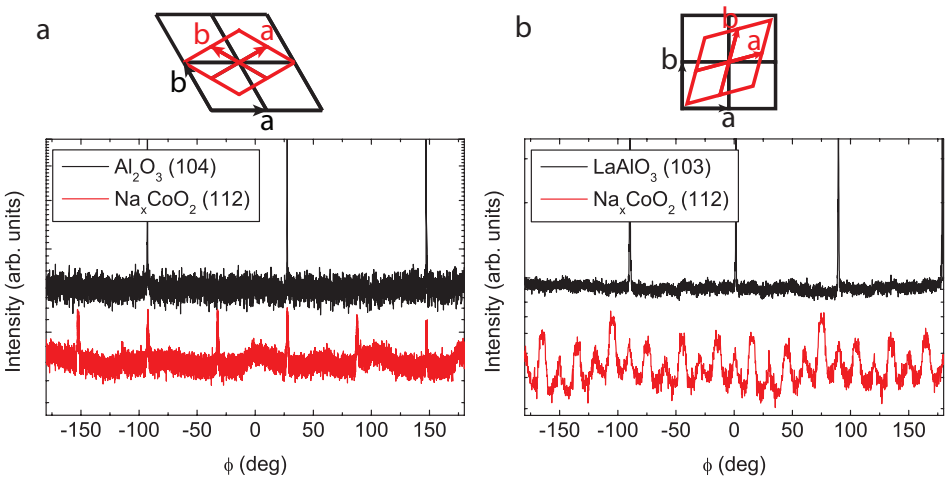

Figure 2.3: X-ray diffraction measurements demonstrating the epitaxial relationship between the Al_2O_3 (a) and the $LaAlO_3$ (b) substrate and the Na_xCoO_2 thin film. The ϕ positions of the (112) Na_xCoO_2 and (104) Al_2O_3 peaks indicate a rotation of the a-axis of the film by 30° compared to that of the Al_2O_3 (a). The ϕ positions of the (112) Na_xCoO_2 and (103) $LaAlO_3$ peaks indicated a rotation of 15° compared to that of the substrate (b). The presence of 24 peaks is a direct consequence of the 4 symmetrically comparable stacking options.

Fig. 2.3a where it is shown that in a ϕ scan the peak positions of the (104) peak of the substrate are found to match that of the (112) film peak, the in-plane configuration is also schematically shown. The a-axis lattice parameter is 2.82 Å for these epitaxial thin films. For the $LaAlO_3$ substrate a different in-plane epitaxial relationship between the substrate and the thin film was found. Because of the cubic structure there is no exact match with the hexagonal Na_xCoO_2 structure, however by rotating the a-axis by 15° with respect to that of the substrate, a partial match can be obtained, as schematically depicted in Fig. 2.3b. This preferred orientation is confirmed by performing a ϕ scan of the (103) peak of the $LaAlO_3$ substrate and the (112) Na_xCoO_2 film peak, which show the expected 15° difference as shown in Fig. 2.3b. The presence of 24 peaks confirms the existence of 4 equivalent stacking options, i.e. twinning, which can be obtained by rotating the a-axis by 15° in either direction, compared to the a-axis of the substrate. Even though a difference in structure as well as lattice parameter results in a significantly different lattice match with the cubic $LaAlO_3$ [20] and the hexagonal Al_2O_3 [21] single crystal substrates, epitaxial growth of Na_xCoO_2 thin films can be achieved on both substrates.

In contrast to previous reports on the narrow range of deposition temperatures for the growth of single-phase thin films, [7] we observed a much wider range (330°C - 650°C) for our deposition conditions. Fig. 2.4 shows a clear difference

in crystallinity for Na_xCoO_2 thin films grown on $LaAlO_3$ substrates at various deposition temperatures. For the samples that are included in this graph, only (00l) Na_xCoO_2 diffraction peaks were observed, indicating that these samples are single phase and all show the same crystallographic orientation. Due to the volatility of sodium, it is expected that the sodium concentration within the sample is depending on the deposition temperature. [8] Therefore, a change in sodium concentration as a function of deposition temperature could lead to a corresponding change in c-axis length of the Na_xCoO_2 unit cell. [13, 22] However, the observed peak shift is relatively small, as can be seen in Fig. 2.4, and a c-axis lattice parameter of 11.05±0.05 Å was determined for these samples. Based on these results it is concluded that the sample stoichiometry is constant for this range of deposition temperatures. For deposition temperatures higher than 650°C in addition to the (00l) Na_xCoO_2 diffraction peaks, the (111) and (222) diffraction peaks of Co_3O_4 were also observed, indicating that at these higher deposition temperatures the sample stoichiometry is changing due to a loss of sodium. These samples with impurity phases were not included in the presented data. Even though the differences are not very pronounced, based on the XRD spectra (Fig. 2.4) it was concluded that a deposition temperature of 430°C results in the best crystallinity, because this sample shows a combination of a high peak intensity and a small FWHM. Therefore a deposition temperature of 430° was used for the following study of the stability and thermoelectric properties of these Na_xCoO_2 thin films.

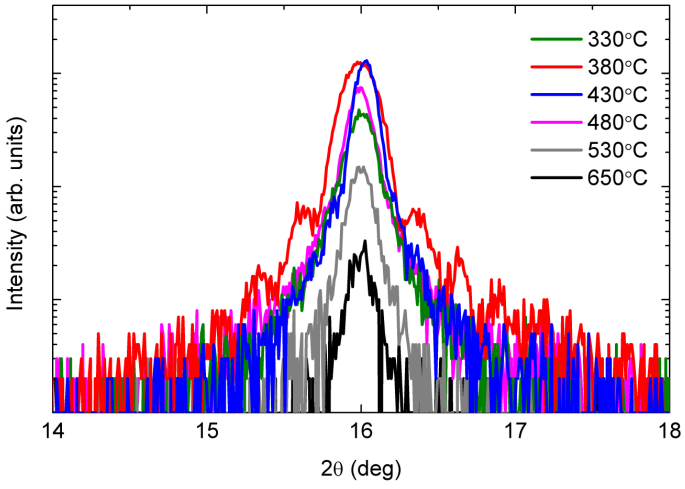

Figure 2.4: X-ray diffraction measurements of the (002) peak of the Na_xCoO_2 thin film on $LaAlO_3$ substrates for varying deposition temperatures. Only small peak shifts are observed, indicating minimal variation in sample composition stoichiometry.

2.3 Chemical Stability and Thermoelectric Potential of Na_xCoO_2 Thin Films

2.3.1 Na_xCoO_2 Stability

The electrical transport properties of thin Na_xCoO_2 films are known to degrade with time in ambient conditions. [7] Stability issues have also been reported for single crystals of Na_xCoO_2, however for these single crystals the degradation is significantly smaller, because of their lower surface to volume ratio, and storing them in vacuum or in a sealed container is typically sufficient. [16, 23] We indeed also observed a strong increase in resistance for Na_xCoO_2 thin films, see Fig. 2.5. For the thin films deposited on Al_2O_3 and $LaAlO_3$ substrates an increase of resistance by a factor of respectively 2.2 and 50 is observed, when exposed to air, over a period of two days, after which it stabilizes. The degradation can be interrupted by placing the sample in a vacuum environment (10^{-5} mbar), while subsequent exposure to ambient conditions continues the degradation process, demonstrating that the effect is not intrinsic but triggered by exposure to ambient conditions. These stability issues have previously hampered accurate analysis of the thermoelectric properties of Na_xCoO_2 thin films, because the intrinsic properties could not be determined.

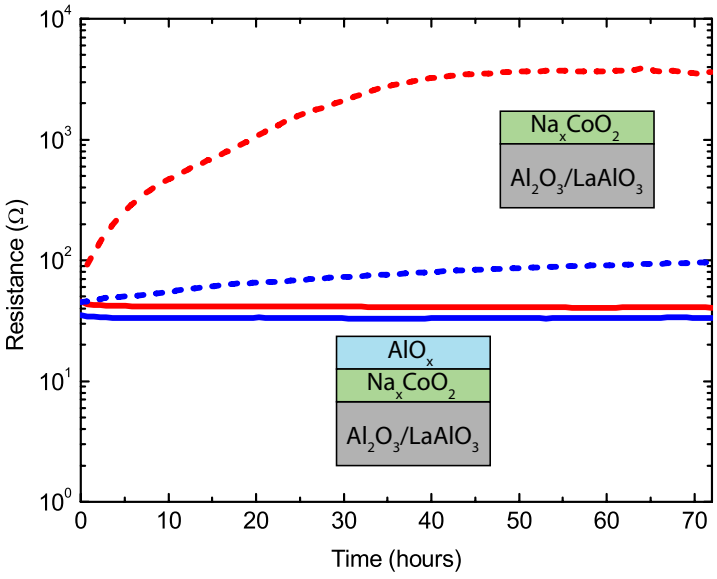

Figure 2.5: Time-dependent resistance measurements of Na_xCoO_2 thin films on Al_2O_3 (blue) and $LaAlO_3$ (red) single crystal substrates at 300K. Measurements are shown for samples with (solid lines) and without (dashed lines) an AlO_x capping layer.

A reaction of sodium from the sample with moisture and carbon dioxide from

the air has been suggested to occur, [7], which can easily take place because the sodium atoms are only loosely bound in between the CoO_2 layers. This reaction results in the formation of sodium carbonate (Na_2CO_3) and will influence the samples by two different mechanisms. Locally the sodium level will be reduced at the surface and grain boundaries where the reactions are taking place, leading to different properties, because of the sensitivity of the electronic properties to the sodium to cobalt ratio. Additionally, the electronic properties will be influenced by the presence of, electrically insulating Na_2CO_3, at the grain boundaries which will influence the transport properties between grains.

In contrast to the changes in electrical resistivity after exposure to ambient conditions for several days, no significant changes in the XRD spectra were observed for these Na_xCoO_2 thin films. This indicates that the reactions are limited to the surface and grain boundaries and that for a large part of the volume of the thin films the structural properties are preserved and that the observed changes in electrical properties are dominated by degradation at the grain boundaries and not by changes of the sodium to cobalt ratio within the grains of the thin film.

To verify the formation of Na_2CO_3 at the surface, X-Ray photoelectron spectroscopy (XPS) measurements were performed on a thin film, which has been transferred into the XPS chamber immediately after deposition. During the sample transfer from PLD to XPS the sample has been shortly exposed to ambient conditions, during which some Na_2CO_3 has already been formed. This was indeed confirmed by XPS analysis, where for carbon 1s a double peak was observed, as shown in Fig. 2.6. One of these peaks was identified as a carbonate peak, whereas the other peak originates from carbohydrates that are adsorbed to the surface when exposed to air. No change in the XPS spectrum was observed after storage in ultra-high vacuum for one week (not shown). However, after exposure to ambient conditions for six days, a clear increase of the carbon 1s peak, originating from the carbonate impurity phase, was measured, as shown in Fig. 2.6. This increase is quantified by calculating the ratio of the area of the carbonate and carbohydrate peaks, after subtracting the background signal, which increases from 0.35 to 1.0 after an exposure of six days. These changes in ratio of the two peaks confirm that the amount of sodium carbonate that is formed on the surface of the sample is increasing upon exposure to ambient conditions and a similar effect is to be expected along the grain boundaries within the thin film. This has a dramatic effect on the electrical transport going through the degrading grain boundaries as shown in Fig. 2.5. The degradation process is significantly stronger for thin films deposited on $LaAlO_3$ substrates, which can be explained by the increased lattice mismatch and the additional formation of twin boundaries, which cause additional exposure.

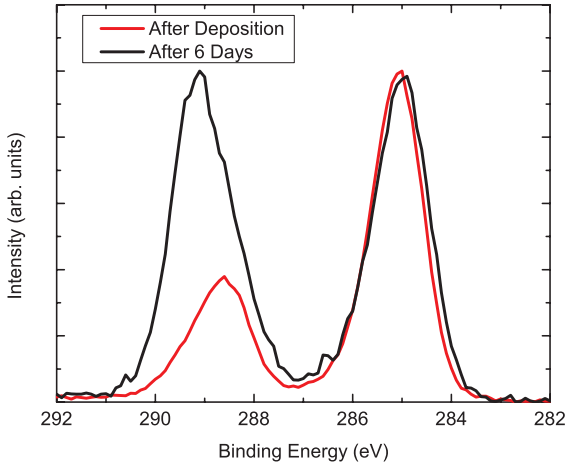

Figure 2.6: XPS measurements of the carbon 1s peak, directly after deposition and after an additional six days of exposure to ambient conditions. Two different peaks are observed, originating from adsorbed carbohydrates (approximately 285 eV) and sodium carbonate (approximately 289 eV). Data is normalized for comparison of the different measurements.

2.3.2 Capping layer

Two possible solutions were proposed to achieve chemical stability in Na_xCoO_2 thin films either by protecting the thin film from direct contact with the surrounding atmosphere [7] or by modifying the reactivity of the material through (partial) substitution of sodium by another cation. [24] The latter attempt has been previously reported and has resulted in stable $Sr_{0.31}Na_{0.21}CoO_2$ thin films. [24] The electrical resistivity of these thin films at room temperature is 1.1 mΩcm and comparable with single crystal samples. [24] The Seebeck coefficient at room temperature was reported as 120 μV/K which is a significantly higher than single crystals, which have a value of about 90 μV/K. It is however difficult to compare these values, because of the additional doping in these $Sr_{0.31}Na_{0.21}CoO_2$ thin films. The disadvantages of this approach are however that it still does not provide the intrinsic material properties of Na_xCoO_2 and that the process of fabrication first involves the preparation of a $Na_{0.8}CoO_2$ thin film which is then converted into $Sr_{0.31}Na_{0.21}CoO_2$ by a Sr^{2+}-ion exchange treatment. The method described in this section aims at the development of a protective capping layer, which could be deposited *in situ* to avoid any exposure to ambient conditions of the Na_xCoO_2 thin films.

A good candidate material is Al_2O_3, since it has been used previously as diffusion barrier, to prevent interface reactions and diffusion between a silicon substrate and a $Pb(Zr_{0.52}Ti_{0.48})O_3$ thin film [25], and it can be deposited by PLD in

either polycrystalline or amorphous layers. For polycrystalline capping layers of Al_2O_3 only a small improvement in the stability was observed, which is most likely caused by an incomplete coverage due to island formation of the polycrystalline capping layer. However, a fully closed coverage of the surface can be expected for an amorphous AlO_x layer. [26] This was indeed confirmed by AFM for an 80nm AlO_x capping layer directly deposited on an $LaAlO_3$ substrate at room temperature and an oxygen pressure of 5×10^{-3} mbar and from a polycrystalline Al_2O_3 target, as shown in figure 2.7c. Deposition of AlO_x at higher oxygen pressures resulted in an increased surface roughness and, therefore, a reduced surface coverage. The surface topography of samples with and without an additional 80 nm amorphous AlO_x capping layer is shown in Fig. 2.7a, 2.7b, 2.7d and Fig. 2.7e for Na_xCoO_2 thin films on respectively Al_2O_3 and $LaAlO_3$ substrates. This thickness was used to ensure a complete coverage of all trenches and islands present at the Na_xCoO_2 surface and to form a suitable barrier layer for CO_2 and moisture. For these samples the RMS-value of the surface roughness is approximately 4 nm and is comparable for samples with and without a capping layer. Detailed analysis of the electrical transport properties showed that the implementation of an additional amorphous AlO_x capping layer completely prevented any degradation in ambient conditions for epitaxial and textured thin films, see Fig. 2.5. Reference samples where only the AlO_x capping layer was deposited were electrically insulating, ensuring that the measured behavior is only from the Na_xCoO_2 thin film. The AlO_x-capped samples remain stable over a period of several months and this enables us to study for the first time in detail the relation between structural and thermoelectric properties in chemically stable Na_xCoO_2 thin films on different single crystal substrates.

2.3.3 Thermoelectric potential

To determine the thermoelectric properties of AlO_x-capped Na_xCoO_2 thin films the temperature dependence of the electrical transport properties are measured in the range of 4-300 K and compared to reported single crystal values. The measurements were performed in a Van der Pauw configuration, with square gold contacts at the corners of the sample. The results are shown in Fig. 2.8. The analysis is given for two samples which are deposited at 430°C and 0.4 mbar on respectively Al_2O_3 and $LaAlO_3$ substrates. These two samples represent typical results for thin films grown on these two substrates and show interesting differences which can be explained by their crystallographic properties. A lower resistivity within the measured temperature range is observed for the sample deposited on Al_2O_3, as compared to the sample deposited on $LaAlO_3$. Assuming a simple single band model and no electron correlations, at room temperature a carrier density of 3.0×10^{21} cm^{-3} and 3.3×10^{21} cm^{-3} for the samples deposited on respectively Al_2O_3 and $LaAlO_3$ are determined from the measured Hall coefficients, which are

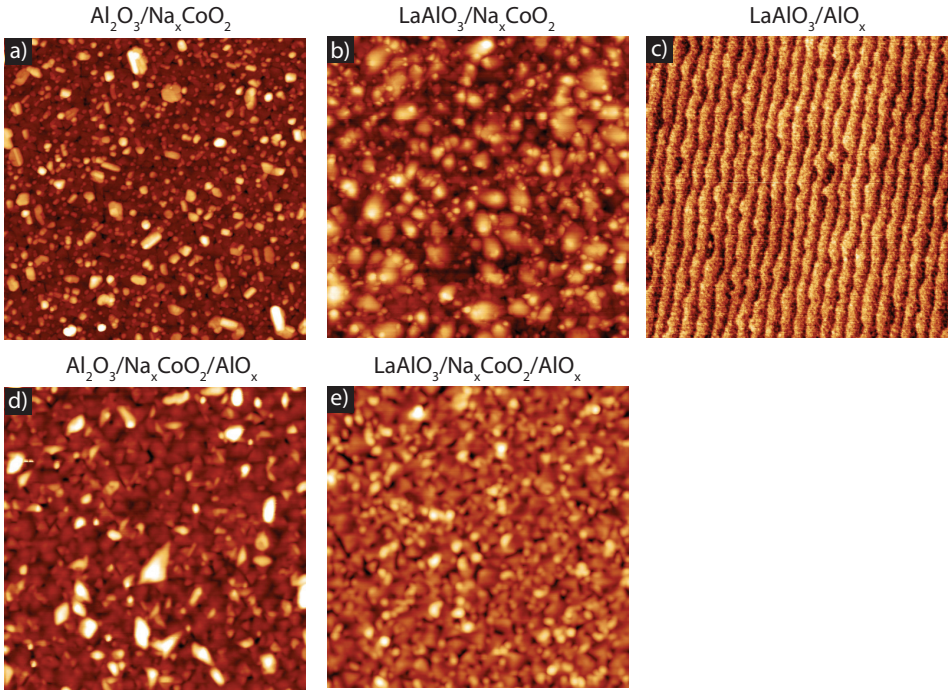

Figure 2.7: Atomic force microscopy images (3×3 μm^2) after growth of a 60 nm Na_xCoO_2 thin film on respectively Al_2O_3 and $LaAlO_3$ substrate (a and b) and after growth of a 80 nm amorphous AlO_x layer (c). Images d and e show the sample surface after growth of 60 nm Na_xCoO_2 and the *in-situ* deposition of an additional 80 nm amorphous AlO_x capping layer.

shown in Fig. 2.8b. Since the carrier densities of these samples are comparable, the change in resistivity is caused by variations in carrier mobility. This difference in carrier mobility can be explained by the crystallographic orientations of the grains within the thin films. Both samples have parallel alignment of the c-axis in all grains. Additionally, the sample deposited on the Al_2O_3 substrate possesses grains, which are also in-plane aligned with respect to each other, whereas for the sample deposited on the $LaAlO_3$ twinning is observed. This additional in-plane alignment for the sample deposited on Al_2O_3 leads to an enhanced carrier mobility, as electron scattering is reduced.

The observed metallic behavior down to low temperatures is in good agreement with previously reported single crystals. [1] However, previous studies reported values for room temperature resistivity of Na_xCoO_2 single crystals with a stoichiometry of x=0.8-0.95 between 1.5 and 22 mΩ·cm [5,27,28], while our thin films exhibit significantly lower values of 0.79 and 0.99 mΩ·cm for growth on respectively Al_2O_3 and $LaAlO_3$ substrates. Additionally, the measured Hall coefficient at room tem-

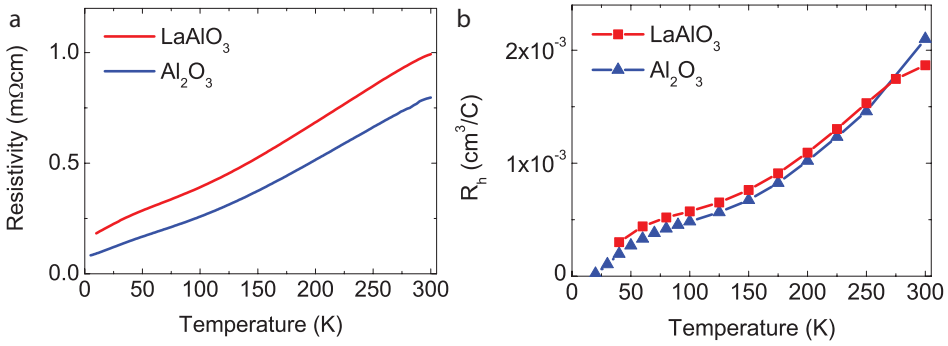

Figure 2.8: Temperature dependence of the resistivity and the Hall coefficient for AlO_x-capped Na_xCoO_2 thin films on Al_2O_3 (blue triangles) and $LaAlO_3$ (red squares) substrates.

perature of ∼0.002 cm^3/C for our thin films is more than 2 orders of magnitude smaller than values observed for $Na_{0.9}CoO_2$ single crystals [5]. Also a decrease of about a factor of 2 in carrier density at lower temperatures was reported for $Na_{0.9}CoO_2$ single crystals, in contrast to the observation of a suppression of more than one order of magnitude for our thin films.

Comparing the transport properties of our thin films with Na_xCoO_2 single crystals with different compositions, a remarkable similarity is observed for $Na_{0.68}CoO_2$ single crystals. [29] For these single crystals a comparable value for the Hall coefficient at room temperature is reported and in addition to this a strong suppression of the Hall coefficient is observed upon cooling. This is in good agreement with our observations and the observed temperature dependence of the Hall coefficient is discussed in more detail in Chapter 3. The observed room temperature resistivity of ∼0.8 mΩ·cm is also very similar to our thin films. These similarities suggest that our thin films have a composition close to $Na_{0.68}CoO_2$. This is supported by the XRD measurements, from which a c-axis lattice parameter of 1.1 nm was obtained. Comparing this lattice parameter with single crystal samples, where a strong dependence between the c-axis lattice parameter and the sodium to cobalt ratio was found, [13–15] an expected composition of approximately $Na_{0.64}CoO_2$ can be determined. [13] Combining the results from the structural and transport measurements, it can be concluded that the composition of our thin films is close to $Na_{0.7}CoO_2$.

The measured thermopower at room temperature is ∼45 μV/K and ∼69 μV/K for thin films grown on respectively Al_2O_3 and $LaAlO_3$ substrates, which is very similar to single crystals with a composition close to $Na_{0.71}CoO_2$, [28] see Table 2.1. These observations are in good agreement with the initial observation of the unusual combination of a high carrier density, low carrier mobility and high thermopower for single crystals of Na_xCoO_2. [1]

Table 2.1: Thermoelectric properties of Na_xCoO_2 thin films and single crystals (x=0.71) at 300 K.

	Al_2O_3	$LaAlO_3$	Single crystal [28]
Resistivity (mΩ·cm)	0.79	0.99	1
Thermopower (μV/K)	45	69	90
Power Factor (μW/K^{2}cm)	2.6	4.8	8.1
Thermal conductivity (W/mK)	4	4	8
ZT	0.01	0.03	0.03

A power factor of 2.6 and 4.8 μW/K^{2}cm is determined at room temperature for thin films on respectively Al_2O_3 and $LaAlO_3$ substrates. Even though based on these electronic measurements no ZT value can be calculated, an approximate value can be obtained by using an estimated value for the thermal conductivity of these thin films. For single crystals a thermal conductivity between 8 and 19 W/mK is reported [28,30,31], which can only be obtained in the case of highly controlled growth with a very low defect density. Therefore, it can be expected that the thermal conductivity in thin films is substantially lower than single crystal values. For an estimated thermal conductivity of 4 W/mK, ZT values of 0.01 and 0.03 are obtained at room temperature for thin films on respectively Al_2O_3 and $LaAlO_3$ substrates, which is in very good agreement with reports on $Na_{0.71}CoO_2$ single crystals, [28] as shown in Table 2.1.

2.4 Conclusions

In summary, we have developed a method to obtain single phase thin films of Na_xCoO_2 which are stable in ambient conditions, due to the *in situ* deposition of an amorphous AlO_x capping layer. These thin films can be deposited epitaxially on both hexagonal (Al_2O_3) as well as cubic ($LaAlO_3$) single crystal substrates.

The thin films remain metallic down to low temperatures, comparable to single crystals of Na_xCoO_2 and the Hall coefficient shows a strong suppression at low temperatures. This unusual temperature dependency is caused by the electronic correlation in Na_xCoO_2 and will be discussed in more detail in chapter 3. The room temperature electronic properties are approaching values of single crystals and a thermoelectric power factor up to 4.8 μW/K^{2}cm for the sample deposited on a $LaAlO_3$ substrate is observed, demonstrating the thermoelectric potential of these chemically stable thin films.

The presented work opens up new possibilities to study the intrinsic thermoelectric properties of Na_xCoO_2 in more detail, since now chemically stable thin films can be obtained by the addition of an amorphous AlO_x capping layer. Additionally, this approach can be used to study the possibility of structural engineering, for example by epitaxial strain, which is only possible in thin films. A more

detailed study of the structural as well as thermoelectric properties, leading to a significant enhancement of the thermoelectric properties by strain engineering, will be presented in chapter 3, where also measurements of the thermal conductivity of several thin films will be reported. Confinement effects of Na_xCoO_2 thin films are described in chapter 4, where the structural as well as thermoelectric properties are studied as a function of the layer thickness.

The development of chemically stable Na_xCoO_2 thin films also enables a study of high-temperature properties (structural as well as thermoelectric) of Na_xCoO_2 thin films. Because of enhanced reactivity of sodium at elevated temperatures, this was previously not possible. A study focusing on the high temperature stability, involving structural and thermoelectric measurements at elevated temperatures, is presented in chapter 5. To conclude, the development of an amorphous AlO_x capping layer, which stabilizes Na_xCoO_2 thin films in ambient conditions, enables more detailed studies of the thermoelectric properties of these thin films and could open up new ways to maximize their thermoelectric performance.

Bibliography

[1] I. Terasaki, Y. Sasago, and K. Uchinokura, "Large Thermoelectric Power in Na_xCoO_2 Single Crystals," *Physical Review B*, vol. 56, pp. R12685–R12687, 1997.

[2] R. Funahashi, I. Matsubara, H. Ikuta, T. Takeuchi, U. Mizutani, and S. Sodeoka, "An Oxide Single Crystal with High Thermoelectric Performance in Air," *Japanese Journal of Applied Physics*, vol. 39, pp. L1127–L1129, 2000.

[3] K. Fujita, T. Mochida, and K. Nakamura, "High-Temperature Thermoelectric Properties of $Na_xCoO_{2-\delta}$ Single Crystals," *Japanese Journal of Applied Physics*, vol. 40, pp. 4644–4647, 2001.

[4] T. Motohashi, E. Naujalis, R. Ueda, K. Isawa, M. Karppinen, and H. Yamauchi, "Simultaneously Enhanced Thermoelectric Power and Reduced Resistivity of Na_xCoO_2 by Controlling Na Nonstoichiometry," *Appl. Phys. Lett.*, vol. 79, pp. 1480–1482, 2001.

[5] M. Mikami, M. Yoshimura, Y. Mori, T. Sasaki, R. Funahashi, and M. Shikano, "Thermoelectric Properties of Two Na_xCoO_2 Crystallographic Phases," *Japanese Journal of Applied Physics*, vol. 42, pp. 7383–7386, 2003.

[6] M. Lee, L. Viciu, L. Li, Y. Wang, M. L. Foo, S. Watauchi, R. A. Pascal Jr., R. J. Cava, and N. P. Ong, "Large Enhancement of the Thermopower in Na_xCoO_2 at High Na Doping," *Nature Materials*, vol. 5, pp. 537–540, 2006.

[7] H. Zhou, X. P. Zhang, B. T. Xie, Y. S. Xiao, C. X. Yang, Y. J. He, and Y. G. Zhao, "Fabrication of Na_xCoO_2 Thin Films by Pulsed Laser Deposition," *Thin Solid Films*, vol. 497, pp. 338–340, 2006.

[8] X. P. Zhang, Y. S. Xiao, H. Zhou, B. T. Xie, C. X. Yang, and Y. G. Zhao, "Surface Morphology, Structure and Transport Property of Na_xCoO_2 Thin Films Grown by Pulsed Laser Deposition," *Materials Science Forum*, vol. 3807, pp. 475–479, 2005.

[9] J. Y. Son, B. G. Kim, and J. H. Cho, "Kinetically Controlled Thin-Film Growth of Layered β- and γ-Na_xCoO_2," *Applied Physics Letters*, vol. 86, p. 221918, 2005.

[10] Y. Krockenberger, I. Fritsch, G. Cristiani, A. Matveev, L. Alff, H. U. Habermeier, and B. Keimer, "Epitaxial Growth of Na_xCoO_2 Thin Films by Pulsed-Laser Deposition," *Applied Physics Letters*, vol. 86, p. 191913, 2005.

[11] A. Venimadhav, A. Soukiassian, D. A. Tenne, Q. Li, X. X. Xi, D. G. Schlom, R. Arroyave, Z. K. Liu, H. P. Sun, X. Pan, M. Lee, and N. P. Ong, "Structural and Transport Properties of Epitaxial Na_xCoO_2 Thin Films," *Applied Physics Letters*, vol. 87, p. 172104, 2005.

[12] L. Yu, L. Gu, Y. Wang, P. X. Zhang, and H. U. Habermeier, "Epitaxial Layered Cobaltite Na_xCoO_2 Thin Films Grown on Planar and Vicinal Cut Substrates," *Journal of Crystal Growth*, vol. 328, pp. 34–38, 2011.

[13] Q. Huang, M. L. Foo, R. A. Pascal Jr., J. W. Lynn, B. H. Toby, H. Tao, H. W. Zandbergen, and R. J. Cava, "Coupling Between Electronic and Structural Degrees of Freedom in the Triangular Lattice Conductor Na_xCoO_2," *Physical Review B*, vol. 70, pp. 134115–, 2004.

[14] R. Berthelot, D. Carlier, and C. Delmas, "Electrochemical Investigation of the P2-Na_xCoO_2 Phase Diagram," *Nature Materials*, vol. 10, pp. 74–80, 2011.

[15] L. Viciu, J. W. G. Bos, H. W. Zandbergen, Q. Huang, M. L. Foo, S. Ishiwata, A. P. Ramirez, M. Lee, N. P. Ong, and R. J. Cava, "Crystal Structure and Elementary Properties of Na_xCoO_2 (x=0.32, 0.51, 0.6, 0.75, and 0.92) in the Three-Layer $NaCoO_2$ Family," *Physical Review B*, vol. 73, p. 174104, 2006.

[16] Q. Li, Y. Zhang, and M. Xu, "Unconventional Magnetic Transition in Na_xCoO_2 ($x \geq 0.7$) Single Crystals," *Journal of Superconductivity and Novel Magnetism*, 2013.

[17] P. R. Wilmott and J. R. Huber, "Pulsed Laser Vaporization and Deposition," *Reviews of Modern Physics*, vol. 72, pp. 315–328, 2000.

[18] D. H. A. Blank, M. Dekkers, and G. Rijnders, "Pulsed laser deposition in Twente: from research tool towards industrial deposition," *Journal of Physics D: Applied Physics*, vol. 47, p. 034006, 2013.

[19] R. Eason, ed., *Pulsed Laser Deposition of Thin Films*. Wiley, New York, 2008.

[20] S. A. Hayward, F. D. Morrison, S. A. T. Redfern, E. K. H. Salje, J. F. Scott, K. S. Knight, S. Tarantino, A. M. Glazer, V. Shuvaeva, P. Daniel, M. Zhang, and M. A. Carpenter, "Transformation Processes in $LaAlO_3$: Neutron Diffraction, Dielectric, Thermal, Optical and Raman Studies," *Physical Review B*, vol. 72, no. 72, p. 054110, 2005.

[21] W. E. Lee and K. P. D. Lagerlof, "Structural and Electron Diffraction Data for Sapphire (α-Al_2O_3)," *Journal of Electron Microscopy Technique*, vol. 2, pp. 247–258, 1985.

[22] Y. Krockenberger, I. Fritsch, G. Christiani, H. U. Habermeier, L. Yu, C. Bernhard, B. Keimer, and L. Alff, "Superconductivity in Epitaxial Thin films of $Na_xCoO_2{\cdot}yD_2O$," *Applied Physics Letters*, vol. 88, p. 162501, 2006.

[23] D. P. Chen, H. C. Chen, A. Maljuk, A. Kulakov, H. Zhang, P. Lemmens, and C. T. Lin, "Single-Crystal Growth and Investigation of Na_xCoO_2 and $Na_xCoO_2{\cdot}yH_2O$," *Physical Review B*, vol. 70, p. 024506, 2004.

[24] K. Sugiura, H. Ohta, K. Nomura, M. Hirano, H. Hosono, and K. Koumoto, "Fabrication and Thermoelectric Properties of Layered Cobaltite, γ-$Sr_{0.32}Na_{0.21}CoO_2$ Epitaxial Films," *Applied Physics Letters*, vol. 88, p. 082109, 2006.

[25] S.-H. Kim, C.-E. Kim, and Y.-J. Oh, "Influence of Al_2O_3 Diffusion Barrier and $PbTiO_3$ Seed Layer on Microstructural and Ferroelectric Characteristics of PZT Thin Films by Sol-Gel Spin Coating Method," *Thin Solid Films*, vol. 305, pp. 312–326, 1997.

[26] F. Di Fonzo, D. Tonini, A. Li Bassi, C. S. Casari, M. G. Beghi, C. E. Bottani, D. Gastaldi, P. Vena, and R. Contro, "Growth Rregimes in Pulsed Laser Deposition of Aluminum Oxide Films," *Applied Physics A*, vol. 93, pp. 765–769, 2008.

[27] T. Ikeda and M. Onoda, "Structural and Electronic Properties of the Triangular Lattice System Na_xCoO_2," *Journal of Physics.: Condensed Matter*, vol. 18, pp. 8672–8682, 2006.

[28] M. Lee, L. Viciu, L. Li, Y. Wang, M. L. Foo, S. Watauchi, R. A. Pascal Jr., R. J. Cava, and N. P. Ong, "Enhancement of the Thermopower in Na_xCoO_2 in the Large-x Regime ($x \geq 0.75$)," *Physica B*, vol. 403, pp. 1564–1568, 2008.

[29] M. Lin Foo, Y. Wang, S. Watauchi, H. W. Zandbergen, T. He, R. J. Cava, and N. P. Ong, "Charge Ordering, Commensurability, and Metallicity in the Phase Diagram of the Layered Na_xCoO_2," *Physical Review Letters*, vol. 92, p. 247001, 2004.

[30] B. C. Sales, R. Jin, K. A. Affholter, P. Khalifah, G. M. Veith, and D. Mandrus, "Magnetic, Thermodynamic, and Transport Characterization of $Na_{0.75}CoO_2$ Single Crystals," *Physical Review B*, vol. 70, p. 174419, 2004.

[31] X. Tang and T. M. Tritt, "Overview of Thermoelectric Sodium Cobaltite: $Na_xCo_2O_4$," *Journal of the South Carolina Academy of Science*, vol. 6, pp. 10–13, 2008.

Chapter 3

Structural Engineering of Thermoelectric Na_xCoO_2 thin films

Abstract

The relation between the structural and thermoelectric properties in Na_xCoO_2 thin films is studied in this chapter. Using X-Ray diffraction and X-Ray photoelectron diffraction, it is shown that Na_xCoO_2 thin films can be grown epitaxially on hexagonal as well as cubic single-crystal substrates. By changing the cubic substrate material, the average grain size can be controlled and a reduction of the grain size results in a significant enhancement of the thermoelectric power factor. Additionally, in these structurally engineered thin films, the thermal conductivity is suppressed compared to Na_xCoO_2 single crystals. This demonstrates the thermoelectric potential of these structurally engineered Na_xCoO_2 thin films.

Part of the work discussed in this chapter is published in: Peter Brinks, Bouwe Kuiper, Eric Breckenfeld, Lane W. Martin, Guus Rijnders, Mark Huijben, "Enhanced Thermoelectric Power Factor of Na_xCoO_2 Thin Films by Structural Engineering", Advanced Energy Materials **4**, 1301927 (2014)

3.1 Introduction

Detailed thermoelectric characterization of Na_xCoO_2 thin films has been hindered by the chemical instability in ambient conditions, which reduced the interest and the amount of reports on Na_xCoO_2 thin films. [1] However, as described in Chapter 2 a recently developed method to obtain chemically stable, single-phase Na_xCoO_2 thin films by pulsed laser deposition, due to the *in-situ* deposition of an amorphous AlO_x capping layer, enables the study of the intrinsic properties of these thermoelectric thin films. [2]

Even though thermoelectric characterization was previously not possible, information about the structural properties of Na_xCoO_2 thin films can be found in previous reports. [1–12] In these reports, Na_xCoO_2 thin films are deposited on different substrate materials, and mostly characterized by X-Ray diffraction. In all reports an oriented growth in the (00l) direction is observed, which is in agreement with the observations described in Chapter 2. In addition to an out-of-plane orientation, it is also demonstrated, by performing ϕ scans, that those thin films can be grown epitaxially on Al_2O_3, $SrTiO_3$ and $LaAlO_3$, also in agreement with the observations described in Chapter 2.

However, because of the lack of thermoelectric characterization, it is difficult to compare the different studies and to understand the observed differences in structural properties. Several reports show electrical characterization, where mostly metallic [1–6, 8–11] but also insulating [4, 11] temperature dependent resistivity curves are reported. A transition from a metallic to an insulating temperature dependent resistivity is also reported after exposure to air of samples that were not chemically stable. [1] Because it is not mentioned in most reports if the thin films were chemically stable, it is difficult to compare the observed electrical properties, especially because of the altered behavior after exposure to air. In addition to this, there is also a relatively large spread in composition of the reported Na_xCoO_2 thin films, ranging from $Na_{0.5}CoO_2$ to $Na_{0.85}CoO_2$. Because of the strong dependence of the electronic properties on the sodium to cobalt ratio in Na_xCoO_2, these results cannot be compared directly. To understand the thermoelectric properties of Na_xCoO_2 thin films and to relate this to their structural properties, a systematic study using chemically stable thin films is required.

Making use of the method to deposit a capping layer, as described in Chapter 2, the intrinsic thermoelectric properties can now be studied in detail and related to their structural properties. In these thin films the structural properties can be uniquely controlled, by for example strain engineering, leading to promising options to enhance the thermoelectric properties of Na_xCoO_2 thin films. In this chapter a detailed study of the relation between the structural and thermoelectric properties of Na_xCoO_2 thin films is presented, where the first part aims at reducing the crystallinity by changing the deposition process. In the second part structural engineering is achieved by changing the substrate material. It is shown that this

has a strong influence on the crystallinity and the grain size of the Na_xCoO_2 thin films, demonstrating that the additional control of the structural properties in thin films, such as strain engineering, can be exploited in thermoelectric Na_xCoO_2 thin films to engineer the thermoelectric properties.

3.2 Results and Discussion

In this study structural engineering is applied as a tool to obtain improved control over the thermoelectric properties of Na_xCoO_2 thin films, which is unique for epitaxial thin films and cannot be obtained in single crystal or polycrystalline samples. To study this effect, Na_xCoO_2 thin films were grown by pulsed laser deposition (PLD) on various single crystal substrates and at different deposition pressures. All Na_xCoO_2 thin films were deposited under the same conditions from a sintered target with a composition of $Na_{0.9}CoO_2$, with the exception of the deposition pressure, and have a thickness of 60 nm. Optimized growth parameters were used as described in Chapter 2 and [2] and also the reported AlO_x capping layer has been used to prevent the formation of impurity phases and to ensure chemical stability of the fabricated thin films. Furthermore, all thin films have been cooled down after growth in 1 atm. of oxygen at a rate of 10°C/min to optimize the oxidation level. This will provide a similar oxygen stoichiometry in all thin films with a negligible amount of oxygen vacancies. Independent of the substrate material and structure, all thin films showed a preferred growth orientation with the (00l) direction parallel to the surface normal and no impurity phases were detected with X-Ray diffraction.

3.2.1 Controlling crystallinity by changing the growth process

In chapter 2 it was shown that the crystallinity of Na_xCoO_2 thin films does not strongly depend on the deposition temperature, and an optimum deposition temperature of 430°C was determined. However, the effect of oxygen deposition pressure on the crystallinity was not systematically studied yet. Here, we observe a significant decrease in crystallinity when the deposition pressure was reduced by one and two orders of magnitude from the previously reported value of 0.4 mbar [2] as shown in Fig. 3.1. Even though the crystallinity was significantly reduced for lower deposition pressures, the preferred crystallographic orientation was still observed and no impurity phases were detected, indicating that these samples are all single-phase and show a similar orientation. This is supported by temperature dependent resistivity measurements where it is observed that these thin films remain metallic down to low temperatures, irrespective of their deposition pressure, as shown in Fig. 3.2a. However, the observed reduction in crystallinity does result in a systematic increase of the room temperature electrical resistivity, as shown in

Fig. 3.2b. The room temperature Seebeck coefficient values for these thin films, also shown in Fig. 3.2, show a suppressed value for the sample with the strongly reduced crystallinity.

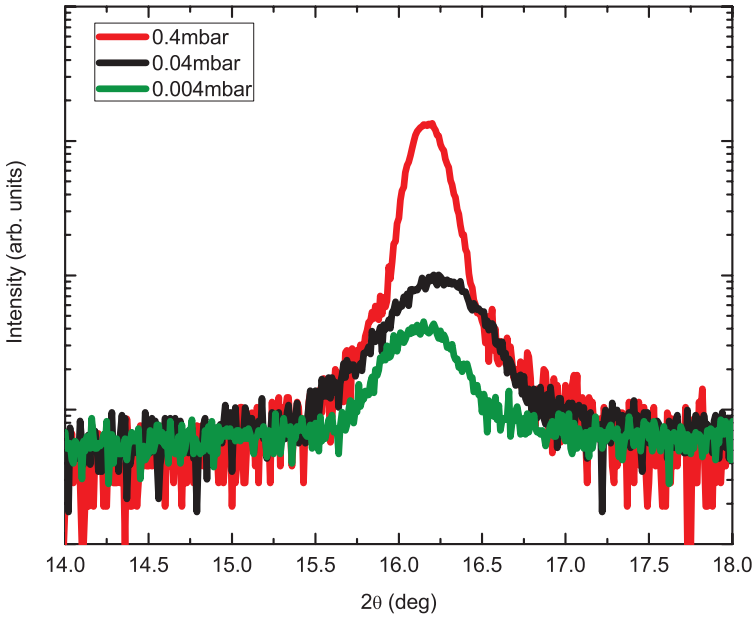

Figure 3.1: X-ray Diffraction spectrum of the (002) diffraction peak of Na_xCoO_2 thin films deposited at different oxygen pressure.

From the measurements of the resisitivity and the Seebeck coefficient the thermoelectric power factor at room temperature was calculated for these thin films as a function of deposition pressure, as shown in Fig. 3.3. A clear trend is observed that the thermoelectric power factor at room temperature is increasing with deposition pressure. Based on these results we can conclude that, although the deposition pressure can clearly be used to tune the crystallinity of these Na_xCoO_2 thin films, it will not provide the required enhanced control over the thermoelectric properties. Therefore the optimized deposition parameters [2] are used, which result in a combination of the optimum crystallinity and thermoelectric properties, as reflected by the highest thermoelectric power factor.

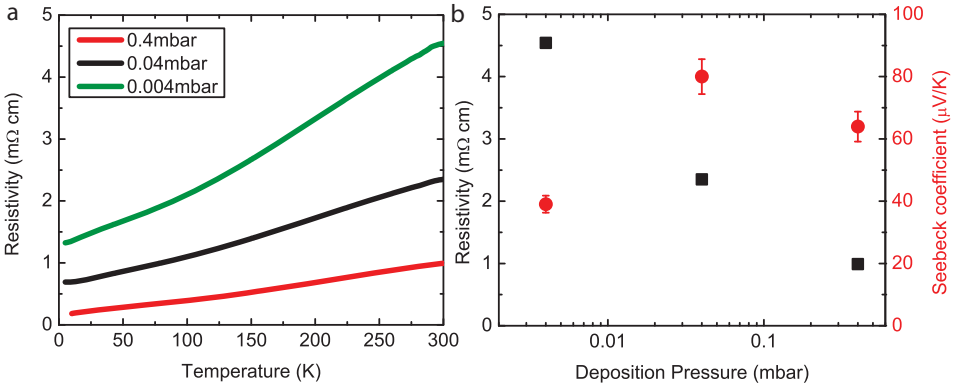

Figure 3.2: a) Temperature dependent resistivity measurements of Na_xCoO_2 thin films deposited at various deposition pressures. b) Electrical resistivity and Seebeck coefficient at room temperature for these samples as a function of deposition pressure.

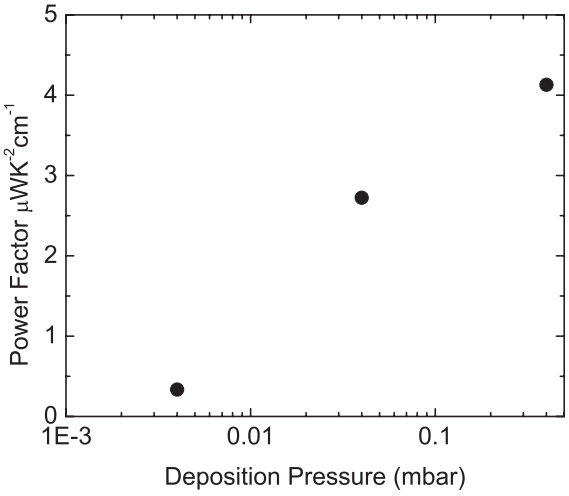

Figure 3.3: Thermoelectric power factor at room temperature for Na_xCoO_2 thin films deposited at various deposition pressures.

3.2.2 Structural Engineering by Changing the Substrate Material

To enable structural engineering of the Na_xCoO_2 thin films, various single crystal substrates have been used with a large variation in lattice parameters of their corresponding crystal structures. All substrates have been annealed to form low roughness surfaces with step-terrace structures exhibiting unit-cell height steps, as determined by atomic force microscopy (AFM) using a Bruker Dimension Icon, as shown in Fig. 3.4. Al_2O_3, MgO and $(LaAlO_3)_{0.3}(Sr_2AlTaO_6)_{0.7}$ (LSAT) were annealed at a temperature of 1050°C for respectively 1, 2 and 10 hours. $LaAlO_3$, $NdGaO_3$, $SrTiO_3$ and $DyScO_3$ were annealed at a temperature of 950°C for respectively 1, 2, 2 and 4 hours and $KTaO_3$ was annealed for 2 hours at a temperature of 500°C. These well defined and smooth surface morphologies form an ideal starting point for the growth of Na_xCoO_2 thin films and differences in structural (and thermoelectric) properties observed for films deposited on these different substrates will therefore not be caused by differences in surface roughness of the substrate, but rather by the differences in crystal structure and lattice parameters.

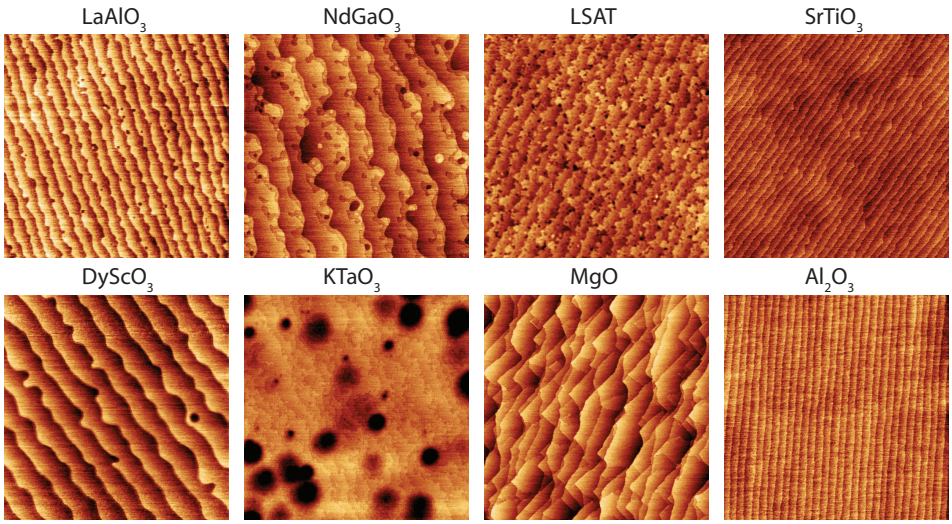

Figure 3.4: AFM images of substrates after annealing. All substrates, with the exception of $KTaO_3$ show a step and terrace surface morphology, with atomically smooth terraces and predominantly unit-cell step heights. The scan area for all images is 3x3 μm.

3.2.2.1 Structural Properties

In Fig. 3.5a the (002) Na_xCoO_2 diffraction peak is shown for thin films grown on different single crystal substrates. X-Ray diffraction measurements were performed with a Bruker D8 Discover and a Panalytical Xpert Pro MRD diffractometer. The

differences in peak height indicate changes of the crystallinity of the thin films depending on the substrate material. The highest crystallinity is observed for the $LaAlO_3$ substrate, as confirmed by the observed Kiessig fringes around the main peak. These Kiessig fringes can only be observed in the case of a highly ordered crystal structure with a well-defined thickness and sharp interfaces. Thin films deposited on $(LaAlO_3)_{0.3}(Sr_2AlTaO_6)_{0.7}$ (LSAT) substrates exhibit the smallest reduction of crystallinity, although an additional peak is observed. This double peak is present in several thin films and is investigated in more detail for the thin film on LSAT. A $2\theta/\omega$ map scan is shown in Fig. 3.5b for the Na_xCoO_2 thin film deposited on LSAT, which reveals the presence of a sharp peak and a diffuse peak, which is even more clearly visible in Fig. 3.5, where a rocking curve (ω scan) is shown. The 2θ position of the two peaks is similar, whereas for the ω position there is a small deviation, indicating that the two peaks are originating from crystalline parts with the same lattice constant but a small tilt angle with respect to each other. This behavior is indicative for the formation of misfit dislocations in heteroepitaxial systems with a relatively large lattice mismatch as previously reported for different thin films and superlattice systems. [13] A relation between the c-axis length of the crystal structure and the sodium concentration has been proposed for single crystal samples, where a shortening of the c-axis indicates a higher sodium concentration in the unit cell. [9, 10, 14–16] Because both observed peaks correspond to one c-axis lattice constant, these measurements indicate that the formation of misfit dislocations depends on the choice of substrate material and that the composition of the samples remains similar and is approximately $Na_{0.67}CoO_2$. [15] This is supported by *in-situ* X-Ray Photoelectron Spectroscopy (XPS) measurements (not shown), which show the same sodium to cobalt ratio for samples deposited on Al_2O_3, $LaAlO_3$ and LSAT substrates.

Previous studies have reported the growth of Na_xCoO_2 thin films on hexagonal (0001) Al_2O_3 as well as on cubic (001) $LaAlO_3$ and (001) $SrTiO_3$ single crystal substrates. [1–7] However, limited information is available on the crystalline ordering between the thin films and the underlying substrate. The weak in-plane ordering of the thin films on various substrates hampered detailed characterization by XRD. Therefore *in-situ* X-Ray Photoelectron Diffraction (XPD) experiments were performed to obtain additional in-plane structural information. XPD measurements were performed on an Omicron Nanotechnology XPS system, using a rotating sample setup with a fixed angle between the monochromatic Al Kα X-Ray source and the detector. XPD provides element specific and surface sensitive information on the intrinsic crystal ordering of the Na_xCoO_2 surface. Stereographic projections of the oxygen 1s core level intensity maps are shown in Fig. 3.6a. XPD measurements were done *in-situ* using 60 nm Na_xCoO_2 thin films deposited on Al_2O_3, $LaAlO_3$ and LSAT substrates, without a capping layer.

Strong in-plane ordering is confirmed for the growth of the hexagonal Na_xCoO_2 crystal structure on the hexagonal Al_2O_3 substrate. Clear 6-fold symmetry is ob-

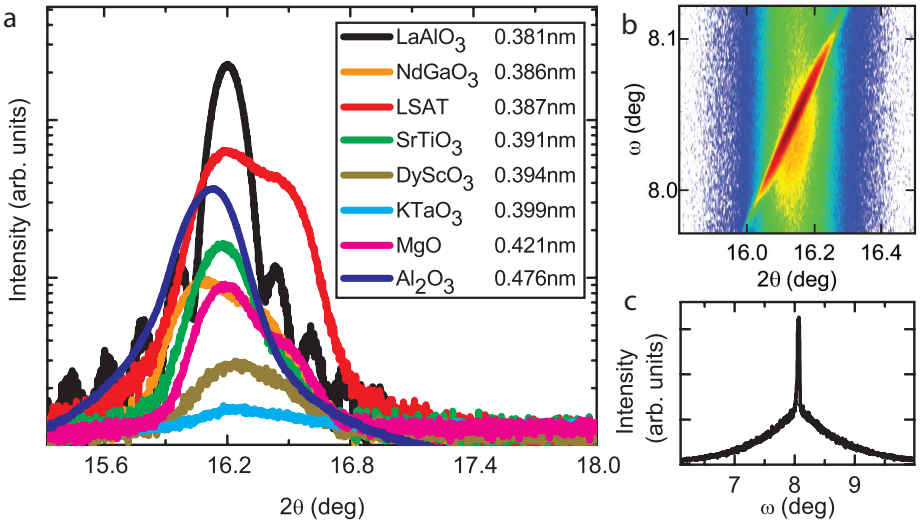

Figure 3.5: a) X-ray Diffraction spectrum of the (002) diffraction peak of Na_xCoO_2 thin films deposited on different single crystal substrates. The corresponding lattice parameters of the substrates are indicated as well. b) 2θ vs. ω map scan of the Na_xCoO_2 (002) diffraction peak for a thin film deposited on LSAT. This scan reveals the presence of a sharp and diffuse peak at the same 2θ angle and a small shift in ω angle. c) Rocking curve (ω scan) through the center of the peak at a 2θ value of 16.1°, showing the presence of a combination of a diffuse and a sharp peak.

served, which is in good agreement with previous reports based on XRD measurements. [2, 4, 6, 7] For the thin films grown on cubic $LaAlO_3$ and LSAT substrates 12-fold symmetry is observed, suggesting two possible orientations in which the 6-fold symmetric Na_xCoO_2 is oriented. These variations in in-plane symmetries can be clearly observed in the additional phi-scans, see Fig. 3.6c. Based on the peak positions and additional information from XRD measurements regarding the in-plane substrate orientation, the in-plane crystallographic ordering of the Na_xCoO_2 thin films on the different substrates was determined. This is schematically shown in Fig. 3.6b, where it should be noted that for cubic substrates the Na_xCoO_2 a-axis can be rotated by 15° in either direction, as compared to the a-axis of the substrate. Based on these measurements it is concluded that the growth of Na_xCoO_2 thin films is crystallographically ordered on cubic as well as hexagonal substrates, however, different levels of crystallinity are achieved. When these Na_xCoO_2 thin films are grown on different (pseudo)cubic substrates, the level of crystal ordering in the thin films will be dependent on the lattice parameter of the substrate. It is expected that the variation in crystal ordering has a strong influence on the electronic and thermal properties of the thin films. Therefore, this method of structural engineering provides a direct control of the thermoelectric properties.

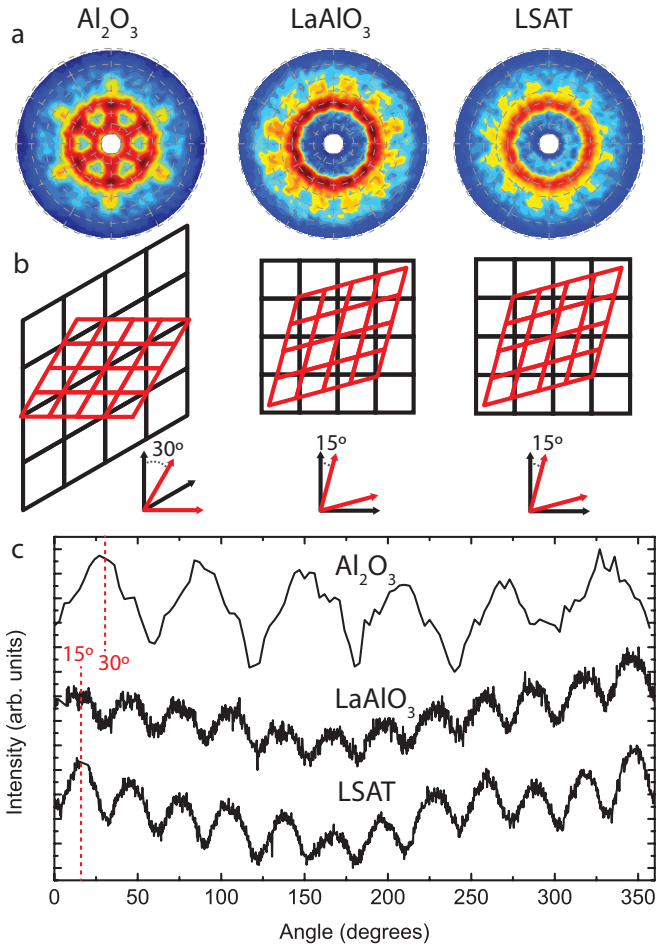

Figure 3.6: a) Oxygen 1s X-Ray Photoelectron Diffraction intensity maps of Na_xCoO_2 thin films deposited on Al_2O_3, $LaAlO_3$ and LSAT single crystal substrates. b) Schematic representation of the in-plane ordering of the crystal structure of Na_xCoO_2 thin film on the specific substrate. The substrate and film structures are shown in respectively black and red. c) Phi-scan at the peak position of the XPD map, revealing in-plane 6 or 12-fold symmetry of the Na_xCoO_2 thin films.

3.2.2.2 Thermoelectric properties

The dependence of the electronic and thermal properties of the Na_xCoO_2 thin films on the structural control by choice of single crystal substrate has been studied in detail. The resistivity as a function of temperature for various Na_xCoO_2 thin films is shown in Fig. 3.7a. These measurements were done in a Van der Pauw configuration with gold contacts, which were sputtered on the corners of the sample corners of the sample, using a Quantum Design PPMS system. It can be clearly observed that all thin films show metallic behavior down to low temperatures, indicating the minimal effect of the strongly suppressed crystallinity (see Fig. 3.5) on the electronic properties. The electrical conductivity and Seebeck coefficient for these thin films at room temperature are shown in Fig. 3.7c as a function of the substrate crystal lattice parameter. The room temperature measurements of the Seebeck coefficient were performed on a custom setup with an accuracy of 7% as determined with a Bi_2Te_3 reference sample (SRM3451) from the National Institute of Standards and Technology (NIST) [17]. Although no clear trend is visible for the electrical conductivity as a function of substrate lattice parameter, the highest electrical conductivity is observed in thin films with the highest crystallinity on substrates of Al_2O_3, $LaAlO_3$ and LSAT.

From Hall measurements in a Van der Pauw geometry a constant carrier density in all thin films in the range between 1.9 and 3.3×10^{21} cm^{-3} was determined at room temperature by fitting to a single band model. Therefore, at room temperature the substrate dependence on the variation in electrical conductivity in the Na_xCoO_2 thin films is dominated by the carrier mobility, which is determined by the crystallinity, or defect density, strongly affecting the scattering processes. We observe a linear increase of the Hall resistance as a function of temperature between 150 and 300 K, as is shown in Fig. 3.7b. This is in good agreement with previous observations in single crystals [18] and thin films [2] and with theoretical predictions based on the t-J model, which take the strong electron correlations in Na_xCoO_2 into account as well as the two-dimensional nature of the triangular CoO_2 layers. [19, 20] These models predict a relatively constant Hall resistance in the low temperature regime and a linear increase of the Hall resistance in the high temperature regime. For our thin films we observe in addition to this linear increase at high temperature, a relatively constant Hall resistance below 150 K, consistent with the models. For thin films on Al_2O_3, $LaAlO_3$ and LSAT, we see a different behavior below 50 K, which resembles the observations in single crystals, in which even a change of sign for the Hall resistance is observed at the transition from the paramagnetic to the antiferromagnetic stage (T_n=21 K in single crystals). [18] We do not observe a change of sign, indicating that in our thin films the Néel temperature is significantly lowered because of the reduction in crystalline ordering as compared to single crystals.

The specific choice of a LSAT substrate showed the smallest decrease in crys-

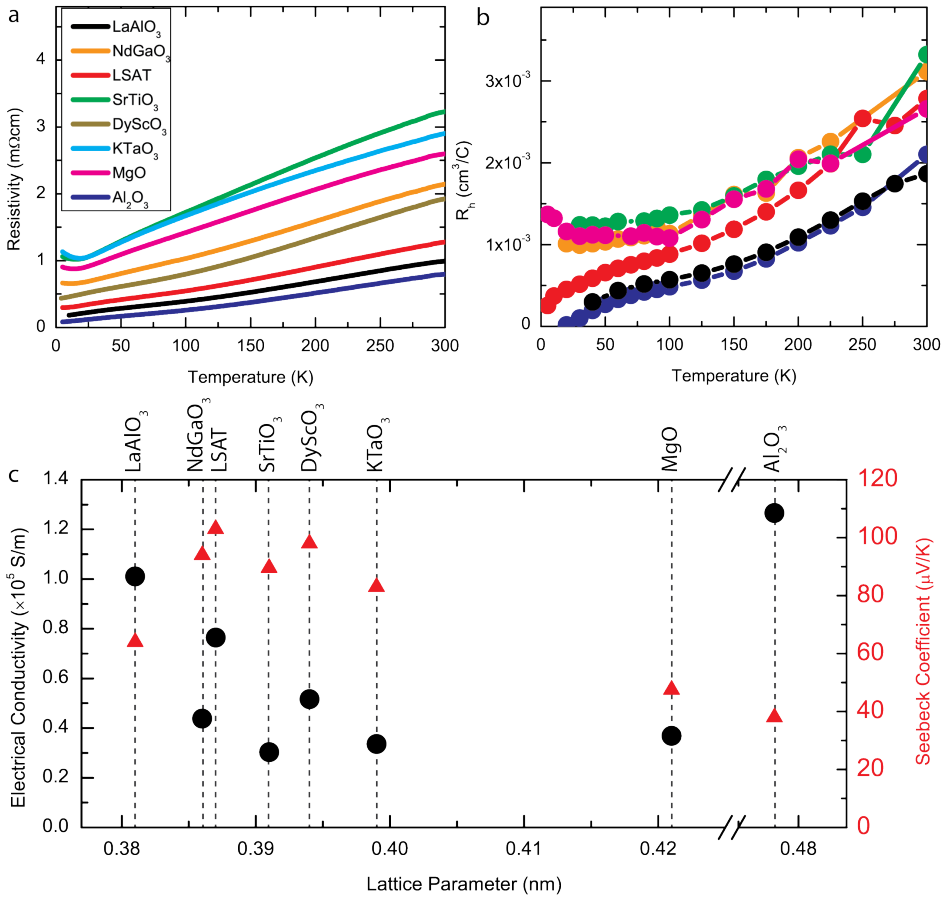

Figure 3.7: a) Resistivity as a function of temperature for Na_xCoO_2 thin films deposited on different substrates, showing metallic behaviour down to low temperatures for all samples. b) Corresponding temperature dependent Hall resistance values. c) Room temperature conductivity and Seebeck coefficient for these thin films as a function of substrate lattice parameter

tallinity as compared to a thin film on a $LaAlO_3$ substrate. However, a significant enhancement of the Seebeck coefficient to values above 100 μV/K was observed, as shown in Fig. 3.7c, as compared to the previously reported value of about 70 μV/K. [2] As the difference in substrate lattice parameter does not provide a direct connection between crystal structure and enhancement of the Seebeck coefficient, the thin films have been characterized by AFM (Fig. 3.8). It is apparent that the thin films have an increased surface roughness of 4-7 nm from the original substrate surfaces (Fig. 3.4) and exhibit a grainy surface structure. The surface morphology of the thin films is depending on the used substrate material.

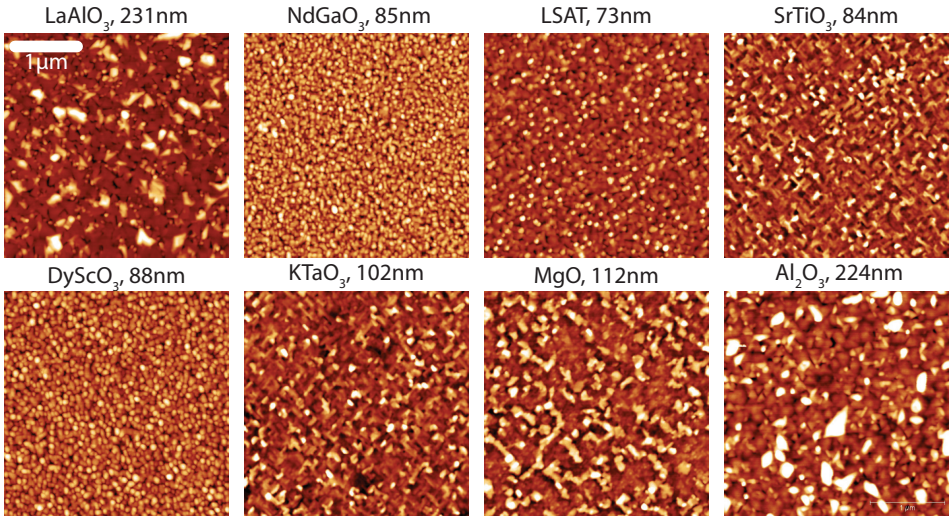

Figure 3.8: AFM images of capped Na_xCoO_2 thin films on various single crystal substrates, scan sizes 3x3μm. The average in-plane grain size, based on a FFT spectrum of the AFM images, is given as well.

The average in-plane grain size is determined from Fast Fourier Transformation (FFT) spectra of the AFM images, see Fig. 3.8. The values are calculated from the Full Width at Half Maximum (FWHM) values of these FFT spectra. These measurements show that, in addition to controlling the crystallinity, the grain size (microstructure) of these thin films can be controlled by changing the substrate material, enabling structural engineering of the Na_xCoO_2 thin films. The effect of variation in grain size on the Seebeck coefficient of the Na_xCoO_2 thin films is shown in Fig. 3.9. It can be clearly seen that for thin films with a reduced grain size the Seebeck coefficient is significantly enhanced. This is in good agreement with reports of PbTe polycrystalline samples with a small grain size. [21] In these PbTe systems the enhancement of the Seebeck coefficient is suggested to be caused by carrier trapping in the grain boundaries. [22]

These newly engineered Na_xCoO_2 thin films with reduced grain sizes provide an optimal combination of thermoelectric properties, as the thin film with the smallest grain size only shows a minor reduction in crystallinity and, therefore, only a slight reduction of the electrical conductivity. Together with an enhanced Seebeck coefficient, this controlled structural engineering provides a promising direction for new thermoelectric materials. The combined results of the electrical conductivity and the Seebeck coefficient are shown in Fig. 3.10 where the thermoelectric power factor is plotted as a function of substrate lattice parameter. A doubling in power factor to 8.1 $\mu WK^{-2}cm^{-1}$ can be observed for chemically stable Na_xCoO_2 thin films on LSAT substrates as compared to previously reported thin films on $LaAlO_3$

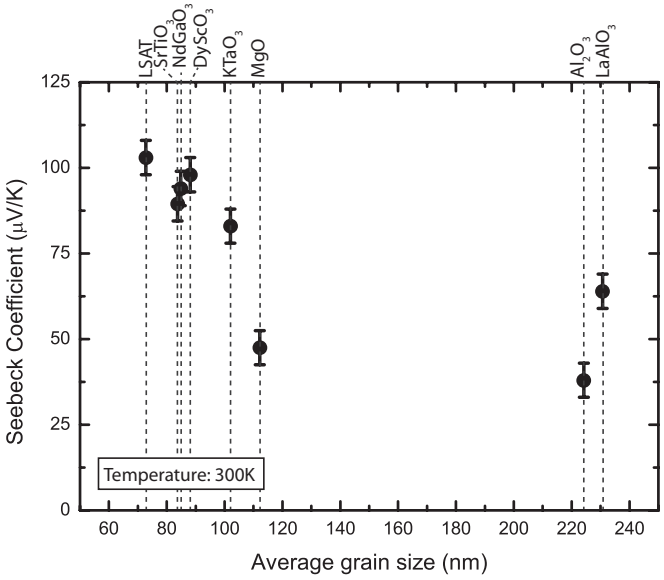

Figure 3.9: Room temperature Seebeck coefficient as a function of average in-plane grain size for Na_xCoO_2 thin films deposited on different single crystal substrates.

and Al_2O_3 substrates. [2, 6, 9] Although this electronic performance is still lower than in single crystal samples with power factors up to 24 $\mu WK^{-2}cm^{-1}$ at 300 K, [23, 24] our structurally engineered thin films outperform polycrystalline samples which have power factors of only 6.0 $\mu WK^{-2}cm^{-1}$. [23, 25]

To determine the effect of structural engineering on the thermal properties of the thin films, the thermal conductivity of several thin films was studied by time-domain-thermoreflectance measurements. The measurements were performed on a custom setup [26], which was verified for metals (high thermal conductivity) [27] and disordered thin films (low thermal conductivity) [28] and also compared with a well established 3ω setup [29]. This technique provides values for the thermal conductivity parallel to the surface normal (cross-plane). For 100 nm thick films of Na_xCoO_2 on $LaAlO_3$ and LSAT the obtained room temperature thermal conductivity is 1.4±0.1 W/mK for both samples, which is significantly lower than both single crystalline as well as polycrystalline samples for which values of respectively 5-19 W/mK [23,24,30] and about 2.0 W/mK [23,25] are reported at room temperature for samples with similar compositions. A similar suppression of the thermal conductivity for samples with reduced grain size is previously reported for PbTe. [21] This indicates that structural engineering also provides control over the thermal properties in addition to the control of the electronic properties. These results clearly show a significant enhancement in the thermoelectric properties, because of a simultaneous enhancement of the thermoelectric power factor and a

reduction of the thermal conductivity. It should however be taken into account that the thermal conductivity is measured parallel to the surface normal (cross-plane), whereas the electronic properties are measured perpendicular to the surface normal (in-plane) and that it is therefore not correct to calculate ZT values based on these measurements. It can be concluded that this structural engineering is a very promising approach to improve the thermoelectric properties of Na_xCoO_2 thin films by simultaneously controlling the electronic as well as thermal properties.

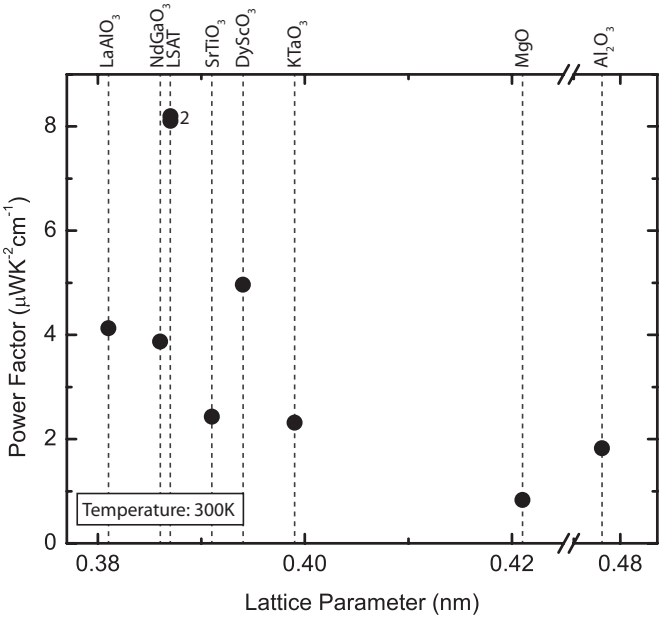

Figure 3.10: Power factor at 300 K of Na_xCoO_2 thin films deposited on different single crystal substrates. A dramatic enhancement in power factor is observed for thin films deposited on LSAT substrates. The number 2 indicates two samples with values too close to distinguish the individual symbols in the graph.

3.3 Conclusions

Na_xCoO_2 thin films with reduced crystallinity were deposited, by changing the oxygen pressure during deposition. Even though the crystallinity was suppressed, the preferred growth in the (00l) direction was similar for these thin films. For the samples with reduced crystallinity a significant and systematic increase of the electrical resistivity at room temperature was observed, whereas for the room temperature Seebeck coefficient no systematic changes were observed. These results indicate that compared to the Seebeck coefficient, the electrical resistivity is much more dependent on the crystalline quality. The resulting thermoelectric power factors show the highest value for the samples with the best crystallinity, indicating the importance to preserve or improve the crystalline quality in Na_xCoO_2 thin films to obtain enhanced thermoelectric properties.

The relation between structural and thermoelectric properties of Na_xCoO_2 thin films deposited on different single crystal substrates has been studied in detail. For these thin films we show that hexagonal Na_xCoO_2 thin films can be deposited on various cubic as well as hexagonal single crystal substrates, with the same preferred (00l) out of plane orientation and an epitaxial relation between the substrate and the thin film.

For the thin films deposited on cubic substrates that show a comparable crystalline quality as thin films deposited on hexagonal substrates, the electrical conductivity is preserved. However, for thin films with a suppressed crystallinity a significant reduction of the electrical conductivity is observed. This supports the previous observations that a good crystallinity is required to preserve the electronic properties of Na_xCoO_2 thin films. For all samples a comparable Hall coefficient is determined at room temperature, showing that the differences in electrical conductivity are dominated by changes of the carrier mobility. The Hall coefficient increases with temperature between 5 and 300K, which is caused by the electron correlations in Na_xCoO_2 and shows similar behavior as theoretically predicted. However, the influence of the ionic conductivity of Na_xCoO_2, making this also an interesting cathode material for battery applications [14], has to be determined in more detail to fully understand the observed differences in electronic properties.

Additionally, it is shown that by changing the cubic substrate material the in-plane average grain size can be reduced, leading to a significant enhancement of the Seebeck coefficient. The samples with preserved crystalline quality and a simultaneous reduction of the average grain size show a combination of a good electrical conductivity and an enhanced Seebeck coefficient, leading to a doubling of the thermoelectric power factor compared to samples with a larger grain size.

It is shown that by structural engineering, controlling crystallinity and grain size, in Na_xCoO_2 thin films, the electronic as well as thermal properties can be controlled. For the optimized Na_xCoO_2 thin films on LSAT substrates, a simultaneous doubling of the thermoelectric power factor and a strong suppression of

the thermal conductivity is achieved, leading to a dramatic enhancement of the overall thermoelectric properties of our Na_xCoO_2 thin films at room temperature. This demonstrates that the additional control of the structural properties, such as strain engineering, that can only be achieved in thin films, can be exploited in thermoelectric materials to obtain a significant improvement of the thermoelectric properties.

Bibliography

[1] H. Zhou, X. P. Zhang, B. T. Xie, Y. S. Xiao, C. X. Yang, Y. J. He, and Y. G. Zhao, "Fabrication of Na_xCoO_2 Thin Films by Pulsed Laser Deposition," *Thin Solid Films*, vol. 497, pp. 338–340, 2006.

[2] P. Brinks, H. Heijmerikx, T. A. Hendriks, G. Rijnders, and M. Huijben, "Achieving Chemical Stability in Na_xCoO_2 Thin Films," *RSC Advances*, vol. 2, pp. 6023–6027, 2012.

[3] L. Yu, L. Gu, Y. Wang, P. X. Zhang, and H. U. Habermeier, "Epitaxial Layered Cobaltite Na_xCoO_2 Thin Films Grown on Planar and Vicinal Cut Substrates," *Journal of Crystal Growth*, vol. 328, 2011.

[4] J. Y. Son, "Epitaxial Layered Cobaltite Na_xCoO_2 Thin Films: x=0.5, 0.7," *Journal of Physics D: Applied Physics*, vol. 41, p. 095405, 2008.

[5] Y. Krockenberger, I. Fritsch, G. Cristiani, A. Matveev, L. Alff, H. U. Habermeier, and B. Keimer, "Epitaxial Growth of Na_xCoO_2 Thin Films by Pulsed Laser Deposition," *Applied Physics Letters*, vol. 86, p. 191913, 2005.

[6] A. Venimadhav, A. Soukiassian, D. A. Tenne, Q. Li, X. X. Xi, D. G. Schlom, R. Arroyave, Z. K. Liu, H. P. Sun, P. Pan, Xiaoqing, M. Lee, and N. P. Ong, "Structural and Transport Properties of Epitaxial Na_xCoO_2 Thin Films," *Applied Physics Letters*, vol. 87, p. 172104, 2005.

[7] J. Y. Son, B. G. Kim, and J. H. Cho, "Kinetically Controlled Thin-Film Growth of Layered β- and γ-Na_xCoO_2 Cobaltate," *Applied Physics Letters*, vol. 86, p. 221918, 2005.

[8] L. Yu, Y. Krockenberger, I. Fritsch, and H. U. Habermeier, "Substrate-Induced Anisotropy of c-axis Textured Na_xCoO_2 thin Films," *Progress in Solid State Chemistry*, vol. 35, 2007.

[9] X. P. Zhang, Y. S. Xiao, H. Zhou, B. T. Xie, C. X. Yang, and Y. G. Zhao, "Surface Morphology, Structure and Transport Property of Na_xCoO_2 Thin Films Grown by Pulsed Laser Deposition," *Materals Science Forum*, vol. 3807, pp. 475–479, 2005.

[10] Y. Krockenberger, I. Fritsch, G. Christiani, H. U. Habermeier, L. Yu, C. Bernhard, B. Keimer, and L. Alff, "Superconductivity in Epitaxial Thin Films of $Na_xCoO_2{\cdot}yD_2O$," *Applied Physics Letters*, vol. 88, p. 162501, 2006.

[11] J. Y. Son, Y. H. Shin, and P. C. S, "Fabrication and Optical Conductivities of Strained Epitaxial Na_xCoO_2 Thin Films: x=0.5, 0.7," *Journal of Solid State Chemistry*, vol. 181, 2008.

[12] S. Hildebrandt, P. Komissinskiy, M. Major, W. Donner, and L. Alff, "Epitaxial Growth and Control of the Sodium Content in Na_xCoO_2 Thin Films," *Thin Solid Films*, vol. 545, 2013.

[13] V. M. Kaganer, R. Köhler, M. Schmidbauer, R. Opitz, and B. Jenichen, "X-Ray Diffraction Peaks due to Misfit Dislocations in Heteroepitaxial Structures," *Physical Review B*, vol. 55, 1997.

[14] R. Berthelot, D. Carlier, and C. Delmas, "Electrochemical Investigations of the p2-Na_xCoO_2 Phase Diagram," *Nature Materials*, vol. 10, p. 74, 2011.

[15] Q. Huang, M. L. Foo, R. A. Pascal, Jr., J. W. Lynn, B. H. Toby, T. He, H. W. Zandbergen, and R. J. Cava, "Coupling Between Electronic and Structural Degrees of Freedom in the Triangular Lattice Conductor Na_xCoO_2," *Physical Review B*, vol. 70, p. 184110, 2004.

[16] L. Viciu, J. W. G. Bos, H. W. Zandbergen, Q. Huang, M. L. Foo, S. Ishiwata, A. P. Ramirez, M. Lee, N. P. Ong, and R. J. Cava, "Crystal Structure and Elementary Properties of Na_xCoO_2 (x=0.32, 0.51, 0.6, 0.75 and 0.92) in the Three-Layer $NaCoO_2$ Family," *Physical Review B*, vol. 73, p. 174104, 2006.

[17] N. D. Lowhorn, W. Wong-Ng, Z. Q. Lu, E. Thomas, M. Otani, M. Green, N. Dilley, J. Sharp, and T. N. Tran, "Development of a Seebeck Coefficient Standard Reference Material," *Applied Physics A*, vol. 96, pp. 511–514, 2009.

[18] P. Mandal and P. Choudhury, "Hall Effect in the Metallic Antiferromagnet Na_xCoO_2 ($0.72 \leq x \leq 0.9$)," *Physical Review B*, vol. 86, 2012.

[19] B. S. Shastry, "Electrothermal Transport Coefficients at Finite Frequencies," *Reports on Progress in Physics*, vol. 72, 2008.

[20] W. Koshibae, A. Oguri, and S. Maekawa, "Hall Effect in CoO_2 Layers with a Hexagonal Structure," *Physical Review B*, vol. 75, 2007.

[21] K. Kishimoto and T. Koyanagi, "Preparation of Sintered Degenerate n-Type PbTe with a Small Grain Size and its Thermoelectric Properties," *Journal of Applied Physics*, vol. 92, p. 2544, 2002.

[22] J. Martin, L. Wang, L. Chen, and G. S. Nolas, "Enhanced Seebeck Coefficient through Energy-Barrier Scattering in PbTe Nanocomposites," *Physical Review B*, vol. 79, p. 115311, 2009.

[23] K. Fujita, T. Mochida, and K. Nakamura, "High-Temperature Thermoelectric Properties of $Na_xCoO_{2-\delta}$ Single Crystals," *Japanese Journal of Applied Physics*, vol. 40, pp. 4644–4647, 2001.

[24] B. C. Sales, R. Jin, K. A. Affholter, P. Khalifah, G. M. Veith, and D. Mandrus, "Magnetic, Thermodynamic, and Transport Characterization of $Na_{0.75}CoO_2$ Single Crystals," *Physical Review B*, vol. 70, p. 174419, 2004.

[25] K. Takahata, Y. Iguchi, D. Tanaka, T. Itoh, and I. Terasaki, "Low thermal Conductivity of the Layered Oxide (Na,Ca)Co_2O_4: Another Example of a Phonon Glass and an Electron Crystal," *Physical Review B*, vol. 61, p. 12551, 2000.

[26] D. G. Cahill, W. K. Ford, K. E. Goodson, G. D. Mahan, A. Majumdar, J. Maris, Humphrey, R. Merlin, and S. R. Phillpot, "Nanoscale Thermal Transport," *Journal of Applied Physics*, vol. 93, 2003.

[27] J. C. Zhao, X. Zheng, and D. G. Cahill, "High-Throughput Diffusion Multiples," *Materials Today*, vol. 8, 2005.

[28] C. Chiritescu, D. G. Cahill, N. Ngoc, D. Johnson, A. Bodapati, P. Keblinski, and P. Zschack, "Ultralow Thermal Conductivity in Disordered, Layered WSe_2 Crystals," *Science*, vol. 315, 2007.

[29] Y. K. Koh, S. L. Singer, W. Kim, J. M. O. Zide, H. Lu, D. G. Cahill, A. Majumdar, and A. C. Gossard, "Comparison of the 3ω Method and Time-Domain Thermoreflectance for Measurements of the Cross-Plane Thermal Conductivity of Epitaxial Ssemiconductors," *Journal of Applied Physics*, vol. 105, 2009.

[30] X. Tang, K. Aaron, J. He, and T. M. Tritt, "Determination of In-Plane Thermal Conductivity of $Na_xCo_2O_4$ Single Crystals via a Parallel Thermal Conductance (PTC) Technique," *Physica Status Solidi. (a)*, vol. 205, pp. 1152–1156, 2008.

Chapter 4

Size Effects on the Thermoelectric Behavior of Na_xCoO_2 Thin Films

Abstract

The effect of confinement of Na_xCoO_2 into thin films is studied in this chapter. Na_xCoO_2 thin films with a thickness between 5 nm and 250 nm are studied to understand the effect of confinement on the structural and thermoelectric properties. For thin films with a thickness of 10 nm and more, misfit dislocations are formed, caused by the difference in lattice parameter and crystal structure between the hexagonal Na_xCoO_2 thin films and the cubic substrates. The electrical resistivity shows a sharp increase for thicknesses below 60 nm, in good agreement with theoretical models. However, for the Seebeck coefficient no trend as a function of layer thickness is observed, in contrast to the models which predict a suppression of the Seebeck coefficient for ultra-thin films. The observed behavior is promising for the use of such ultra-thin layers as building blocks in thermoelectric superlattice structures, because of the preservation of the thermoelectric properties in ultra-thin films.

Part of the work discussed in this chapter is also used in a manuscript: Peter Brinks, Guus Rijnders, Mark Huijben, "Size effects on thermoelectric behavior of ultrathin Na_xCoO_2 thin films", manuscript submitted

4.1 Introduction

For the successful application of cobaltates in thermoelectric energy converters further improvement of the thermoelectric properties is required. In Chapter 3 it is shown that enhanced thermoelectric properties can be achieved in Na_xCoO_2 by structural engineering of Na_xCoO_2 thin films, making these thin films promising thermoelectric candidate materials. The effect of confinement of Na_xCoO_2 into ultrathin films on the thermoelectric properties, has however not been studied in detail. This confinement of thermoelectric materials down to nanometer dimensions offers a promising method to further improve the thermoelectric properties, as previously shown for other materials systems when combined into superlattice structures. [1] To understand the overall effect of confinement on the thermoelectric performance, the influence of confinement on the electrical conductivity, the Seebeck coefficient and the thermal conductivity should be separately studied.

The thermal conductivity can be strongly influenced by confining materials into ultrathin films. If the layers are made sufficiently thin, enhanced phonon scattering at the interfaces will lead to a strong suppression of the thermal conductivity. These effects have been previously reported for other material systems, where a reduction of about one order of magnitude was achieved for the thermal conductivity at room temperature. [2, 3] Similar studies have not yet been reported for thermoelectric cobaltate thin films, however it has been shown (Chapter 3) that the thermal conductivity at room temperature can be significantly smaller than single crystal samples. [4]

Furthermore, because of enhanced electron scattering at surfaces in ultrathin films, a decrease in electrical conductivity is also expected, based on Fuchs-Sondheimer theory [5,6] and more specifically Tellier's model. [7] This model is experimentally verified for thermoelectric Bi_2Te_3 thin films, where a good agreement with Tellier's model was observed for polycrystalline thin films. [8,9] According to the models, the increase of the resistivity is dependent on the crystalline ordering of the thin films. The strongest effect is observed for polycrystalline samples, whereas in the limit of a single crystalline film the effect cannot be observed, because in single crystalline thin films all charge carriers are specularly scattered at the surface. Therefore, control over the structural quality in ultrathin films is imperative to maintain a high electrical conductivity in these thin films. A systematic study focusing on the structural as well as electronic properties is therefore required in order to understand the size effects on the electronic transport properties.

Besides the thickness dependent conductivity, also the Seebeck coefficient of thin films is predicted to change with layer thickness, according to Pichard's model, [10] which is an extension of the previously mentioned Tellier's model. [7] In addition to the crystalline ordering, this model also uses an energy dependent scattering term to describe the Seebeck coefficient. This model has been previously experimentally verified in thermoelectric Bi_2Te_3 thin films. [8,9] In analogy

to Tellier's model for the electrical conductivity, the amount of crystalline ordering also plays a determining role for the strength of the thickness dependency of the Seebeck coefficient. For single crystalline thin films the thickness dependency is expected to be reduced, because of the specular scattering of the charge carriers in these well ordered films.

As described above, the three relevant properties for thermoelectric materials are all expected to significantly change with the layer thickness. A systematic study focusing on the thickness dependence of these material properties is therefore required in order to reveal the thermoelectric potential of Na_xCoO_2 thin films. By combining this with a detailed study of the structural properties, the thermoelectric properties can be related to the structural properties as well as the proposed models. Such a study has been reported for the related cobaltate material $Bi_2Sr_2Co_2O_y$ [11], which does not show a metallic temperature dependent resistivity, in contrast to Na_xCoO_2. For very thin films an increased resistivity is reported which is in agreement with Tellier's model. However, the thermopower did not show a clear change as a function of the layer thickness, opposed to Pichard's model. The reported $Bi_2Sr_2Co_2O_y$ thin films were not grown epitaxially in contrast to the epitaxial Na_xCoO_2 thin films described in Chapter 3. Therefore they cannot be directly compared because of the dependence of the crystalline ordering on the size effects in these thin films. In this chapter, size effects in thermoelectric ultrathin Na_xCoO_2 films, with a thickness between 5 and 250 nm, are studied to determine the influence of the confinement on the thermoelectric properties.

It is expected that if preservation of the high crystalline ordering in these ultrathin films can be achieved, the electronic properties (electrical conductivity and Seebeck coefficient) will remain constant with layer thickness. Simultaneouly, because of enhanced phonon scattering in ultrathin films a significant suppression of the thermal conductivity is expected. Achieving such an improvement in thin films of Na_xCoO_2 will enable the use of these ultrathin films as building blocks in superlattice structures. A reduction of the thermal conductivity, by the additional interface scattering, has previously been reported for superlattices of tellurides and this resulted in a strong improvement of the ZT value. [1,12] The study presented in this chapter on size effects in Na_xCoO_2 thin films aims at understanding whether a similar approach could be used in cobaltate thin films.

4.2 Results and Discussion

To study size effects on the thermoelectric performance of Na_xCoO_2 thin films, the dependence of the film thickness, between 5 and 250 nm, was determined on the structural and thermoelectric properties. The thin films were deposited by Pulsed Laser Deposition (PLD) on single crystal $LaAlO_3$ (001) and LSAT (001) substrates (Crystec GmbH). The $LaAlO_3$ and LSAT substrates were annealed respectively

at 950°C for 1 hour and at 1050°C for 10 hours in an oxygen flow of 150 ml/min to exhibit smooth surfaces with clear unit-cell-height steps in atomic force microscopy. [4] The thin films were deposited in an oxygen background pressure of 0.4 mbar and at a substrate temperature of 430°C, while a sintered $Na_{0.9}CoO_2$ target was ablated with a laser fluence of 4 J/cm^2 and at a repetition rate of 1 Hz. After growth the thin films were slowly cooled to room temperature in 1 bar of oxygen at a rate of 10°C/min to optimize the oxidation level. In order to maintain the chemical stability of the thin films, an amorphous AlO_x capping layer was deposited in situ on top of the Na_xCoO_2 thin films. [13] More detailed information about the chemical stability, growth and characterization can be found in Chapters 2 and 3.

In order to verify the correct thermoelectric phase exhibiting metallic behavior, the resistivity as a function of temperature is measured using a Physical Property Measurement System (PPMS, Quantum Design). It can be clearly observed, in Fig. 4.1, that thin films with a strongly reduced layer thickness of 15 nm display similar metallicity as previously reported thin films [4] with thicknesses of 60 nm, indicating controlled electrical properties with preservation of the overall transport behavior irrespective of layer thickness and substrate material. This is supported by Hall measurements (not shown), which demonstrate a constant carrier density of 1-2×10^{21} cm^{-3}, calculated by a simple single band model, for all thin films at room temperature in combination with a constant carrier mobility of 1-2 cm^{2}V^{-1}s^{-1} in good agreement with previous reports. [4, 13]

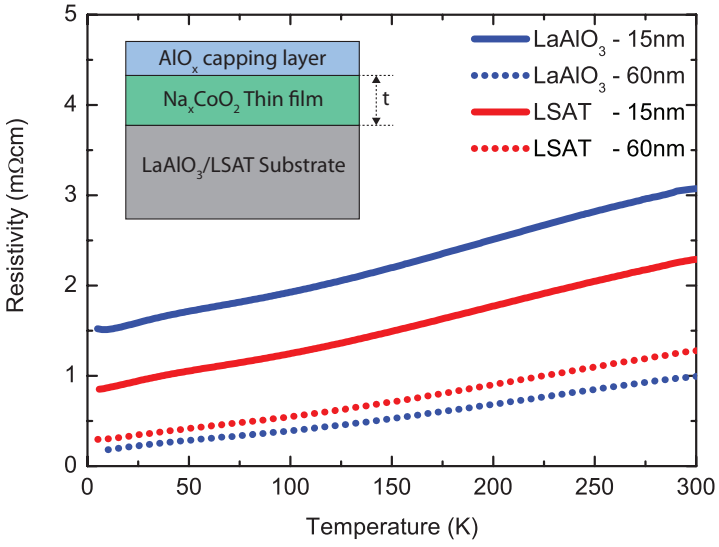

Figure 4.1: The temperature dependence of resistivity for Na_xCoO_2 thin films with varying thickness t deposited on $LaAlO_3$ (001) and LSAT (001) single crystal substrates.

The absence of impurity phases is confirmed by XRD, which is measured with a Panalytical XPert Pro MRD diffractometer. Only (00l) Na_xCoO_2 peaks for $2\theta/\omega$ scans between 10 and 110° are observed, indicating oriented growth with the c-axis perpendicular to the surface of the thin films. Detailed reciprocal space maps (RSM's) around the (002) Na_xCoO_2 diffraction peak are shown in Fig. 4.2 for thin films with varying thickness on both $LaAlO_3$ as well as LSAT substrates. For thin films deposited on both substrates clear structural differences are observed with varying layer thickness. For ultrathin films a sharp line is observed in the $2\theta/\omega$ direction, with only a very limited spread in the ω direction, which represents a crystalline phase with a very well defined orientation (tilt). The observed spread in $2\theta/\omega$ direction is a direct consequence of the finite thickness of the thin films. The presence of multiple peaks (sharp lines) for the thin films on $LaAlO_3$ is originating from the substrates, for which also several crystallographic domains are commonly observed. If the layer thickness is increased, a second peak with a significantly larger spread in the ω direction is appearing. This spread is caused by an increasing variation of tilt angles of the unit cell which is increasing with layer thickness. This is known to occur by the formation of misfit dislocations for thin films with a relatively large lattice mismatch with their substrate, as previously predicted and observed for different material systems [14, 15] as well as for Na_xCoO_2 thin films [4].

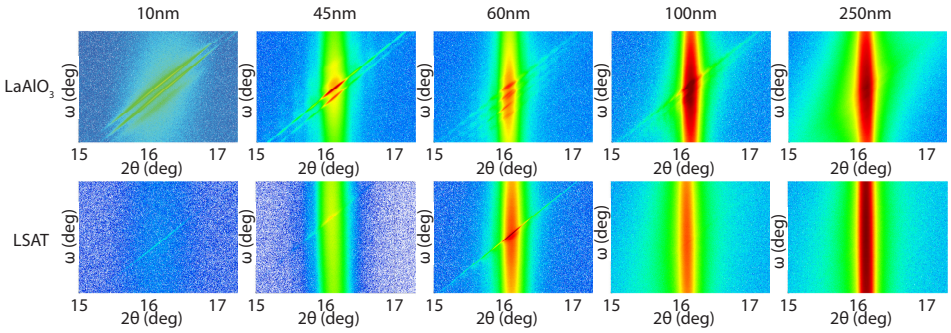

Figure 4.2: XRD RSM for Na_xCoO_2 thin films with varying layer thickness deposited on $LaAlO_3$ (top) and LSAT (bottom) single crystal substrates. Scans are made around the (002) Na_xCoO_2 diffraction peak. Color scale is linear and equal for all scans on the same substrate for comparison of the intensity distributions

The critical thickness at which misfit dislocations start to form is dependent on the lattice mismatch between the substrate and thin film [16–18] and is rather complicated for these thin films because of the difference in crystal symmetry between substrate and film in addition to the difference in lattice parameter. From Fig. 4.2, the critical thickness for the onset of misfit dislocations is estimated to be smaller than 10 nm for thin films deposited on $LaAlO_3$, whereas it is estimated to be around 10 nm for thin films deposited on LSAT.

It is clear from these RSM's that these two different diffraction peaks are originating from similar 2θ values, demonstrating that the lattice parameter remains the same. The c-axis lattice parameter in Na_xCoO_2 is previously reported to vary with the composition [19–23] and the observed value suggests a composition of $Na_{0.67}CoO_2$ for these thin films, [4, 19] irrespective of the layer thickness and the formation of misfit dislocations.

To study the structural properties in more detail, $2\theta/\omega$ scans and rocking curves (ω scans) of these thin films are shown in Fig. 4.3. In the rocking curves the presence of a diffuse and a sharp peak is confirmed and the ratio of the two different contributions can be clearly observed. It is seen that the diffuse peak is increasing rapidly and is becoming more significant with increasing thickness. This is especially clear for the samples on LSAT, where the sharp peak can no longer be observed for a thickness of 100 and 250 nm. This is a direct consequence of the increasing amount of volume of the sample which has a less defined orientation (tilt). Overall it is clear that the samples on $LaAlO_3$ are more crystalline, which can be best observed by comparing the thin films with a thickness of 10 nm, where for the sample on $LaAlO_3$ the peak is significantly more pronounced than for the sample on LSAT in the $2\theta/\omega$ as well as the rocking curve scans. Even though the crystallinity is reduced for the samples deposited on LSAT, it can be concluded that for very thin layers below the critical thickness for the onset of misfit dislocations, the layers have a significantly lower orientational spread.

Based on theoretical predictions, it is expected that by reducing the layer thickness of metallic thin films, surface scattering is enhanced, leading to a strong increase of the resistivity. Additionally, the Seebeck coefficient is expected to decrease for very thin layers. For both the resistivity ρ_f as well as the Seebeck coefficient S_f an inverse thickness dependence is expected based on Tellier's [7] and Pichard's [10] models:

$$\rho_f(t) = \rho_b(1 + \frac{3l_b}{8t}(1-p)) \tag{4.1}$$

$$S_f(t) = S_b(1 - \frac{3l_b}{8t}(1-p)\frac{U_b}{1+U_b}) \tag{4.2}$$

where ρ_b is the bulk resistivity, S_b is the bulk Seebeck coefficient, l_b the bulk electron mean free path, p the specularity parameter, U_b the energy-dependent scattering term and t the layer thickness. The appearance of this size effect is mainly dependent on the electron mean free path, which determines the thickness at which the resistivity starts to increase and the specularity parameter, p, which determines the strength of the effect. The value of p is a measure of the atomic order (crystallinity) of the thin films, which limits are zero for fully disordered polycrystalline thin films and 1 for perfect single crystalline epitaxial thin films. In the latter case no size effect can be observed.

The room temperature resistivity of Na_xCoO_2 thin films deposited on $LaAlO_3$ and LSAT substrates as a function of layer thickness is shown in Fig. 4.4. It

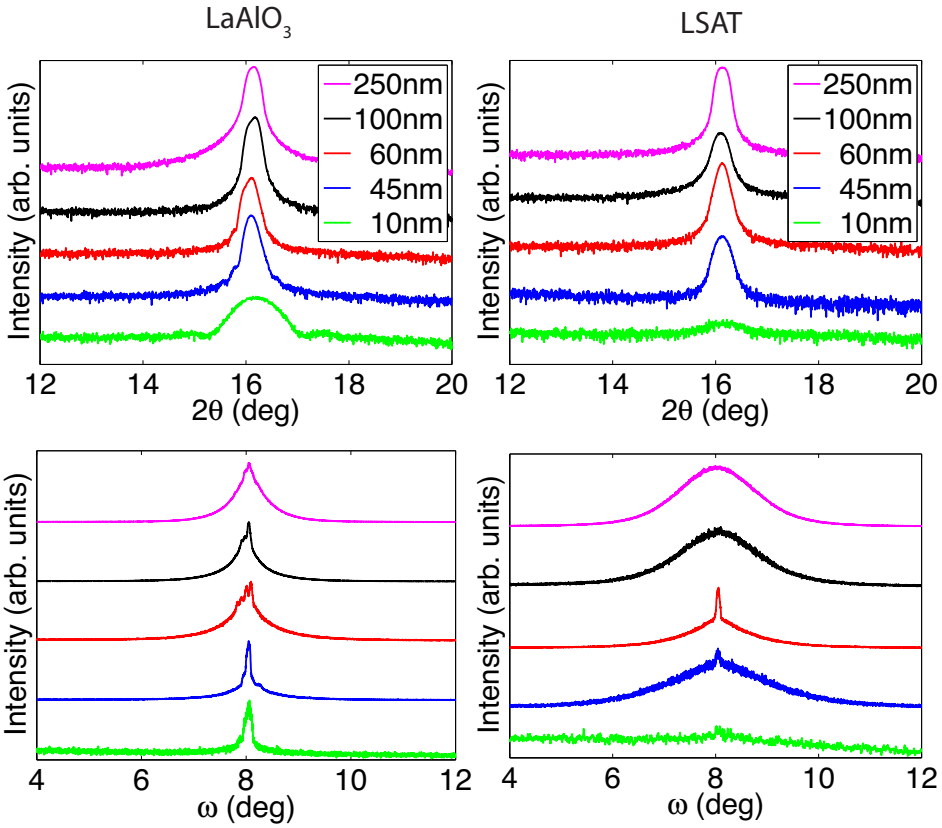

Figure 4.3: XRD scans around the (002) diffraction peak of Na_xCoO_2 thin films with varying layer thickness deposited on $LaAlO_3$ (left) and LSAT (right) single crystal substrates. The top figures show $2\theta/\omega$ scans for thin films deposited on respectively $LaAlO_3$ and LSAT substrates (scale is logarithmic). These curves are vertically shifted for clarity. Corresponding rocking curve scans for these samples are shown in the bottom images (scale is linear). The rocking curves are normalized and vertically shifted. Because of the small peak height of the 10 nm thin film on LSAT this curve was smoothened by a moving average filter.

can be clearly observed that the resistivity increases when the film thickness is reduced, as expected from Tellier's model. To obtain a good fit, the value of the bulk resistivity, ρ_b, is determined by averaging values for films above a thickness of 60 nm, while the value of the bulk mean free path, l_b, is determined from the slope of the resistivity versus 1/t and assuming the ideal case with p-value of zero. With these values of l_b and ρ_b, the complete data set was fitted to obtain the specularity parameter p. The resulting fits for the thin films on $LaAlO_3$ and LSAT are very comparable and the fit for the thin films on LSAT is shown in Fig. 4.4. The value obtained for the electron mean free path, l_b, of the fit is 56 nm, which is much larger than values calculated from the room temperature Hall measurements, which lead to an electron mean free path of only 0.7 nm based on a single band model with an effective electron mass of $5m_e$ [24] and assuming no electron correlations. However, even larger values up to 550 nm were reported for thermoelectric tellurides [8, 9]. It should however be taken into account that our Na_xCoO_2 thin films remain metallic down to low temperatures, in contrast to $Bi_2Sr_2Co_2O_y$ and the tellurides, since the used models are only valid for metallic thin films. Additionally, the value calculated from the Hall measurements is only an approximation, because the used single band model does not take the strong electron correlations (as mentioned in Chapter 3) in account, explaining the difference between the results from the model and the measurements. Using the obtained ρ_b and l_b values, the best fit is obtained for a specularity parameter, p, of 0.3, which is in good agreement with previous observations that these thin films on LSAT form an ordered structure for both out-of-plane and in-plane orientations but do not form a single-crystalline film. [4]

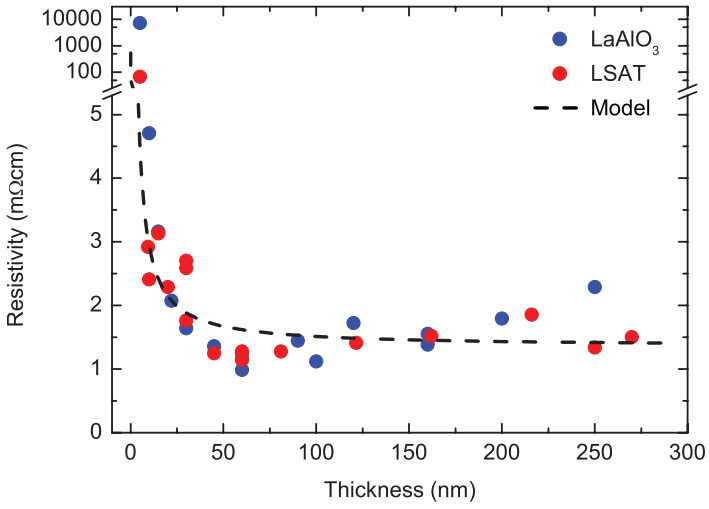

Figure 4.4: Room temperature resistivity as a function of Na_xCoO_2 layer thickness for thin films deposited on $LaAlO_3$ and LSAT single crystal substrates. Measurement errors remain within the symbol size. Dashed line is a fit based on Tellier's model.

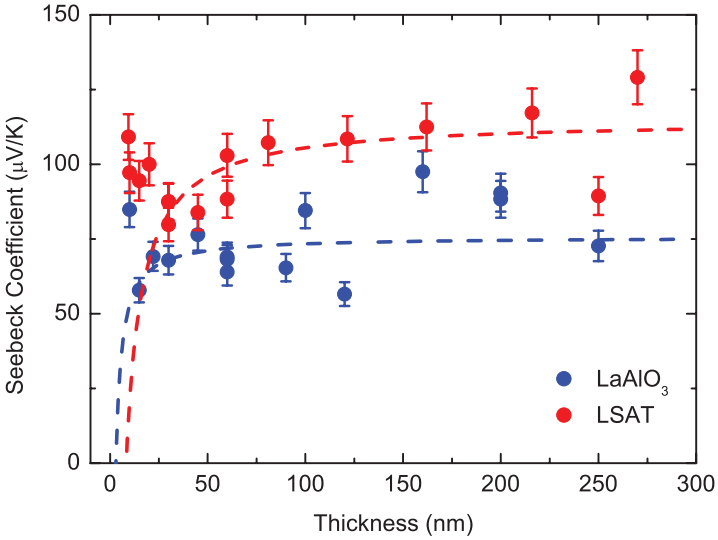

Figure 4.5: Room temperature Seebeck coefficient as a function of Na_xCoO_2 layer thickness for thin films deposited on $LaAlO_3$ and LSAT single crystal substrates. Measurement errors remain within the symbol size. Dashed lines are fits based on Pichard's model.

The Seebeck coefficient for Na_xCoO_2 thin films deposited on $LaAlO_3$ and LSAT substrates with varying layer thickness is shown in Fig. 4.5. The presented Seebeck measurements were performed using a custom built Seebeck measurement setup, verified with a NIST standard reference sample. [25] For both type of substrates fits to Pichard's model of the thickness dependent Seebeck coefficient are shown, based on the results of the fits for the corresponding resistivity data. The bulk Seebeck value S_b is determined by averaging values for films above a thickness of 60 nm. By fitting to Pichard's model the combined values for the bulk Seebeck coefficient and the initial resistivity fits, the energy dependent scattering term U_b can be determined. For thin films deposited on LSAT substrates a reasonable fit provides a value for U_b of approximately 1, which is much larger than that observed for Bi_2Te_3-based samples. [9] For ultrathin films down to a thickness of 10 nm a constant Seebeck coefficient of $\sim$100 μVK^{-1} is measured, in strong contrast to the predicted downturn in Seebeck coefficient according to the simple Pichard's model. Qualitatively comparable behavior is observed for thin films deposited on $LaAlO_3$ substrates. This behavior can be understood by realizing that the structural properties for ultrathin films are not comparable to thin films with a larger thickness. The increase of orientational spread in these thin films above the critical thickness lead to an enhanced carrier scattering, which is not taken into account by Tellier's and Pichard's models, in which structurally comparable films are assumed. Additionally, the strong electron correlations in Na_xCoO_2 should also be taken into

account to fully understand the transport behavior of these thin films, as previously described in Chapter 3. The strong electron correlations are proposed to play a determining role for the high Seebeck coefficient in Na_xCoO_2 [11, 26, 27]. Previous reports indicate that for thermoelectric cobaltates the Seebeck coefficient is not dependent on the scattering mechanism and remains constant for ultrathin films [11], in good agreement with our observations. These observations demonstrate again the importance of electron correlations in cobaltate thin films and show Na_xCoO_2 as a promising thermoelectric material, because of the preserved high Seebeck coefficient in ultrathin films.

4.3 Conclusions

The thickness dependence of structural and thermoelectric properties of Na_xCoO_2 thin films is studied. It is observed that thin films deposited on LSAT and $LaAlO_3$ single crystal substrates show metallic behavior between 5 and 300K. Based on XRD measurements it is concluded that the critical thickness for the formation of misfit dislocations is around and below 10 nm, for respectively LSAT and $LaAlO_3$ substrates, and can be explained by the difference in symmetry in addition to the relatively large lattice mismatch. Based on XRD measurements it is concluded that the stoichiometry of the thin films is $Na_{0.67}CoO_2$ and remains constant when the layer thickness or substrate material are changed.

We have observed an increasing resistivity for metallic Na_xCoO_2 thin films, deposited on $LaAlO_3$ as well as LSAT substrates, with a thickness lower than 60 nm, which is in accordance with theoretical predictions and previous observations for $Bi_2Sr_2Co_2O_y$ thin films. However, the Seebeck coefficient for these thin films remains constant, irrespective of layer thickness, which is a signature of the strong electron correlations in Na_xCoO_2.

This separate control over the resistivity and Seebeck coefficient is very promising for Na_xCoO_2 as a thermoelectric material, because the observed high Seebeck coefficient of ultrathin films enables the use of these thin films as thermoelectric material. Because the increase of the resistivity for ultrathin films remains limited, in combination with the constant Seebeck coefficient, these thin films are very promising candidates as basic building blocks in thermoelectric superlattices.

Bibliography

[1] R. Venkatasubramanian, E. Siivola, T. Colpitts, and B. O'Quinn, "Thin Film Thermoelectric Devices with High Room-Temperature Figures of Merit," *Nature*, vol. 413, 2001.

[2] M. S. Aubain and P. R. Bandaru, "In-Plane Thermal Conductivity Determination Through Thermoreflectance Analysis and Measurements," *Journal of Applied Physics*, vol. 110, 2011.

[3] M. Maldovan, "Micro to Nano Scale Thermal Energy Conduction in Semiconductor Thin Films," *Journal of Applied Physics*, vol. 110, 2011.

[4] P. Brinks, B. Kuiper, E. Breckenfeld, G. Koster, L. W. Martin, G. Rijnders, and M. Huijben, "Enhanced Thermoelectric Power Factor of Na_xCoO_2 Thin Films by Structural Engineering," *Advanced Energy Materials*, vol. 4, 2014.

[5] K. Fuchs, H. H. Wills, and N. F. Mott, "The Conductivity of Thin Metallic Films According to the Electron Theory of Metals," *Mathematical Proceedings of the Cambridge Philosophical Society*, vol. 34, 1938.

[6] E. H. Sondheimer, "The Mean Free Path of Electrons in Metals," *Advances in Physics*, vol. 1, 1952.

[7] C. R. Tellier, "A Theoretical Description of Grain Boundary Electron Scattering by an Effective Mean Free Path," *Thin Solid Films*, vol. 51, 1978.

[8] Z. Zeng, P. Yang, and Z. Hu, "Temperature and Size Effects on Electrical Properties and Thermoelectric Power of Bismuth Telluride Thin Films Deposited by Co-Sputtering," *Applied Surface Science*, vol. 268, 2013.

[9] K. W. Cho and I. H. Kim, "Thermoelectric Properties of the Flash-Evaporated n-type $Bi_2Te_{2.4}Se_{0.6}$ Thin Films," *Materials Letters*, vol. 59, 2005.

[10] C. R. Pichard, C. R. Tellier, and A. J. Tosser, "Thermoelectric Power of Thin Polycrystalline Metal Films in an Effective Mean Free Path Model," *Journal of Physics F: Metal Physics*, vol. 10, 1980.

[11] J. Ravichandran, A. K. Yadav, W. Siemons, M. A. McGuire, V. Wu, A. Vailionis, A. Majumdar, and R. Ramesh, "Size Effects on Thermoelectricity in a Strongly Correlated Oxide," *Physical Review B*, vol. 85, 2012.

[12] R. Venkatasubramanian, "Lattice Thermal Conductivity Reduction and Phonon Localizationlike Behavior in Superlattice Structures," *Physical Review B*, vol. 61, 2001.

[13] P. Brinks, H. Heijmerikx, T. A. Hendriks, G. Rijnders, and M. Huijben, "Achieving Chemical Stability in Thermoelectric Na_xCoO_2 Thin Films," *RSC Advances*, vol. 2, 2012.

[14] J. W. Matthews and A. E. Blakeslee, "Defects in Epitaxial Multilayers," *Journal of Crystal Growth*, vol. 27, 1974.

[15] V. M. Kaganer, R. Köhler, M. Schmidbauer, R. Opitz, and B. Jenichen, "X-ray Diffraction Peaks due to Misfit Dislocations in Heteroepitaxial Structures," *Physical Review B*, vol. 55, 1997.

[16] S. M. Hu, "Misfit Dislocations and Critical Thickness of Heteroepitaxy," *Journal of Applied Physics*, vol. 69, 1991.

[17] A. Braun, K. M. Briggs, and P. Böni, "Analytical Solution to Matthews' and Blakeslee's Critical Dislocation Formation Thickness of Epitaxially Grown Thin Films," *Journal of Crystal Growth*, vol. 241, 2002.

[18] D. C. Houghton, C. J. Gibbings, C. G. Tuppen, M. H. Lyons, and M. A. G. Halliwell, "Equilibrium critical thickness for $Si_{1-x}Ge_x$ strained layers on (100) Si," *Applied Physics Letters*, vol. 56, 1990.

[19] Q. Huang, M. L. Foo, R. A. Pascal, J. W. Lynn, B. H. Toby, T. He, H. W. Zandbergen, and R. J. Cava, "Coupling Between Electronic and Structural Degrees of Freedom in the Triangular Lattice Conductor Na_xCoO_2," *Physical Review B*, vol. 70, 2004.

[20] Y. Krockenberger, I. Fritsch, G. Christiani, H. U. Habermeier, L. Yu, C. Bernhard, B. Keimer, and L. Alff, "Superconductivity in Epitaxial Thin Films of $Na_xCoO_2{\cdot}yD_2O$," *Applied Physics Letters*, vol. 88, 2006.

[21] L. Viciu, J. W. G. Bos, H. W. Zandbergen, Q. Huang, M. L. Foo, S. Ishiwata, A. P. Ramirez, M. Lee, N. P. Ong, and R. J. Cava, "Crystal Structure and Elementary Properties of Na_xCoO_2 (x=0.32, 0.51, 0.6, 0.75, and 0.92) in the Three-Layer Family," *Physical Review B*, vol. 73, 2006.

[22] R. Berthelot, D. Carlier, and C. Delmas, "Electrochemical Investigation of the P2-Na_xCoO_2 Phase Diagram," *Nature Materials*, vol. 10, 2010.

[23] X. P. Zhang, Y. S. Xiao, H. Zhou, B. T. Xie, C. X. Yang, and Y. G. Zhao, "Surface Morphology, Structure and Transport Property of Na_xCoO_2 Thin Films Grown by Pulsed Laser Deposition," *Materials Science Forum*, vol. 3807, 2005.

[24] S. Lupi, M. Ortolani, and P. Calvani, "Optical Conductivity of Single Crystals of $Na_{0.57}CoO_2$," *Physical Review B*, vol. 69, 2004.

[25] N. D. Lowhorn, W. Wong-Ng, Z. Q. Lu, E. Thomas, M. Otani, M. Green, N. Dilley, J. Sharp, and T. N. Tran, "Development of a Seebeck Coefficient Standard Reference Material," *Applied Physics A*, vol. 96, 2009.

[26] W. Koshibae, A. Oguri, and S. Maekawa, "Hall Effect in CoO_2 Layers with a Hexagonal Structure," *Physical Review B*, vol. 75, 2007.

[27] B. S. Shastry, "Electrothermal Transport Coefficients at Finite Frequencies," *Reports on Progress in Physics*, vol. 72, 2009.

Chapter 5

High-Temperature Thermoelectric Potential of Cobaltate Thin Films

Abstract

The high-temperature thermoelectric properties of cobaltate thin films of Na_xCoO_2 and $Ca_3Co_4O_9$ are studied. These measurements are combined with temperature dependent X-ray diffraction measurements. By systematic cycling up to increasingly high temperatures and simultaneous electronic measurements during heating as well as cooling, it is shown that such electronic measurements are a much more sensitive tool to study the thermal stability of cobaltate thermoelectric thin films. Additionally, the sensitivity of these cobaltate thin films for the oxygen partial pressure during heating is demonstrated. A significant enhancement of the thermal stability is observed when the cobaltate thin films are heated in an oxygen-rich environment. For these thin films with enhanced thermal stability, a significant improvement of the thermoelectric properties at elevated temperatures is achieved compared to bulk samples.

Part of the work discussed in this chapter is also used in a manuscript: Peter Brinks et al., "High-temperature stability and thermoelectric properties of $Ca_3Co_4O_9$ thin films", manuscript in preparation

5.1 Introduction

In Chapters 2-4 the stability, structural properties, and size effects on the thermoelectric performance in thin films of Na_xCoO_2 have been discussed. These studies focussed on the room temperature properties of these thermoelectric Na_xCoO_2 thin films, although as discussed in Chapter 1, the promising regime of oxide thermoelectrics is at high-temperature. Previous reports have shown that the best thermoelectric behavior is obtained at approximately 550°C for single crystals of Na_xCoO_2. [1] At this temperature a maximum ZT value of 1.2 was obtained, which is a strong enhancement compared to the value of 0.03 which was obtained at room temperature.

Even though several previous studies of Na_xCoO_2 thin films have been reported, [2–13] very limited data about the high-temperature properties of these thin films is published. [14] Therefore, the focus of the first part of this chapter is the high-temperature stability and thermoelectric properties of Na_xCoO_2 thin films. Because of the presence of the volatile sodium, which already lead to stability problems in air at room temperature, as described in Chapter 2, not only the high-temperature properties are measured, but also the structural stability is studied. By combining these studies the high-temperature potential of these Na_xCoO_2 thin films will be revealed.

In analogy to Na_xCoO_2 single crystals, similar thermoelectric properties have been reported for $Ca_3Co_4O_9$ single crystals, where the ZT value increases up to approximately 1.2 at a temperature of 600°C. [15] This related compound does not contain the volatile sodium layers and is therefore expected to show a higher thermal stability. In the second part of this chapter the high-temperature stability of $Ca_3Co_4O_9$ thin films is studied and compared to bulk samples. This will demonstrate the potential of $Ca_3Co_4O_9$ thin films as thermoelectric materials.

The main focus of this chapter is to understand the high-temperature stability and thermoelectric behavior of cobaltate thin films. The structural as well as thermoelectric properties at high-temperature of the two related compounds Na_xCoO_2 and $Ca_3Co_4O_9$ are investigated. Because the stability of these materials at high-temperature has not been studied in detail previously, especially for thin films, this stability is first studied to understand if the obtained thermoelectric measurements reflect the intrinsic material properties, rather than that of unstable degrading samples. Previous reports have shown that the background gas in which these thermoelectric cobaltates are heated significantly influences the electronic properties. [16] This is a strong indication that structural changes, such as the formation of oxygen vacancies, occur during these thermal treatments and shows the importance of a controlled environment in which the measurements are performed. These effects can be directly studied by controlling the background gas, and more specifically the partial oxygen pressure, during the measurements at high-temperature. By analyzing the samples during heating as well as cooling

and by sequentially increasing the maximum temperature of the measurements, differences in stability are directly observed. To the best of our knowledge, such a systematic study has not been reported. These effects are studied in this chapter for cobaltate thin films, by temperature dependent electronic measurements at elevated temperatures with different background gases. This study will demonstrate the sensitivity of these cobaltate thin films to the environment when heated to elevated temperatures.

5.2 Experimental Section: High-Temperature Measurements

To study the high-temperature structural properties, XRD measurements at elevated temperatures are performed. The measurements are done on a Bruker D8 and a Panalytical XPert pro MRD diffractometer, equipped with an Anton Paar domed hot stage (THS-900). For the high-temperature XRD measurements described in this chapter, the samples were heated in air, providing a partial oxygen pressure of approximately 210 mbar.

High-temperature measurements of the electrical resistivity and Seebeck coefficient were performed using a Linseis LSR3-1100 system, equipped with a high-temperature furnace. In this system samples are vertically clamped in between two platinum electrodes, which serve as the current electrodes for the four-point resistivity measurements. Two additional probes, which are S-type thermocouples, are pressed on the surface and function as voltage probes, from which the resistivity values are calculated. For the Seebeck measurements, a temperature gradient in the sample is established by a heater element, which is thermally connected to the bottom electrode. To measure the local temperature as well as the voltage difference on the sample, which is required to calculate the Seebeck coefficient, the two probes on the surface are used. These two probes function as temperature probes (thermocouples) as well as voltage probes. This whole setup is enclosed in a furnace, of which the temperature can be controlled between room temperature and 1100°C.

Because the high-temperature measurements are performed inside a closed furnace, the atmosphere at which the measurements are done can be controlled, even though the absolute pressure during the measurements should always be kept around 1.1 bar. Generally, such high-temperature Seebeck measurements are done with helium as a background gas, because helium provides good thermal contacts in the system, making it relatively easy to establish the required temperature gradient across the sample. The design of the LSR3 system provides the possibility to measure in different atmospheres, such as inert or oxidizing, because of the corrosion resistant materials, such as platinum electrodes and S-type thermocouples. Because the partial oxygen pressure during the measurements at high-temperature

is expected to be important for the stability of the studied cobaltate thin films, this system provides a tool to directly compare measurements at different partial oxygen pressures.

For the cobaltate thin films that are studied in this chapter, it will be shown that a sufficient thermal contact was obtained up to an oxygen partial pressure of approximately 100 mbar. At this partial oxygen pressure of 100 mbar, the helium gas still provides a sufficient thermal contact to obtain the required temperature gradient across the sample, whereas for larger partial oxygen pressures, at high-temperature the gradient across the sample slowly reduces to zero. The procedure to obtain reproducible and reliable measurements in this controlled atmosphere is to flush the closed furnace twice with oxygen and/or helium, after pumping down to approximately 10^{-1} mbar. After this flushing the furnace is filled with either helium, oxygen or a mixture of these two. If only resistivity measurements are performed, the system can also be used with pure oxygen as a background gas, because a temperature gradient is not required for these measurements. For the high-temperature Seebeck measurements described in this chapter, either helium or a mixture of 100 mbar of oxygen and 1 bar of helium is used. High temperature resistivity measurements are performed in the same background gases, but also several measurements in pure oxygen are presented.

5.3 Na_xCoO_2 Thin Films: High-Temperature Stability and Thermoelectric properties

To study the thermoelectric properties at high-temperature, knowledge about the stability of the materials is required. Na_xCoO_2 thin films deposited on LSAT and with a thickness of 60 nm were used for this study, because the structural and thermoelectric properties of these thin films as well as size effects in these thin films have been studied in respectively Chapters 3 and 4. An amorphous AlO_x capping layer was deposited to ensure chemical stability in air, as discussed in Chapter 2. These optimized thin films show enhanced thermoelectric properties at room temperature and are therefore interesting for a study of their high-temperature stability and thermoelectric properties. Such study focussing on the high-temperature stability of Na_xCoO_2 thin films has not been previously reported.

In order to determine the structural stability at elevated temperatures, temperature dependent XRD measurements are performed on a 60 nm Na_xCoO_2 thin film on LSAT. The measurements were performed in air. At increasing temperatures a $2\theta/\omega$ scan was made around the (002) Na_xCoO_2 diffraction peak, which is the strongest observed film peak in these thin films. From these scans, the normalized peak intensity and the c-axis lattice parameter were calculated, as shown in Fig. 5.1.

Initially, the peak intensity increases as a function of temperature, after which it

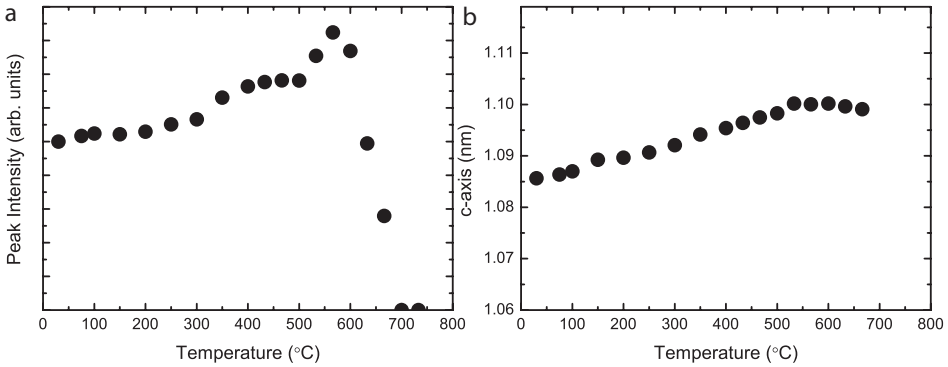

Figure 5.1: XRD measurements of a 60 nm Na_xCoO_2 thin film on LSAT. (a) Shows the peak intensity of the (002) Na_xCoO_2 diffraction peak, normalized to the first measurement at room temperature, as a function of temperature. (b) Shows the c-axis lattice parameter as a function of temperature.

suddenly shows a sharp drop at a temperature of approximately 575°C. An increase in intensity is also seen for the substrate peaks and can be explained because of the elevated temperature near the sample, causing reduced scattering of the X-rays because of the lower air pressure. However, the increase of intensity of the substrate peaks is significantly smaller than that of the (002) Na_xCoO_2 film peak, indicating that other effects play an important role as well. Either recrystallisation, a temperature dependent structure factor or (small) structural changes such as the formation of oxygen vacancies could contribute to such an intensity increase. After this initial increase, a sharp transition at approximately 575°C is observed. This effect is much more pronounced and indicates decomposition of Na_xCoO_2, because the (002) peak cannot be observed at temperatures of 700°C and higher. After the sample is cooled down to room temperature, no Na_xCoO_2 diffraction peaks are found, confirming that Na_xCoO_2 is decomposed.

The c-axis lattice parameter shows a linear increase between room temperature and 530°C, which can be explained by thermal expansion. Above 530°C the c-axis lattice parameter shows a transition and slowly decreases, indicating a change in crystal structure. From these temperature dependent XRD measurements it is concluded that the samples are structurally stable up to a temperature of 530°C in air. This is supported by the observations of XRD measurements of Na_xCoO_2 thin films deposited at different temperatures, as shown in Chapter 2 (Fig. 2.4). The observed decomposition temperature around 530°C is close to the optimum temperature of 550°C for single crystals at which the best thermoelectric properties were observed and also matches the observed decomposition temperature of bulk samples of approximately 500°C. [1, 17]

The high-temperature electrical resistivity and Seebeck coefficient of these

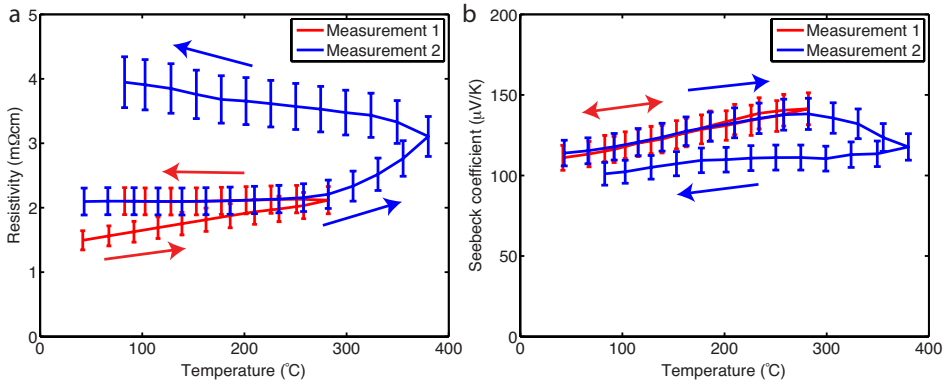

Figure 5.2: (a) Temperature dependent resistivity measurements of a Na_xCoO_2 thin film on LSAT. (b) Temperature dependent Seebeck coefficient of the same Na_xCoO_2 thin film. The arrows indicate the sequence of the temperature sweeps. Measurements were performed in a mixture of 100 mbar O_2 and 1 bar He.

Na_xCoO_2 thin films have also been measured, as shown in Fig. 5.2. To prevent a loss of oxygen at elevated temperatures, the measurements were performed in a mixture of 100 mbar oxygen and 1 bar helium, as described in Section 5.2. To verify that the samples have remained stable during the measurement procedure, measurements were performed during heating as well as cooling of the samples.

A first measurement was performed for the resistivity as well as the Seebeck coefficient, as shown by the red curves in Fig. 5.2a and b. For the resistivity a different behavior is observed during cooldown, compared to the values obtained during heating. Even though the absolute difference between the values remains limited, the observed trends during heating and cooling are rather different. During heating the resistivity shows an increase with temperature, whereas during the cooldown the resistivity remains constant with temperature. For the Seebeck coefficient a linear increase as a function of temperature to a maximum of 140 μV/K is observed and no differences are observed during the heating and cooling.

A second measurement up to a temperature of approximately 380°C was performed, as shown by the blue curves in Fig. 5.2. For the resistivity a much larger difference for the values obtained during heating and cooling is observed, compared to the first measurements. These measurements clearly show that significant changes to the sample occurred, leading to a difference in electronic behavior. For this measurement, also a small difference in values for the Seebeck coefficient during heating and cooling is observed, although this difference is not as significant as that observed for the resistivity.

In contrast to the previously described temperature dependent XRD measurements, from these electronic measurements it is clearly observed that the Na_xCoO_2 thin films are not stable at temperatures of 300-400°C in a mixture of oxygen and

helium. Combining these different measurements it is concluded that temperature dependent resistivity measurements are a much more sensitive tool to study the high-temperature stability of these Na_xCoO_2 thin films. As an example, the formation of oxygen vacancies can often not be observed with XRD, whereas this will have a pronounced effect on the electronic transport properties, as shown for $SrTiO_3$. [18, 19] For these Na_xCoO_2 thin films, a number of effects can take place and because of the presence of a capping layer to ensure chemical stability in air the situation is even more complex. In order to fully understand the observed instability at elevated temperatures possible reactions between sodium and the capping layer, the substrate material and the environment should be studied, as well as the possible formation of oxygen vacancies as a function of the partial oxygen pressure and the temperature and the formation of (minor) impurity phases. Even though it cannot be fully understood from these measurements why these Na_xCoO_2 thin films are not stable at elevated temperatures, the poor thermal stability has been clearly shown. Even at a temperature of 300°C the transport properties are already changing and therefore alternative cobaltate thin films are considered for high-temperature studies.

5.4 $Ca_3Co_4O_9$ High Temperature Properties and Stability

Even though the thermoelectric properties of the layered cobaltates are shown to be most promising at elevated temperatures, as shown in the previous Section the thermal stability of these cobaltates should also be considered. If the samples are not stable during the measurements at elevated temperatures, the obtained values are extrinsic and will strongly depend on experimental details such as the heating rate and/or the measurement time. Because of the lack of thermal stability of Na_xCoO_2 thin films, the related $Ca_3Co_4O_9$ is studied as an alternative material. This has the advantage that the volatile sodium is replaced by less volatile Ca_2CoO_3 layers, removing the necessity of the AlO_x capping layer and its related complexity. To understand the high-temperature stability of these $Ca_3Co_4O_9$ thin films, high-temperature measurements are performed, but also the stability of bulk samples is studied in the next Sections.

5.4.1 Bulk Stability

To study the thermal stability of bulk $Ca_3Co_4O_9$, thermogravimetric analysis (TGA) was performed on $Ca_3Co_4O_9$ powder samples up to 1000°C with air and N_2 as a background gas, as shown in Fig. 5.3a. Measurements were performed using a commercially available setup (Netzsch STA-449 F3 Jupiter). These measurements show a small mass increase around 400°C and a significant mass loss of

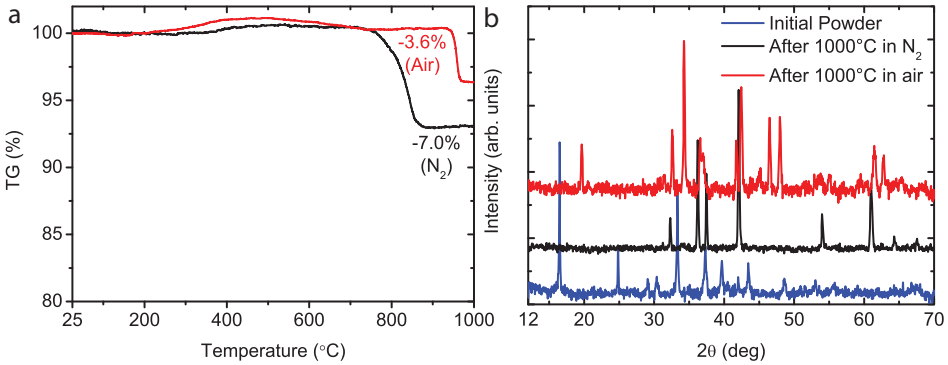

Figure 5.3: Measurements of the stability of bulk $Ca_3Co_4O_9$ samples. (a) Shows TGA measurements of bulk $Ca_3Co_4O_9$ powders in air and N_2 atmosphere, showing improved stability in air up to 930°C. (b) Shows XRD measurements of the initial powder and of samples after TGA measurements up to 1000°C in air and N_2.

3.6% and 7.0% at higher temperatures when measured in respectively air and N_2. It is observed that the mass loss starts at 940°C in air and at 740°C in N_2. These observations are in good agreement with previous reports of TGA measurements of bulk $Ca_3Co_4O_9$, where a comparable mass loss, which was attributed to the decomposition of $Ca_3Co_4O_9$, was observed around 970°C when heated in air. [20] The observed mass increase during the first part of the measurement of respectively approximately 0.5% and 1% when heated in respectively N_2 and air, was not previously observed. This mass increase could possibly be explained by the uptake of respectively nitrogen or oxygen, thereby changing the oxygen content of the $Ca_3Co_4O_9$ samples between 200° and 700°C.

To understand the processes taking place that lead to the observed mass loss in the TGA measurements, XRD measurements of these samples were made after the TGA measurements. These XRD spectra are compared with the measured spectrum of a non-heated $Ca_3Co_4O_9$ sample, as shown in Fig. 5.3b. The most important observation from these spectra is that the $Ca_3Co_4O_9$ phase is decomposed for both samples that were heated to 1000°C, as was already indicated by the observed mass losses in the TGA measurements. For the sample that was heated in N_2, the observed diffraction peaks are in good agreement with those of CoN and CaO, whereas for the sample that was heated in air, the diffraction peaks are in good agreement with those of $Ca_3Co_2O_6$ and CoO. This is consistent with the $Ca_3Co_4O_9$ phase diagram in air. [21] The observed mass differences in the TGA measurements are in agreement with the theoretical mass differences of the decomposition of $Ca_3Co_4O_9$ into the previously mentioned phases and a corresponding loss of oxygen.

To confirm that the structural properties are stable up to temperatures below that corresponding to the observed mass loss in the TGA measurements, a sample

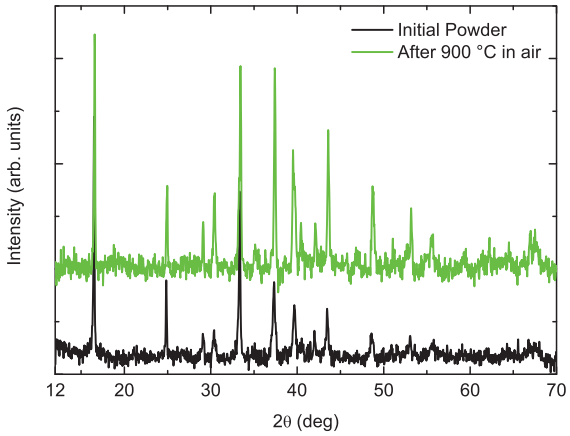

Figure 5.4: XRD measurements of the initial powder and a powder after heating to 900°C in air. The observation of similar peaks confirmed that the sample was not decomposed during the heat treatment.

was measured in the TGA up to 900°C in air. A comparable measurement as that shown in Fig. 5.3a was observed, however the observed mass loss at 940°C was not observed, because the measurement was stopped at 900°C. The XRD spectrum of this sample after the TGA measurement is compared to that of a non-heated sample, as shown in Fig. 5.4. As expected, the spectra are comparable, confirming the stability of the $Ca_3Co_4O_9$ phase in bulk samples when heated in air to 900°C.

It is concluded that in these bulk samples the $Ca_3Co_4O_9$ phase is stable up to approximately 740°C and 940°C when heated in a controlled environment of respectively nitrogen and air. This clearly demonstrates the importance of the background gas for the thermal stability of $Ca_3Co_4O_9$, which should also be taken into account when the high-temperature electronic properties are measured.

5.4.2 High-Temperature Properties of $Ca_3Co_4O_9$ thin films

As an alternative material to the Na_xCoO_2 thin films, which show very limited thermal stability, as described in Section 5.3, the stability and high-temperature properties of $Ca_3Co_4O_9$ thin films are studied. Thin films of $Ca_3Co_4O_9$ were previously studied, [22–28] however only a limited number of these studies analyzed the high-temperature thermoelectric properties. [29–31] In the remainder of this section a systematic study combining the structural stability and thermoelectric properties at high-temperature is presented, which has not been reported to date.

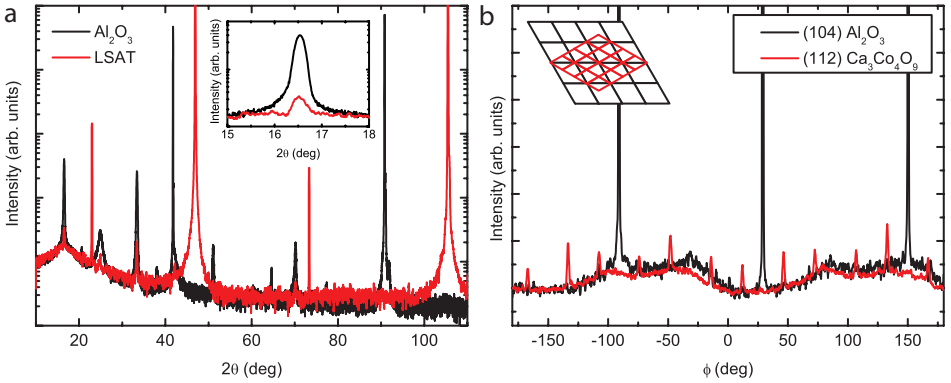

Figure 5.5: XRD measurements of the $Ca_3Co_4O_9$ thin films deposited on Al_2O_3 and LSAT substrates. (a) Shows a $2\theta/\omega$ scan, showing only (00l) peaks of the deposited $Ca_3Co_4O_9$ thin films. In the inset a zoom of the (002) $Ca_3Co_4O_9$ diffraction peak is shown. (b) Shows a ϕ scan of the (104) and (112) peak of respectively the substrate and the thin film, demonstrating the epitaxial relationship between $Ca_3Co_4O_9$ and Al_2O_3, as indicated by the inset.

5.4.2.1 Growth of $Ca_3Co_4O_9$ thin films

The $Ca_3Co_4O_9$ thin films that are analyzed in this chapter were grown by pulsed laser deposition, using a KrF excimer laser with a wavelength of 248 nm (Lambda-Physik LPX 210) with a laser fluence of 4 J/cm^2, a spotsize of 1.1 mm^2 and a repetition rate of 1 Hz. During deposition, an oxygen pressure of 0.01 mbar was used, because this deposition pressure resulted in $Ca_3Co_4O_9$ thin films with an optimized crystallinity. Because the volatile sodium of Na_xCoO_2 is replaced by the more stable Ca_2CoO_3, the low deposition temperature that was used for Na_xCoO_2 thin films is no longer required and it was found that optimized crystallinity was obtained for samples deposited at 750°C, whereas the thermoelectric properties show only little variation with the deposition temperature. Therefore, a deposition temperature of 750°C was used for the $Ca_3Co_4O_9$ thin films studied in this chapter. After growth the samples were slowly cooled down to room temperature in 1 atm. of oxygen at a rate of 10°C/min to optimize the oxidation level. As substrate material, (001) oriented single crystals of Al_2O_3 and LSAT were used. Before deposition the Al_2O_3 and LSAT substrates were annealed at 1050°C for respectively 1 hour and 10 hours, to obtain a smooth surface with predominantly unit-cell-height steps, as shown in Chapter 3 (Fig. 3.4). Hexagonal Al_2O_3 was used because of the good structural match with $Ca_3Co_4O_9$, whereas LSAT was used because this has shown to result in a significant enhancement of the thermoelectric properties of cobaltate thin films, as described in Chapter 3.

Using the deposition parameters as described above, single-phase thin films were deposited, which show a preferred (00l) orientation on Al_2O_3 and LSAT sub-

strates, as confirmed by XRD measurements (Fig. 5.5a). In the inset a $2\theta/\omega$ scan, focusing on the (002) diffraction peak of $Ca_3Co_4O_9$ is shown. Here it is clearly observed that a much stronger diffraction peak is observed for the sample deposited on Al_2O_3, indicating a significant loss of crystallinity when the hexagonal $Ca_3Co_4O_9$ is deposited on the cubic LSAT. The $Ca_3Co_4O_9$ thin film deposited on Al_2O_3 was found to be grown epitaxially, as shown by the phi-scans of the (104) and (112) diffraction peaks of respectively the substrate and the thin film in Fig. 5.5b. From these results it was concluded that the a-axis of $Ca_3Co_4O_9$ is rotated by 30° compared to that of the Al_2O_3, as indicated in the inset in Fig. 5.5b. This epitaxial relationship is comparable to that observed for Na_xCoO_2 thin films, as described in Chapter 2. For the sample deposited on LSAT no epitaxial relationship could be found by XRD, because of the significantly lower intensity, as already observed in Fig. 5.5a for the out-of-plane direction.

For these $Ca_3Co_4O_9$ thin films, a room temperature resistivity of 6 mΩcm and 26 mΩcm is measured, for the sample deposited on respectively Al_2O_3 and LSAT. The Seebeck coefficient of these samples is 133 μV/K and 141 μV/K when deposited on respectively Al_2O_3 and LSAT. From these measurements it is clear that thin films deposited on Al_2O_3 show better thermoelectric properties at room temperature and therefore Al_2O_3 is used as substrate material for the $Ca_3Co_4O_9$ thin films that are studied at high-temperature in the remainder of this chapter. These samples have the additional advantage of a better crystallinity, compared to samples deposited on LSAT, making it easier to observe small structural changes by XRD, because of the higher intensity of the diffraction peaks for these samples.

5.4.2.2 High-Temperature stability and thermoelectric properties of $Ca_3Co_4O_9$ Thin Films

To study the structural stability at elevated temperatures, temperature dependent XRD measurements of a 60 nm $Ca_3Co_4O_9$ thin film deposited on Al_2O_3 were performed in air. At varying temperatures, $2\theta/\omega$ measurements were done around the (002) $Ca_3Co_4O_9$ diffraction peak, which is the strongest diffraction peak for these thin films, as described in the previous Section. From these measurements, the (normalized) peak intensity and the c-axis lattice parameter were determined as a function of temperature, as shown in Fig. 5.6a and b.

The peak intensity is initially increasing, comparable to previous observations in Na_xCoO_2 thin films, whereas a sharp decrease of the peak intensity is observed above a temperature of 750°C. This sharp decrease is an indication of decomposition of the $Ca_3Co_4O_9$, which is confirmed by the absence of any $Ca_3Co_4O_9$ at room temperature after cooling down from these high-temperature measurements.

For the temperature dependent c-axis lattice parameter, a linear increase is observed between room temperature and 775°C, after which the c-axis lattice parameter reduces. The observed linear increase is caused by thermal expansion

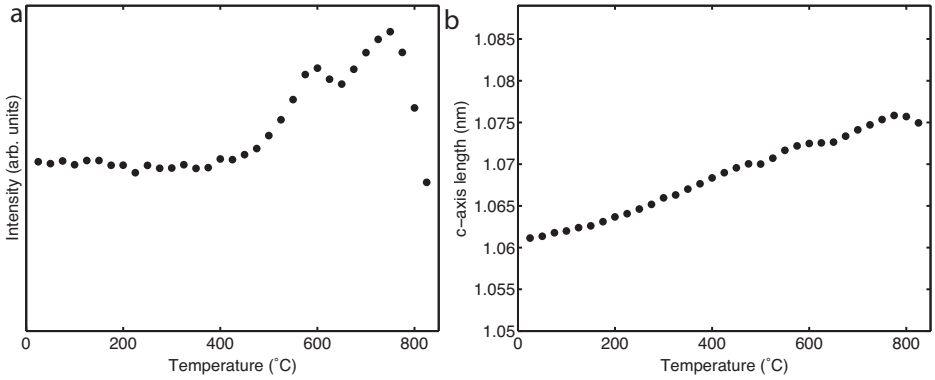

Figure 5.6: High-temperature XRD measurements of a $Ca_3Co_4O_9$ thin film on Al_2O_3. The (normalized) peak intensity of the (002) $Ca_3Co_4O_9$ (a) and the c-axis lattice parameter (b) are shown as a function of temperature.

and a deviation from this linear trend is an indication that changes are occurring to the crystal structure, supporting the observed decomposition at approximately 750°C. Based on these temperature dependent XRD measurements it is concluded that these $Ca_3Co_4O_9$ thin films are structurally stable in air up to a temperature of approximately 750°C, after which decomposition is occurring.

To determine the high-temperature thermoelectric properties of these $Ca_3Co_4O_9$ thin films, temperature dependent resistivity and Seebeck measurements are performed. Because the stability of these thin films is also studied, the measurements are performed in a sequence of heating cycles. For each heating cycle the maximum temperature to which the sample is heated is increased compared to the previous cycle. Using this measurement procedure, the data obtained during heating and cooling are compared to confirm that the sample has not changed during the measurement procedure. These measurements are shown in Fig. 5.7.

The top figures (Fig. 5.7a and b) are measurements performed with helium as a background gas, which is the standard measurement gas because of its high thermal conductivity. As clearly seen in the resistivity measurements, the values obtained during the heating and cooling already significantly differ when the sample is only heated to approximately 300°C. These observed changes indicate that these thin films are not stable when heated to 300°C in helium and the obtained values are not the intrinsic values of these thin films. For the Seebeck coefficient, no clear differences are observed during the heating and the cooling, even though a relatively strong increase of the Seebeck coefficient as a function of temperature is observed. Because helium was used as a background gas during these measurements, oxygen vacancies can be easily created at elevated temperatures in these oxide materials, which could possibly explain the observed poor thermal stability. To study the influence of the oxygen partial pressure on the thermal

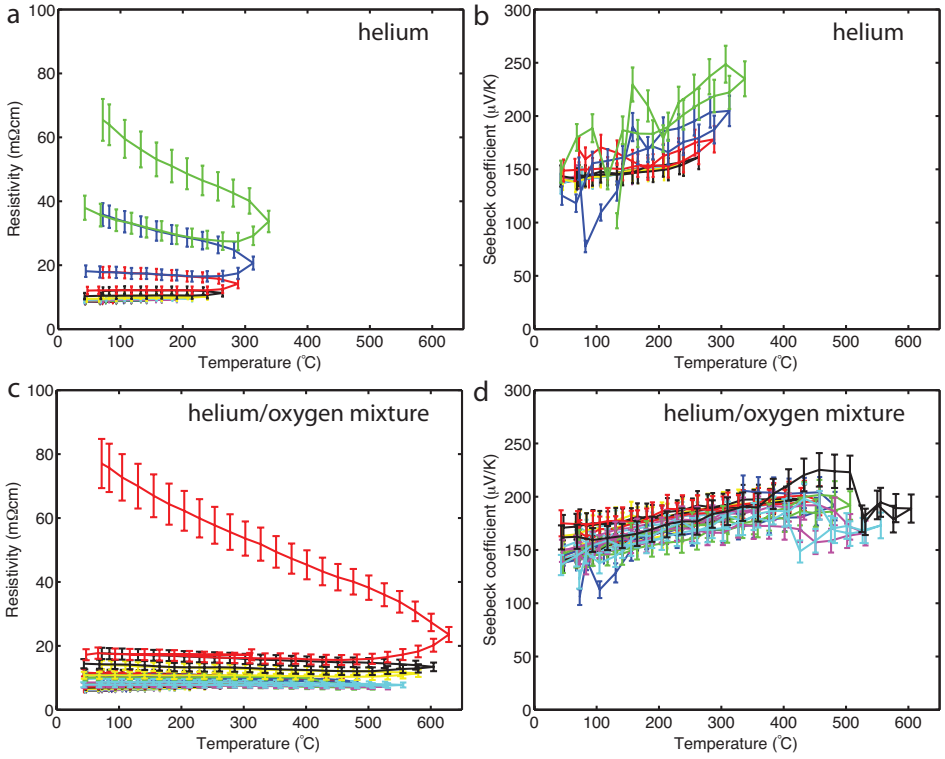

Figure 5.7: High-temperature resistivity and Seebeck coefficient measurements. Measurements are performed with helium (a and b) and a mixture of 100 mbar oxygen and 1 bar of helium (c and d) as a background gas. Values are measured during heating as well as during cooling to observe the thermal stability. The different curves represent consecutive measurements up to increasing temperatures.

stability of these $Ca_3Co_4O_9$ thin films, similar measurements were performed in a mixture of 100 mbar of oxygen and 1 bar of helium. This mixture still provides sufficient thermal contact to establish the required temperature gradient for the Seebeck coefficient measurements, as explained in Section 5.2. The results of these measurements are shown in Fig. 5.7c and d.

Compared to the measurements in helium, indeed a significant improvement of the high-temperature stability is obtained when the samples are measured in a mixture of oxygen and helium. Up to a temperature of approximately 550°C the resistivity during heating and cooling overlap, within the error margin of the measurements. When measured to even higher temperatures, a similar degradation, leading to an increase of the resistivity, is observed as in the thin films that were measured in helium. By comparing the different measurements, it is also observed that the sample is more rapidly degrading when the temperature is increased, similar as observed for the measurements that were performed in helium. The Seebeck coefficient does not show a clear effect from the sample degradation, and the curves obtained from heating and cooling are relatively similar. Some (small) changes are observed, however these are caused by variations in thermal and electrical contact to the samples. This is confirmed by additional measurements, in a custom-built setup, that show the same Seebeck coefficient at room temperature before and after the high-temperature measurement procedure. These observations match those of previous reports that the resistivity is much more sensitive to the background gas during thermal treatments than the Seebeck coefficient in bulk $Ca_3Co_4O_9$. [16] This could be explained by a non-homogeneous sample degradation, starting at the sample surface. For these thin films, the surface to volume ratio is significantly larger than for bulk samples, leading to a significant change of the resistivity (because the volume of the conducting phase is considerably changing) when a surface layer is formed. At the same time, this will not have such a pronounced influence on the Seebeck coefficient, because these measurements are not dependent on the volume of the film and will not change if sufficient thermal and electrical contact is made with the thermoelectric phase.

The observed increase of the Seebeck coefficient is relatively comparable to reports of bulk $Ca_3Co_4O_9$, which also report an increasing Seebeck coefficient at high-temperature. However, the absolute values between 140 μV/K and 220 μV/K are significantly higher than previously reported for bulk $Ca_3Co_4O_9$. [32] The electrical resistivity is relatively constant with temperature, in contrast to previous reports of bulk $Ca_3Co_4O_9$ where a maximum is observed around 150°C. [32] The best thermoelectric properties for thin films that remain stable during the complete measurement cycle are observed around a temperature of 500°C. At this temperature an electrical resistivity and a Seebeck coefficient of respectively 7.1 mΩcm and 192 μV/K are obtained. This is a significant improvement compared to bulk samples for which an electrical resistivity and Seebeck coefficient of respectively 9.5 mΩcm and 170 μV/K are reported at a similar temperature. From these values

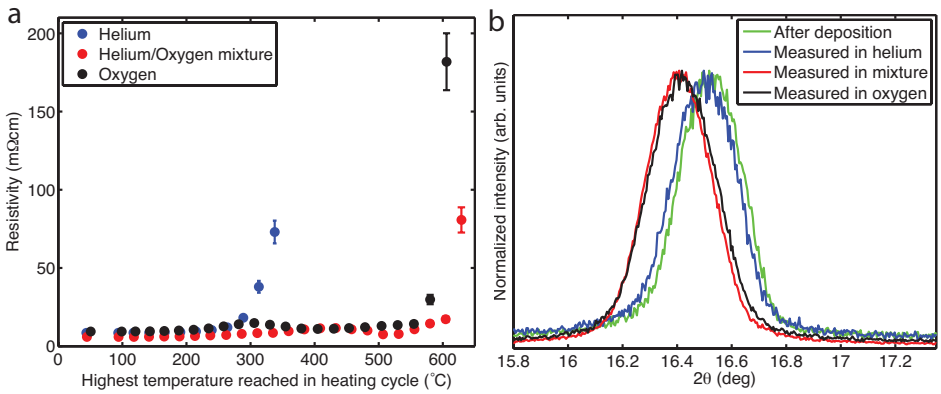

Figure 5.8: (a) Resistivity measurements of $Ca_3Co_4O_9$ thin films at room temperature, after heating cycles to the maximum temperature shown on the horizontal axis. (b) Normalized XRD measurements of the (002) diffraction peak of $Ca_3Co_4O_9$ thin films. Curves are shown for a sample after deposition, and after a sequence of high-temperature measurements in respectively helium, helium/oxygen mixture and oxygen.

a thermoelectric power factor of $5.2{\cdot}10^{-4}$ $Wm^{-1}K^{-2}$ is calculated at 500°C, which is significantly higher than the reported value of $3.0{\cdot}10^{-4}$ $Wm^{-1}K^{-2}$ for bulk samples. [32] These results clearly demonstrate the high thermoelectric performance of $Ca_3Co_4O_9$ thin films at elevated temperatures.

Comparing the high-temperature XRD measurements and the resistivity measurements a remarkable difference is observed. From the XRD measurements it is concluded that the samples remain stable up to a temperature of approximately 750°C, whereas the electronic properties are already changing when the thin films are heated to 550°C. This indicates that these electronic measurements at high-temperature are more sensitive for the stability than temperature dependent XRD measurements. To further investigate this difference, the room temperature resistivity values after heating the samples to a specific temperature are shown in Fig. 5.8a. The data is shown for the samples that were heated in either helium or a mixture of helium and oxygen, as previously shown, and data is also included for a sample that was heated in pure oxygen.

From these room temperature values after heating, the difference in stability between measurements in helium and a mixture of oxygen and helium is clearly confirmed. Additionally, it is also observed that the stability in a mixture of oxygen and helium is comparable to that in oxygen, as these two samples show a comparable increase after heating. This shows that by adding 100 mbar of oxygen, a sufficient partial oxygen pressure is already obtained to minimize oxygen vacancies. The partial oxygen pressure is not limiting the stability of these thin films at these gas mixtures.

Based on these results it is expected that the low partial oxygen pressure when

measured in helium results in the formation of oxygen vacancies, and thereby influence the electronic properties. To confirm this, Hall measurements were performed and compared with a sample before and after thermal cycling. From initial measurements of the sample before thermal cycling, a carrier density of $4{\cdot}10^{20}$ cm^{-3} at room temperature was calculated, using a simple single band model. This value is in exact agreement with previous reports of $Ca_3Co_4O_9$ thin films. [33] After the thermal cycling (during the high-temperature experiments), a carrier density of $1\text{-}2{\cdot}10^{20}$ cm^{-3} has been determined. Even though a more precise value could not be determined because of a strong observed directional anisotropy of the electronic transport, these results show a clear reduction of the carrier density for the two measured directions. This confirms the formation of oxygen vacancies, because the oxygen vacancy functions as a donor, leading to a reduction of the carrier density in a p-type material. Before and after these high temperature measurements in helium similar XRD spectra were measured, as shown in Fig. 5.8b. This supports the formation of oxygen vacancies and the absence of the formation of impurity phases, because oxygen vacancies can often not be observed by XRD. [18, 19]

As indicated by the measurements in pure oxygen, the oxygen partial pressure of the used mixture of helium and oxygen was sufficient to prevent the formation of oxygen vacancies. For these samples that were heated in an oxygen-rich environment, before and after these high-temperature measurements a peak shift to lower 2θ values was observed as presented in Fig. 5.8, showing that the c-axis lattice parameter was increased. This structural change indicates that the cation stoichiometry is changed, which is previously reported to result in a change of the c-axis lattice parameter. [16] In addition to the change of stoichiometry of the $Ca_3Co_4O_9$ phase, this is expected to result in the formation of impurity phases, such as $Ca_3Co_2O_6$ as also observed for bulk $Ca_3Co_4O_9$ as described in Section 5.4.1. These impurity phases are not observed by XRD, which can be explained by the small volume of the impurity phases. The $Ca_3Co_4O_9$ phase is still intact in a large volume fraction of the thin films, as shown by the XRD scans in Fig. 5.8. Even though the volume fraction is small, the formation of such an insulating impurity phase will have a strong influence on the electrical resistivity, as confirmed by the measurements after thermal cycling.

The effect of the formation of minor impurity phases on the Seebeck coefficient is observed to be negligible, as shown by the room temperature Seebeck coefficient measurements after these high-temperature measurements, which resulted in similar values as those directly after deposition. This is in good agreement with previous observations of bulk $Ca_3Co_4O_9$, [34] and can be explained by theoretical predictions of the Seebeck coefficient of a composite consisting of a metallic and an insulating phase. [35]

Combining these high-temperature electronic measurements with the high-temperature XRD measurements, it is concluded that $Ca_3Co_4O_9$ thin films have promising high-temperature thermoelectric properties up to a temperature of ap-

proximately 550°C in an oxygen-rich environment. At high temperatures or different environments, the samples are not stable because of the formation of (minor) impurity phases or oxygen vacancies. These results can only be obtained by systematic thermal cycling and performing measurements during heating as well as cooling of the samples, because the transport properties of these layered cobaltates are much more sensitive to small changes in the structural properties than direct structural measurements, such as XRD. The presented method to use thermal cycling in combination with electronic measurements in different atmospheres is a powerful tool to study the thermoelectric potential as well as the thermal stability of thermoelectric materials. Without such a systematic study which also focuses on measurements during the cool down it is not clear whether the obtained results are the intrinsic material properties or reflect those of a changing system with for example additional oxygen vacancies or minor impurity phases.

5.5 Conclusions

The thermal stability of Na_xCoO_2 thin films has shown to be limited. The Na_xCoO_2 phase remains stable up to a temperature of approximately 530°C in air, as shown by XRD. However, when the thermoelectric properties are measured, significant changes occur already after heating to temperature of 300°C in an oxygen-rich environment. From these observations it is concluded that the thermal stability of Na_xCoO_2 is very limited, and that systematic high-temperature electronic measurements, including cycling, are a much more sensitive tool to study the thermal stability of thermoelectric materials.

The related $Ca_3Co_4O_9$ was studied as alternative material. From TGA measurements of bulk $Ca_3Co_4O_9$ a thermal stability up to approximately 940°C in air was determined, in good agreement with literature. The structural stability of $Ca_3Co_4O_9$ thin films was determined by temperature dependent XRD measurements, showing no significant changes up to 750°C when measured in air, showing a limited thermal stability of $Ca_3Co_4O_9$ thin films compared to bulk samples.

By systematic cycling up to increasingly high-temperatures and electronic measurements during heating as well as cooling, the stability of $Ca_3Co_4O_9$ thin films was studied. By varying the background gas during the measurements from helium to oxygen the effect of oxygen vacancies was determined. When heated in helium, the thin films are only stable up to approximately 250°C, and it is concluded that the observed changes are caused by the formation of oxygen vacancies when heated in helium.

When the $Ca_3Co_4O_9$ thin films are heated in an oxygen-rich environment, an enhanced stability up to a temperature of 550°C is observed. When heated to higher temperatures, an increased resistivity is observed, which is caused by the formation of impurity phases as indicated by a change of the cation stoichiometry

after thermal cycling. The effect of these impurity phases on the Seebeck coefficient is negligible.

Based on the observed difference in thermal stability from temperature dependent XRD and electronic measurements, it is concluded that a combination of these studies is required to fully understand the thermal stability of layered cobaltates. Systematic cycling and simultaneous electronic measurements in various environments is a powerful tool to study small changes in thin films of $Ca_3Co_4O_9$. This is partly caused by the small volume of possible impurity phases in thin films, because of the overall small volume of a thin film, but also because the electronic transport is very sensitive to the formation of oxygen vacancies as well as the formation of impurity phases. From these observations it is concluded that thermal cycling and simultaneous electronic measurements are a more suitable approach to determine the thermal stability of $Ca_3Co_4O_9$ thin films. Such systematic thermal cycling results in a direct observation of changes to the sample, during cooling, and thereby can help to differentiate between intrinsic and extrinsic properties of measurements at high temperatures by also taking the thermal stability into account.

In the stable regime of these $Ca_3Co_4O_9$ thin films, up to approximately 550°C, the thermoelectric properties are characterised. Compared to bulk samples, a simultaneous reduction of the electrical resistivity and an enhancement of the Seebeck coefficient are measured, leading to a significant enhancement of the thermoelectric properties. The best thermoelectric performance was obtained at 500°C, where a thermoelectric power factor of $5.2{\cdot}10^{-4}$ $Wm^{-1}K^{-2}$ is achieved. This is significantly higher than the reported value of $3.0{\cdot}10^{-4}$ $Wm^{-1}K^{-2}$ for bulk samples at a similar temperature. These results clearly demonstrate the thermoelectric potential of cobaltate thin films at elevated temperatures.

Bibliography

[1] K. Fujita, T. Mochida, and K. Nakamura, "High-Temperature Thermoelectric Properties of $Na_xCoO_{2-\delta}$ Single Crystals," *Japanese Journal of Applied Physics*, vol. 40, pp. 4644–4647, 2001.

[2] S. Hildebrandt, P. Komissinskiy, M. Major, W. Donner, and L. Alff, "Epitaxial Growth and Control of the Sodium Content in Na_xCoO_2 Thin Films," *Thin Solid Films*, vol. 545, pp. 291–295, 2013.

[3] L. Yu, L. Gu, Y. Wang, P. X. Zhang, and H. U. Habermeier, "Epitaxial Layered Cobaltite Na_xCoO_2 Thin Films Grown on Planar and Vicinal Cut Substrates," *Journal of Crystal Growth*, vol. 328, pp. 34–38, 2011.

[4] J. Y. Son, Y. H. Shin, and C. S. Park, "Fabrication and Optical Conductivities of Strained Epitaxial Na_xCoO_2 Thin Films: x=0.5, 0.7," *Journal of Solid State Chemistry*, vol. 181, pp. 2020–2023, 2008.

[5] J. Y. Son, "Epitaxial Layered Cobaltite Na_xCoO_2 Thin Films: x= 0.5, 0.7," *Journal of Physics D: Applied Physics*, vol. 41, p. 095405, 2008.

[6] J. Y. Son, H.-B.-R. Lee, and J. H. Cho, "Stress Dependence of Growth Mode Change of Epitaxial Layered Cobaltite γ-$Na_{0.7}CoO_2$," *Applied Surface Science*, vol. 254, pp. 436–440, 2007.

[7] H. Zhou, X. P. Zhang, B. T. Xie, Y. S. Xiao, C. X. Yang, Y. J. He, and Y. G. Zhao, "Fabrication of Na_xCoO_2 Thin Films by Pulsed Laser Deposition," *Thin Solid Films*, vol. 497, pp. 338–340, 2006.

[8] Y. Krockenberger, I. Fritsch, G. Christiani, H. U. Habermeier, L. Yu, C. Bernhard, B. Keimer, and L. Alff, "Superconductivity in Epitaxial Thin Films of $Na_xCoO_2{\cdot}yD_2O$," *Applied Physics Letters*, vol. 88, p. 162501, 2006.

[9] Y. Krockenberger, I. Fritsch, G. Cristiani, A. Matveev, L. Alff, H. U. Habermeier, and B. Keimer, "Epitaxial Growth of Na_xCoO_2 Thin Films by Pulsed-Laser Deposition," *Applied Physics Letters*, vol. 86, p. 191913, 2005.

[10] J. Y. Son, B. G. Kim, and J. H. Cho, "Kinetically Controlled Thin-Film Growth of Layered β- and γ-Na_xCoO_2 Cobaltate," *Applied Physics Letters*, vol. 86, p. 221918, 2005.

[11] K. Sugiura, H. Ohta, K. Nomura, M. Hirano, and H. Hosono, "Fabrication and Thermoelectric Properties of Layered Cobaltite, γ-$Sr_{0.32}Na_{0.21}CoO_2$ Epitaxial Films," *Applied Physics Letters*, vol. 88, p. 082109, 2006.

[12] L. Yu, Y. Krockenberger, I. Fritsch, and H. U. Habermeier, "Substrate-Induced Anisotropy of c-Axis Textured Na_xCoO_2 Thin Films," *Progress in Solid State Chemistry*, vol. 35, pp. 545–551, 2007.

[13] A. Venimadhav, A. Soukiassian, D. A. Tenne, Q. Li, X. X. Xi, D. G. Schlom, R. Arroyave, Z. K. Liu, H. P. Sun, X. Pan, M. Lee, and N. P. Ong, "Structural and Transport Properties of Epitaxial Na_xCoO_2 Thin Films," *Applied Physics Letters*, vol. 87, p. 172104, 2005.

[14] X. P. Zhang, Y. S. Xiao, H. Zhou, B. T. Xie, C. X. Yang, and Y. G. Zhao, "Surface Morphology, Structure and Transport Property of Na_xCoO_2 Thin Films Grown by Pulsed Laser Deposition," *Materials Science Forum*, vol. 3807, pp. 475–479, 2005.

[15] R. Funahashi, I. Matsubara, H. Ikuta, T. Takeuchi, U. Mizutani, and S. Sodeoka, "An Oxide Single Crystal with High Thermoelectric Performance in Air," *Japanese Journal of Applied Physics*, vol. 39, pp. L1127–L1129, 2000.

[16] D. Moser, L. Karvonen, S. Populoh, M. Trottmann, and A. Weidenkaff, "Influence of the Oxygen Content on Thermoelectric Properties of $Ca_{3-x}Bi_xCo_4O_{9+\delta}$ System," *Solid State Sciences*, vol. 13, pp. 2160–2164, 2011.

[17] T. Motohashi, E. Naujalis, R. Ueda, K. Isawa, M. Karppinen, and H. Yamauchi, "Simultaneously Enhanced Thermoelectric Power and Reduced Resistivity of Na_xCoO_2 by Controlling Na Nonstoichiometry," *Applied Physics Letters*, vol. 79, pp. 1480–1482, 2001.

[18] D. Freedman, D. Roundy, and T. Arias, "Elastic Effects of Vacancies in Strontium Titanate: Short- and Long-Range Strain Fields, Elastic Dipole Tensors, and Chemical Strain," *Physical Review B*, vol. 80, p. 064108, 2009.

[19] T. Ohnishi, K. Shibuya, T. Yamamoto, and M. Lippmaa, "Defects and Transport in Complex Oxide Thin Films," *Journal of Applied Physics*, vol. 103, p. 103703, 2008.

[20] N. V. Nong, C.-J. Liu, and M. Ohtaki, "Improvement on the High Temperature Thermoelectric Performance of Ga-Doped Misfit-Layered $Ca_3Co_{4-x}Ga_xO_{9+\delta}$ (x=0, 0.05, 0.1, and 0.2)," *Journal of Alloys and Compounds*, vol. 491, pp. 53–56, 2010.

[21] E. Woermann and A. Muan, "Phase Equilibria in the System CaO-Cobalt Oxide in Air," *Journal of Inorganic and Nuclear Chemistry*, vol. 32, pp. 1455–1459, 1970.

[22] T. Sun, H. H. Hng, Q. Yan, and J. Ma, "Effects of Pulsed Laser Deposition Conditions on the Microstructure of $Ca_3Co_4O_9$ Thin Films," *Journal of Electronic Materials*, vol. 39, pp. 1611–1615, 2010.

[23] R. Moubah, S. Colis, C. Ulhaq-Bouillet, and A. Dinia, "Defects Analysis at the Nanometric Scale in $Ca_3Co_4O_9$ Thin Films," *Applied Physics Letters*, vol. 96, p. 041902, 2010.

[24] A. Sakai, T. Kanno, S. Yotsuhashi, A. Odagawa, and H. Adachi, "Control of Epitaxial Growth Orientation and Anisotropic Thermoelectric Properties of Misfit-Type $Ca_3Co_4O_9$ Thin Films," *Japanese Journal of Applied Physics*, vol. 44, pp. 966–969, 2005.

[25] H. W. Eng, W. Prellier, S. Hébert, D. Grebille, L. Méchin, and B. Mercey, "Influence of Pulsed Laser Deposition Growth Conditions on the Thermoelectric Properties of $Ca_3Co_4O_9$ Thin Films," *Journal of Applied Physics*, vol. 97, p. 013706, 2005.

[26] Y. F. Hu, W. D. Si, E. Sutter, and Q. Li, "In Situ Growth of c-axis-Oriented $Ca_3Co_4O_9$ Thin Films on Si (100)," *Applied Physics Letters*, vol. 86, p. 082103, 2005.

[27] Y. F. Hu, E. Sutter, W. D. Si, and Q. Li, "Thermoelectric Properties and Microstructure of c-axis-Oriented $Ca_3Co_4O_9$ Thin Films on Glass Substrates," *Applied Physics Letters*, vol. 87, p. 171912, 2005.

[28] Q. Qiao, A. Gulex, T. Paulauskas, S. Kolesnik, B. Dabrowski, M. Ozdemir, C. Boyrax, D. Mazumdar, A. Gupta, and R. F. Klie, "Effect of Substrate on the Atomic Structure and Physical Properties of Thermoelectric $Ca_3Co_4O_9$ Thin Films," *Journal of Physics: Condensed Matter*, vol. 23, p. 305005, 2011.

[29] M.-G. Kang, K.-H. Cho, S.-M. Oh, J.-S. Kim, C.-Y. Kang, S. Nahm, and S.-J. Yoon, "High-Temperature Thermoelectric Properties of Nanostructured $Ca_3Co_4O_9$ Thin Films," *Applied Physics Letters*, vol. 98, p. 142102, 2011.

[30] K. Sugiura, H. Ohta, K. Nomura, M. Hirano, H. Hosono, and K. Koumoto, "High Electrical Conductivity of Layered Cobalt Oxide $Ca_3Co_4O_9$ Epitaxial Films Grown by Topotactic Ion-Exchange Method," *Applied Physics Letters*, vol. 89, p. 032111, 2006.

[31] Y. Zhou, "Effect of Grain Size on Electric Resistivity and Thermopower of $(Ca_{2.6}Bi_{0.4})Co_4O_9$ Thin Films," *Journal of Applied Physics*, vol. 95, pp. 625–628, 2004.

[32] N. Van Nong, N. Pryds, S. Linderoth, and M. Ohtaki, "Enhancement of the Thermoelectric Performance of p-Type Layered Oxide $Ca_3Co_4O_{9+\delta}$ Through Heavy Doping and Metallic Nanoinclusions," *Advanced Materials*, vol. 23, pp. 2484–2490, 2011.

[33] H. W. Eng, P. Limelette, W. Prellier, C. Simon, and R. Fresard, "Unconventional Hall Effect in Oriented $Ca_3Co_4O_9$ Thin Films," *Physical Review B*, vol. 73, p. 033403, 2006.

[34] X. D. Zhou, L. R. Pederson, E. Thomsen, Z. Nie, and G. Coffey, "Nonstoichiometry and Transport Properties of $Ca_3Co_{4\pm x}O_{9+\delta}$ (x=0-0.4)," *Electrochemical and Solid State Letters*, vol. 12, pp. F1–F3, 2009.

[35] O. Levy and D. J. Bergman, "Scaling Behaviour of the Thermopower in a Two-Component Composite Near a Percolation Threshold," *Journal of Physics A*, vol. 25, pp. 1875–1884, 1992.

Chapter 6

Cobaltate Superlattices

Abstract

Thermoelectric superlattices of cobaltates are studied in this chapter, aiming to preserve the electronic properties and simultaneously suppress the thermal conductivity by enhanced phonon scattering at the introduced interfaces. Superlattices of Na_xCoO_2 and electrically insulating materials could not be fabricated with a high degree of crystalline ordering due to limitations to the deposition process because of the volatile nature of the sodium. This lack of crystalline ordering results in a strong degradation of the electronic properties in these superlattices. Additionally, a new approach of thermoelectric superlattices is studied, where the two thermoelectric materials Na_xCoO_2 and $Ca_3Co_4O_9$ are combined and no electrically insulating materials are used. In these superlattices, a high degree of crystalline ordering is achieved because the similar CoO_2 layers in these two materials provide a good crystallographic match. Such thermoelectric superlattices show similar electronic properties as thin films of these two materials. Even though additional studies focusing on the thermal properties of such superlattices are required, these superlattices form a promising and novel approach to improve the thermoelectric performance of cobaltate-based materials.

6.1 Introduction

Thin films of cobaltates are promising as thermoelectric materials and their properties can be engineered in several ways, as described in the previous chapters. By engineering the average grain size in Na_xCoO_2 thin films, a doubling of the thermoelectric power factor was obtained, as described in Chapter 3. Size effects of these thin films were studied in Chapter 4, showing that the electronic properties can be preserved in ultra-thin Na_xCoO_2 films.

Even though the thermal conductivity of several thin films was determined, the work described in this thesis focused on the relation between the structural and the electronic properties of cobaltate thin films. As shown in Chapter 3, the thermal conductivity of thin films of Na_xCoO_2 is significantly lower than single-crystals, in combination with a significant improvement of the electronic properties. The thermal conductivity of such heterostructures can be even more reduced by enhanced phonon scattering at interfaces, as described in Chapter 1. This can be obtained in superlattice structures, where the interfaces act as phonon scatterers. This was successfully shown for PbTe-based superlattices [1] as well as Bi_2Te_3-based superlattices [2–4], leading to an enhancement of the ZT value up to 2.4. [3]

Such superlattices were also fabricated with $SrTiO_3$ as thermoelectric material. [5–9] For these superlattices, $SrTiO_3$ and $SrTi_{0.8}Nb_{0.2}O_3$ were used with various thicknesses of the different layers. These studies focused on electron confinement and its effect on the Seebeck coefficient. This electron confinement was successfully used to obtain an enhancement of the Seebeck coefficient up to a factor of 5. For the best superlattices, ZT values up to 2.4 were reported, however for these calculations only the 2-dimensional electron gas (2DEG) to which the electrons are confined was used to obtain the ZT value. Even though the ZT value reduces to 0.24 after correcting for the total volume of the deposited stack, this is still a factor of three larger than values obtained in bulk $SrTiO_3$ at room temperature.

In this chapter, the thermoelectric potential of cobaltate-based superlattices is studied. Using thin films of Na_xCoO_2 and $Ca_3Co_4O_9$ as basic building blocks, various combinations are characterized. In analogy to previous studies of different material systems, superlattices of Na_xCoO_2 and insulating barrier materials (Al_2O_3 and $LaAlO_3$) are fabricated to study their thermoelectric properties. Because of limitations to the deposition temperature for Na_xCoO_2 thin films, due to the volatility of sodium, it was found to be very challenging to preserve crystallinity throughout the entire stack. This preservation of the crystallinity is expected to be required to preserve the electronic properties, as described in Chapter 3.

As an alternative, superlattices of a combination of Na_xCoO_2 and $Ca_3Co_4O_9$ are fabricated. Such superlattices have the advantage of combining two thermoelectric materials, thereby making the use of an insulating barrier material redundant. Another advantage of this approach is the good crystallographic match of these two materials, because both have similar CoO_2 sheets embedded in the

structure. Such a good crystallographic fit is expected to simplify the preservation of crystallinity throughout the entire stack. The main question that will be addressed in this outlook chapter is if the electronic properties can be preserved in a cobaltate superlattice in which Na_xCoO_2 and $Ca_3Co_4O_9$ are combined. If the electronic properties can be preserved, these superlattices are very promising as thermoelectric materials, because a significant reduction of the thermal conductivity is expected in such superlattice structures, as schematically shown in Fig. 6.1.

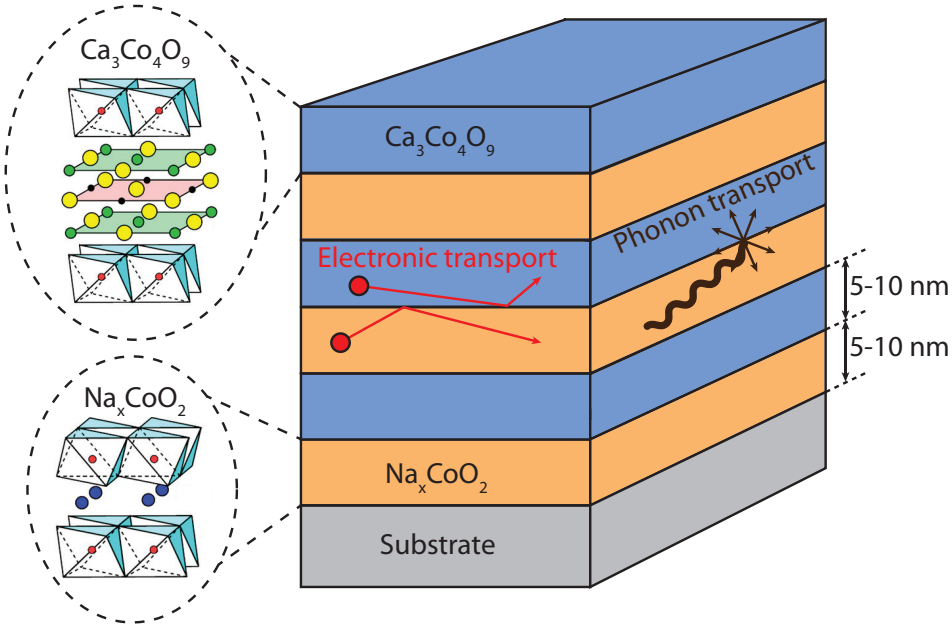

Figure 6.1: Schematic representation of a thermoelectric cobaltate superlattice, composed of alternating layers of Na_xCoO_2 and $Ca_3Co_4O_9$. Because of the similar CoO_2 layers in Na_xCoO_2 and $Ca_3Co_4O_9$ the layers form a good crystallographic match and can be fabricated with a high degree of crystalline ordering. The aim is to achieve unaffected electronic transport, compared to thin films of both materials and a simultaneous suppression of the thermal conductivity through enhanced phonon scattering at the interfaces.

6.2 Results and Discussion

Using the knowledge of thin films of Na_xCoO_2 and $Ca_3Co_4O_9$ as described in the previous chapters in this thesis, superlattice structures of these cobaltates are fabricated. Initially, superlattices of Na_xCoO_2 and an insulating barrier layer were fabricated. For the barrier layer, Al_2O_3 and $LaAlO_3$ were used, because on

these two materials Na_xCoO_2 can be grown with good crystalline properties, as shown in Chapter 2 and 3. For these superlattices, it was found that the resistivity increased by at least one order of magnitude in these samples and that the crystallinity was not preserved in the complete stack. The barrier layers were not crystalline, because of the low deposition temperature of 430°C that was required for the growth of the Na_xCoO_2 layers, which prevented the crystalline growth of subsequent Na_xCoO_2 layers. As an alternative, superlattices of a combination of Na_xCoO_2 and $Ca_3Co_4O_9$ were fabricated. These superlattices have the advantage of a good crystallographic match, because of the similar CoO_2 sheets in these two materials. Additionally, in these superlattices both materials are thermoelectric, resulting in a superlattice without insulating barrier layers, which should help to preserve the electrical conductivity of the complete stack. The superlattices are fabricated in such a way that Na_xCoO_2 and $Ca_3Co_4O_9$ are stacked in various thicknesses and compared with thin films of these two materials.

Because the volatility of sodium in Na_xCoO_2 limits the deposition parameters, especially the deposition temperature, optimized deposition parameters for Na_xCoO_2 were used for the fabrication of the cobaltate superlattices, as described in Chapter 2 and [10]. To ensure chemical stability of the samples in air, the reported AlO_x capping layer was also deposited on top of all superlattices. Because the thermoelectric properties of Na_xCoO_2 show a significant enhancement when deposited on LSAT, [11] whereas for $Ca_3Co_4O_9$ not such a clear dependence was found, as described in Chapters 3 and 5, LSAT was used as substrate materials for the deposition of these cobaltate superlattices.

As shown in chapter 4, the thermoelectric properties of Na_xCoO_2 thin films can be preserved when reducing the layer thickness down to 5 nm. A similar study was done for thin films of $Ca_3Co_4O_9$, where a more significant increase for the resistivity was observed already for thin films with a reduced layer thickness of 10 nm. [12] Based on these observations, layer thicknesses of 5 nm and 10 nm were chosen to demonstrate the thermoelectric potential of cobaltate superlattice structures. The total thickness of the superlattices was kept constant at a total thickness of 200 nm, thereby also keeping the total thickness of Na_xCoO_2 and $Ca_3Co_4O_9$ constant at 100 nm. By keeping these total thicknesses constant, only the number of periods of the superlattices is changing for the different superlattices. Using this approach, superlattices with 5 nm and 10 nm layer thicknesses were fabricated and characterized, which are denoted as $(10\text{nm } Na_xCoO_2/10\text{nm } Ca_3Co_4O_9)_{10x}$ and $(5\text{nm } Na_xCoO_2/5\text{nm } Ca_3Co_4O_9)_{20x}$.

The superlattices of Na_xCoO_2 and $Ca_3Co_4O_9$ are compared with thin films of these two materials with a thickness of 10 nm and 100 nm, because these are respectively the individual layer thicknesses and the total layer thickness of the two materials. As shown in Chapter 4 the crystallinity in ultra-thin films of Na_xCoO_2 plays a determining role for the electronic transport in such ultra-thin films. Similar effects can be expected in superlattice structures, where it is

expected that optimized crystalline properties of the separate layers is required to preserve the electronic properties of the overall stack.

X-ray diffraction measurements of the superlattices as well as the thin films show only (00l) diffraction peaks of Na_xCoO_2 and $Ca_3Co_4O_9$, in agreement with previous observations as described Chapters 2-5. Looking in more detail, significant influence of the stacking of Na_xCoO_2 and $Ca_3Co_4O_9$ is observed, as shown in Fig. 6.2. Here, the (002) peaks of 100 nm thin films of Na_xCoO_2 are compared with the superlattice samples. For the $Ca_3Co_4O_9$ thin film no diffraction peak is observed, because of the low deposition temperature. However, for the superlattice samples, a stronger diffraction peak, compared to that of the Na_xCoO_2 thin film, is observed and the peak position is shifted to a higher 2θ value, close to that of the (002) diffraction peak of $Ca_3Co_4O_9$.

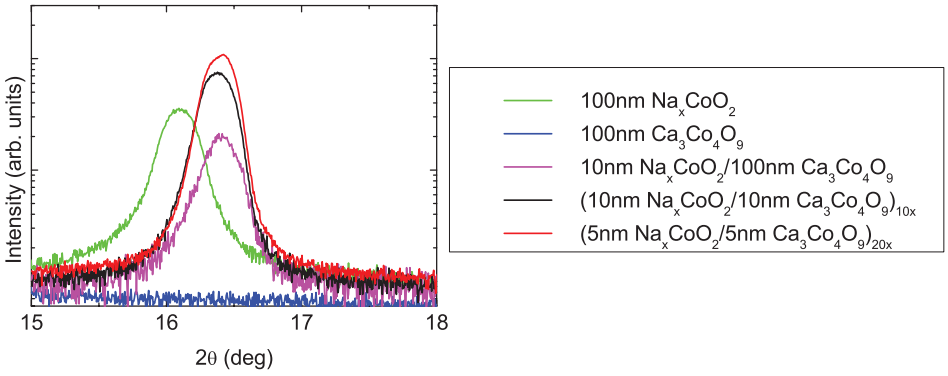

Figure 6.2: XRD measurements of Na_xCoO_2 thin films, $Ca_3Co_4O_9$ thin films and $Na_xCoO_2/Ca_3Co_4O_9$ superlattices. A scan around the (002) diffraction peak of Na_xCoO_2 and $Ca_3Co_4O_9$ is shown.

To understand the influence of the presence of underlying Na_xCoO_2 layers on the growth of $Ca_3Co_4O_9$, a reference sample with 100 nm of $Ca_3Co_4O_9$ on top of 10 nm of Na_xCoO_2 is also included. These results clearly show that by starting with a thin layer of Na_xCoO_2, the growth of $Ca_3Co_4O_9$ can be significantly influenced, leading to a strong enhancement of the crystallinity of the complete stack. These results also demonstrate that cobaltate superlattice structures can be grown with preserved or even enhanced crystallinity, even at the low deposition temperature which is required for the growth of Na_xCoO_2.

In analogy to thin films of Na_xCoO_2, as described in Chapter 4, this is expected to lead to a preservation of the electrical resistivity in these superlattices. The resistivity and Seebeck coefficient at room temperature of the superlattice samples and values for thin films as a reference are shown in Table 6.1. All samples shown in the table are fabricated using similar deposition parameters, as earlier described, thereby leading to somewhat lower thermoelectric performance of the $Ca_3Co_4O_9$

thin films, as compared to those described in Chapter 5.

Table 6.1: Thermoelectric properties of cobaltate heterostructures at 300K

Reference Samples	Resistivity (mΩ·cm)	Thermopower (μV/K)
10nm Na_xCoO_2	2.4	97
100nm Na_xCoO_2	1.4	107
10nm $Ca_3Co_4O_9$	641	118
100nm $Ca_3Co_4O_9$	4.5	76
10nm Na_xCoO_2/100 nm $Ca_3Co_4O_9$	18	82
Superlattice Samples		
(10nm Na_xCoO_2/10nm $Ca_3Co_4O_9)_{10x}$	6.2	95
(5nm Na_xCoO_2/5nm $Ca_3Co_4O_9)_{20x}$	14	97

Compared to the reference samples, the superlattice samples show similar thermoelectric properties, especially the superlattice with layer thicknesses of 10 nm. The superlattice with layer thicknesses of 5 nm shows an increased resistivity, however this value is still much lower compared to a thin film of $Ca_3Co_4O_9$. For the Seebeck coefficient, values close to 100 μV/K are obtained for both superlattice samples, which clearly shows that this is not degraded as a consequence of the introduced interfaces in these samples.

These results demonstrate the successful fabrication of cobaltate superlattice structures, with preservation of the crystallinity throughout the entire stack. Because of this preserved crystallinity, the electronic properties at room temperature also remain similar to ultra-thin films of these cobaltate materials. Even though the thermal conductivity of these superlattices has not been determined yet, for comparable thin films of 100 nm of Na_xCoO_2 and $Ca_3Co_4O_9$ a thermal conductivity of respectively 1.4 W/mK and 2.1 W/mK was measured. These values are lower than values previously reported for single crystals of Na_xCoO_2 and $Ca_3Co_4O_9$. [13, 14]

This shows that confinement into thin films of 100 nm already has the desired effect to suppress the thermal conductivity. It should however be noted that the thermal conductivity measurements have been performed in the out-of-plane direction, whereas the electronic properties were measured in the in-plane direction. From these initial measurements on single layers, a further suppression of the thermal conductivity in superlattice samples is expected, because of the additionally introduced interfaces. These results clearly demonstrate that cobaltate-based superlattices are very promising as thermoelectric materials and additional studies will be required to fully reveal their thermoelectric potential.

6.3 Conclusions and Outlook

In analogy to observations for thin films of Na_xCoO_2, a high degree of crystalline ordering is required to preserve the electrical conductivity in cobaltate-based superlattices. Combinations of Na_xCoO_2 and insulating barrier layers could not be deposited with sufficient crystalline ordering to preserve the electronic transport properties, because of constraints to the deposition process, caused by the volatile nature of sodium. As a consequence of this lack of crystalline ordering in such Na_xCoO_2-based superlattices, the electronic properties were inferior to thin films of this material.

Superlattices of a combination of Na_xCoO_2 and $Ca_3Co_4O_9$ have been successfully deposited with a high degree of crystalline ordering. The crystallinity of the $Ca_3Co_4O_9$ layers is significantly improved by the initial growth of a layer of Na_xCoO_2. This underlying layer acts as a buffer layer because of the crystalline similarities of the CoO_2 layers. Because of the high degree of crystalline ordering, the electronic properties of these cobaltate superlattices match those of a combination of thin films of these two materials.

Even though the results presented in this chapter are preliminary and do not represent a complete and detailed study, it can be concluded that cobaltate-based superlattices form a promising approach to obtain enhanced thermoelectric performance in oxide materials. The new idea to combine two thermoelectric materials into a superlattice structure, rather than a thermoelectric and an insulating material, eliminates the issue of a reduced electrical conductivity of the entire stack due to the electrically insulating layers. If the superlattices can be fabricated in a controlled way, the electronic properties of the superlattice structure can match or even outperform those of thin films of the same thermoelectric materials, as clearly demonstrated with the results shown in this chapter.

More detailed studies will be required to fully understand and to design optimized superlattices of these thermoelectric cobaltates. Variations in the thickness of the layers of both materials should be considered, taking into account the differences in thermoelectric properties of these two materials. Because of the lower electrical resistivity of Na_xCoO_2 thin films, compared to $Ca_3Co_4O_9$ thin films, a higher volume fraction of Na_xCoO_2 is expected to result in a decrease of the electrical resisitivity. Another promising option is to fabricate superlattices in which the layer thickness is varied in a disordered way. Such an approach has previously been used to create phonon blocking structures [15] and might also be used to create ultra-low thermal conductivity superlattice structures. Additionally, it will also be interesting to combine $Bi_2Sr_2Co_2O_y$ within such superlattices as a third material, or make even different combinations. This could also be done by adding different dopants to different layers, thereby further reducing the order in the superlattice structures. The addition of dopants, such as Ag or Ga, has already lead to a significant enhancement of the thermoelectric properties in bulk

materials [16–18] and could also be used to further improve the thermoelectric performance of cobaltate superlattices. Because of the similar crystal structure of the CoO_2 layers within these layered cobaltates, various promising pathways to design optimized superlattice structures can be attempted. The suggested approaches are all aiming at reducing the thermal conductivity through enhanced phonon scattering at the additional interfaces that are created in such samples. Even though this suppression of the thermal conductivity has not been shown for cobaltate superlattice samples, such a suppression has been observed for thin films of both Na_xCoO_2 as well as $Ca_3Co_4O_9$, compared to single-crystalline and polycrystalline samples. The main aspect that should be studied in future work is the thermal conductivity of such cobaltate superlattices. The focus of such work should be to study phonon transport to confirm that enhanced phonon scattering is obtained in these cobaltate superlattices. To obtain more information about the phonon spectra of these superlattices, Raman scattering experiments could be performed, as was previously done for Si/Ge superlattices. [19] By gaining sufficient understanding of the phonon transport in such superlattices, this knowledge can be used to design optimized superlattice structures of layered cobaltates with enhanced thermoelectric performance.

Bibliography

[1] L. Hicks, T. Harman, X. Sun, and M. Dresselhaus, "Experimental Study of the Effect of Quantum-Well Structures on the Thermoelectric Figure of Merit," *Physical Review B*, vol. 53, p. 10493, 1996.

[2] R. Venkatasubramanian, T. Colitts, E. Watko, M. Lamvik, and N. El-Masry, "MOCVD of Bi_2Te_3, Sb_2Te_3 and their superlattice structures for thin-film thermoelectric applications," *Journal of Crystal Growth*, vol. 170, pp. 817–821, 1997.

[3] R. Venkatasubramanian, E. Siivola, T. Colpitts, and B. O'Quinn, "Thin-Film Thermoelectric Devices with High Room-Temperature Figures of Merit," *Nature*, vol. 413, pp. 597–602, 2001.

[4] R. Venkatasubramaniam, "Lattice Thermal Conductivity Reduction and Phonon Localizationlike Behavior in Superlattice Strucures," *Physical Review B*, vol. 61, p. 3091, 2000.

[5] H. Ohta, "Thermoelectrics Based on Strontium Titanate," *Materials Today*, vol. 10, pp. 44–49, 2007.

[6] H. Ohta, S. Kim, Y. Mune, T. Mizoguchi, K. Nomura, S. Ohta, T. Nomura, Y. Nakanishi, Y. Ikuhara, M. Hirano, H. Hosono, and K. Koumoto, "Giant

Thermoelectric Seebeck Coefficient of a Two-Dimensional Electron Gas in $SrTiO_3$," *Nature Materials*, vol. 6, pp. 129–134, 2007.

[7] H. Ohta, K. Sugiura, and K. Koumoto, "Recent Progress in Oxide Thermoelectric Materials: p-Type $Ca_3Co_4O_9$ and n-Type $SrTiO_3$," *Inorganic Chemistry*, vol. 47, pp. 8429–8436, 2008.

[8] Y. Mune, H. Ohta, K. Koumoto, T. Mizoguchi, and Y. Ikuhara, "Enhanced Seebeck Coefficient of Quantum-Confined Electrons in $SrTiO_3/SrTi_{0.8}Nb_{0.2}O_3$ Superlattices," *Applied Physics Letters*, vol. 91, p. 192105, 2007.

[9] H. Ohta, "Two-dimensional Thermoelectric Seebeck Coefficient of $SrTiO_3$-based Superlattices," *Physica Status Solidi (b)*, vol. 245, pp. 2363–2368, 2008.

[10] P. Brinks, H. Heijmerikx, T. A. Hendriks, G. Rijnders, and M. Huijben, "Achieving Chemical Stability in Thermoelectric Na_xCoO_2 Thin Films," *RSC Advances*, vol. 2, 2012.

[11] P. Brinks, B. Kuiper, E. Breckenfeld, G. Koster, L. W. Martin, G. Rijnders, and M. Huijben, "Enhanced Thermoelectric Power Factor of Na_xCoO_2 Thin Films by Structural Engineering," *Advanced Energy Materials*, vol. 4, 2014.

[12] M. Ihns, "Structural Engineering of $Ca_3Co_4O_9$ Thermoelectric Thin Films," *M.Sc. thesis*, 2013.

[13] M. Lee, L. Viciu, L. Li, Y. Wang, M. L. Foo, S. Watauchi, R. A. Pascal Jr., R. J. Cava, and N. P. Ong, "Large Enhancement of the Thermopower in Na_xCoO_2 at high Na doping," *Nature Materials*, vol. 5, pp. 537–540, 2006.

[14] M. Shikano and R. Funahashi, "Electrical and Thermal Properties of Single-Crystalline $(Ca_3CoO_3)_{0.7}CoO_2$ with a $Ca_3Co_4O_9$ Structure," *Applied Physics Letters*, vol. 82, pp. 1851–1853, 2003.

[15] P. Sesion, C. Albuquerque, E.L. Chesman, and V. Freire, "Acoustic Phonon Transmission Spectra in Piezoelectric AlN/GaN Fibonacci Phononic Crystals," *The European Physical Journal B - Condensed Matter and Complex Systems*, vol. 58, pp. 379–387, 2007.

[16] N. Van Nong, N. Pryds, S. Linderoth, and M. Ohtaki, "Enhancement of the Thermoelectric Performance of p-Type Layered Oxide $Ca_3Co_4O_{9+\delta}$ Through Heavy Doping and Metallic Nanoinclusions," *Advanced Materials*, vol. 23, pp. 2484–2490, 2011.

[17] N. V. Nong, S. Yanagiya, S. Monica, N. Pryds, and M. Ohtaki, "High-Temperature Thermoelectric and Microstructural Characteristics of Cobalt-Based Oxides with Ga Substituted on the Co-Site," *Journal of Electronic Materials*, vol. 40, pp. 716–722, 2011.

[18] N. V. Nong, C.-J. Liu, and M. Ohtaki, "High-temperature Thermoelectric Properties of Late Rare Earth-Doped $Ca_3Co_4O_{9+\delta}$," *Journal of Alloys and Compounds*, vol. 509, pp. 977–981, 2011.

[19] R. Schorer, G. Abstreiter, S. de Gironcoli, E. Molinari, H. Kibbel, and H. Presing, "In-Plane Raman Scattering of (001)-Si/Ge Superlattices," *Physical Review B*, vol. 49, p. 5406, 1994.

Summary

Thermoelectric energy conversion is a promising technology as it can be used to directly convert a temperature gradient into electrical energy. In general more than half of the used energy is lost as waste heat and converting this energy back into useful electrical energy has tremendous potential to reduce the overall energy consumption. However, to date the efficiency of such thermoelectric energy conversion processes remains limited. Major improvements of the efficiency of this process could be achieved by engineering new materials with better thermoelectric properties. The performance indicator of these thermoelectric materials is the dimensionless figure of merit (ZT value), which is calculated from the Seebeck coefficient, the electrical conductivity and the thermal conductivity. For large scale applications a threshold ZT value of approximately 3 is typically assumed, whereas most current commercially available thermoelectric materials have a ZT value of about 1.

The main challenge to improve the performance of thermoelectric materials originates from the interconnection of the Seebeck coefficient, the electrical conductivity and the thermal conductivity. These three parameters all depend on the electronic carrier concentration, enabling optimization of the ZT value as a function of the carrier concentration. Further improvement is possible by suppression of phonon transport, which is responsible for a carrier independent contribution to the thermal conductivity. To reduce the phonon transport in thermoelectric materials different approaches have been proposed which share the common idea to enhance phonon scattering by introducing disorder or small features in the otherwise crystallographically ordered materials. A promising example of such an approach is to use phonon scattering at the interfaces in thin films and superlattices, which has been shown to give a significant improvement for Bi_2Te_3-based materials.

Oxide materials form a promising class of materials for thermoelectric applications, because of their good thermal and chemical stability. Among these oxides, the layered cobaltates, such as Na_xCoO_2 and $Ca_3Co_4O_9$, have been reported to have the interesting combination of a high Seebeck coefficient and a relatively good electrical conductivity, resulting in a promising thermoelectric performance. ZT

values exceeding unity have been reported for Na_xCoO_2 single crystals at 800K. However, further improvement of the thermoelectric performance of these cobaltates is hindered by their high thermal conductivity. Most literature reports of these thermoelectric cobaltates describe single crystal and polycrystalline samples, whereas very limited literature about heterostructures of these cobaltates is available.

In this thesis, heterostructures of layered cobaltates are studied, aiming at understanding as well as improving the thermoelectric performance of such heterostructures. By confinement into thin films and superlattice structures additional control over the structural properties can be achieved such as strain engineering, which is not possible in single crystal or polycrystalline samples. The presented study focuses on the investigation of size effects by studying the relation between the structural and the thermoelectric properties of these thermoelectric cobaltates which are confined into nanoscale heterostructures.

Epitaxial thin films of Na_xCoO_2 are grown by pulsed laser deposition on various single crystal substrates without the formation of impurity phases. When these samples are electrically characterised it is found that the electrical resistivity is increasing by more than one order of magnitude within several days, indicating that the samples are not stable when exposed to air. These stability issues are studied in Chapter 2, and are found to be caused by the reactive nature of the sodium, which forms sodium carbonate with moisture and carbon dioxide from air. The stability issues are overcome by the *in-situ* deposition of an amorphous AlO_x capping layer, resulting in chemically stable Na_xCoO_2 thin films. This capping layer enables thermoelectric characterization of the intrinsic properties of these thin films and similar thermoelectric properties at room temperature are observed compared to Na_xCoO_2 single crystals.

The relation between the structural and thermoelectric properties in Na_xCoO_2 thin films is studied in Chapter 3. Using a combination of X-ray diffraction and X-ray photoelectron diffraction it is shown that Na_xCoO_2 thin films can be grown epitaxially on hexagonal as well as cubic single-crystal substrates. The average grain size is controlled by changing the substrate material and a reduction of the grain size is found to result in a significant enhancement of the thermoelectric power factor. It is also shown that in these structurally engineered Na_xCoO_2 thin films the thermal conductivity is significantly suppressed, compared to Na_xCoO_2 single crystals, further demonstrating the thermoelectric potential of these structurally engineered Na_xCoO_2 thin films.

In Chapter 4 size effects in Na_xCoO_2 thin films are studied. The effect of confinement on the structural as well as thermoelectric properties is investigated by fabricating thin films with thicknesses between 5 nm and 250 nm. Misfit dislocations start to form for thin films with a thickness of 10 nm and more, because of the large lattice mismatch between Na_xCoO_2 and the substrate material. The electrical resistivity shows a sharp increase for thicknesses below 60 nm, which

is in good agreement with theoretical models. However, for the Seebeck coefficient no clear trend as a function of layer thickness is observed, in contrast to the models which predict a suppression of the Seebeck coefficient for ultra-thin films. Because of the preservation of the Seebeck coefficient in ultra-thin Na_xCoO_2 thin films, these ultra-thin layers are very promising for their use as building blocks in superlattice structures.

The high-temperature thermoelectric properties of thin films of Na_xCoO_2 and $Ca_3Co_4O_9$ are studied in Chapter 5. In addition to this, also the thermal stability is studied by temperature dependent X-ray diffraction measurements. By systematic cycling up to increasingly high temperatures and simultaneous electronic measurements during heating as well as cooling, it is shown that such electronic measurements are a much more sensitive tool to study the thermal stability of cobaltate thermoelectric thin films. Additionally, the sensitivity of these cobaltate thin films for the oxygen partial pressure during heating is demonstrated. The thermal stability is found to be increased when the samples are heated in an oxygen-rich environment. For these thin films with enhanced thermal stability, a significant improvement of the thermoelectric properties at elevated temperatures is achieved, compared to bulk samples.

In the final chapter (Chapter 6) thermoelectric superlattices of cobaltates are investigated. The aim of such superlattices is to preserve the electronic properties and suppress the thermal conductivity by enhanced phonon scattering at the interfaces. Superlattices of Na_xCoO_2 and insulating materials were found to have degraded electronic properties, as a consequence of the limited crystallinity of these superlattices. This limited crystallinity is caused by the low deposition temperature that is required for Na_xCoO_2 because of the volatile sodium. Additionally, a new approach is studied, where the two thermoelectric materials Na_xCoO_2 and $Ca_3Co_4O_9$ are combined into a superlattice, without any electrically insulating materials. In such superlattices a high degree of crystalline ordering was achieved, because of the good crystallographic match of these two materials. Because of the preserved crystallinity the electronic properties of such superlattices are comparable to thin films of these cobaltate materials. Even though additional studies focusing on the thermal properties of such superlattices are required, these superlattices form a promising and novel approach to improve the thermoelectric performance of cobaltate-based materials.

Samenvatting

Thermo-elektrische energieomzetting is een veelbelovende methode vanwege de mogelijkheid om een temperatuurgradiënt rechtstreeks om te zetten in elektrische energie. In het algemeen gaat meer dan de helft van de gebruikte energie verloren in de vorm van restwarmte en het terugwinnen van deze restwarmte tot bruikbare elektrische energie kan leiden tot een afname van de totaal geconsumeerde energie. De efficiëntie van het omzetten van energie door middel van thermo-elektrische processen is tot op heden echter beperkt. Grote verbeteringen van deze efficiëntie kunnen bereikt worden door het manipuleren van nieuwe materialen met betere thermo-elektrische eigenschappen. De prestatie-indicator voor thermo-elektrische materialen is de eenheidsloze "figure of merit" (ZT waarde), die berekend wordt uit de Seebeck coefficiënt, de elektrische geleiding en de warmtegeleiding. Voor grootschalige toepassingen wordt een minimale ZT waarde van 3 als drempel aangenomen, terwijl commercieel beschikbare materialen momenteel een ZT waarde van ongeveer 1 hebben.

De belangrijkste uitdaging om de prestaties van thermo-elektrische materialen te verbeteren, ontstaat uit de gezamenlijke afhankelijkheid van de Seebeck coefficiënt, de elektrische geleiding en de warmtegeleiding ten opzichte van de ladingsdragersdichtheid. Ten gevolge van deze gezamenlijke afhankelijkheid kan de ZT waarde geoptimaliseerd worden als functie van de ladingsdragersdichtheid. Verdere verbetering van de ZT waarde is mogelijk door het onderdrukken van fonon transport, wat een bijdrage levert aan de warmtegeleiding die onafhankelijk is van de ladingsdragersdichtheid. Om fonon transport te onderdrukken in thermo-elektrische materialen zijn verschillende benaderingen voorgesteld, waarbij de gemeenschappelijke factor het versterken van de verstrooiing van fononen is door het introduceren van wanorde of kleine elementen in de kristallijn geordende materialen. Een veelbelovend voorbeeld van een dergelijke aanpak is het gebruik van fonon verstrooiing op grensvlakken in heterostructuren en multilaag structuren, waarvoor is aangetoond dat het een significante verbetering op kan leveren voor op Bi_2Te_3 gebaseerde multilagen.

Oxides zijn een veelbelovende materiaalklasse voor thermo-elektrische toepassingen vanwege hun goede thermische en chemische stabiliteit. Van deze oxides

hebben de gelaagde cobaltaten, zoals Na_xCoO_2 en $Ca_3Co_4O_9$, de interessante combinatie van een hoge Seebeck coefficiënt en een relatief goede elektrische geleiding, wat resulteert in goede thermo-elektrische prestaties. ZT waardes groter dan één op een temperatuur van 800K zijn reeds gepubliceerd. Verdere verbeteringen van de thermo-elektrische prestaties van deze cobaltaten wordt echter gehinderd door hun hoge warmtegeleiding. In literatuur worden voornamelijk monokristallijne en polykristallijne materialen beschreven en slechts enkele publicaties beschrijven dunne films van deze cobaltaten.

In dit proefschrift worden heterostructuren van gelaagde cobaltaten bestudeerd met als doel om de thermo-elektrische eigenschappen hiervan te begrijpen en te verbeteren. Door begrenzing in dunne films en multilaag structuren kan extra controle over de structurele eigenschappen worden verkregen, zoals manipulatie van de rek, wat niet mogelijk is in monokristallijne of polykristallijne materialen. Het beschreven onderzoek richt zich op het onderzoeken van schaaleffecten door het bestuderen van de relatie tussen de structurele en de thermo-elektrische eigenschappen van deze cobaltaten die begrensd worden in heterostructuren.

Epitaxiale dunne films van Na_xCoO_2 zijn gegroeid met gepulste laser depositie zonder de vorming van ongewenste fasen op verschillende monokristallijne substraatmaterialen. Door de monsters elektrisch te karakteriseren is gebleken dat onder invloed van lucht de soortelijke weerstand meer dan een orde van grootte toeneemt over een periode van enkele dagen. De geobserveerde instabiliteit in lucht is bestudeerd in hoofdstuk 2, waar beschreven staat dat dit veroorzaakt wordt door de reactiviteit van natrium. In combinatie met koolstofdioxide en vocht uit de lucht wordt natriumcarbonaat gevormd. Deze stabiliteitsproblemen zijn opgelost door het *in-situ* deponeren van een amorfe AlO_x beschermlaag. Door deze beschermlaag kunnen de intrinsieke thermo-elektrische eigenschappen van Na_xCoO_2 dunne films bepaald worden en op kamertemperatuur zijn thermo-elektrische eigenschappen gemeten die vergelijkbaar zijn met monokristallen van Na_xCoO_2.

De relatie tussen de structurele en de thermo-elektrische eigenschappen van Na_xCoO_2 dunne films is bestudeerd in hoofdstuk 3. Door een combinatie van röntgendiffractie en röntgen photoelectron diffractie te gebruiken is aangetoond dat Na_xCoO_2 dunne films epitaxiaal gegroeid kunnen worden op zowel hexagonale als kubische monokristallijne substraten. De gemiddelde deeltjesgrootte kan beïnvloedt worden door het substraat materiaal te veranderen en een afname van de deeltjesgrootte resulteert in een significante verbetering van de thermo-elektrische "power factor". Het is ook aangetoond dat in deze structureel gemodificeerde Na_xCoO_2 dunne films de warmtegeleiding significant onderdrukt is ten opzichte van Na_xCoO_2 monokristallen. Deze twee bevindingen demonstreren dat deze structureel gemodificeerde dunne films veelbelovende thermo-elektrische eigenschappen bezitten.

In hoofdstuk 4 worden schaaleffecten in Na_xCoO_2 dunne films bestudeerd. Het effect van begrenzing op de structurele en thermo-elektrische eigenschappen

is onderzocht door het fabriceren van dunne films met een variërende dikte van 5 nm tot 250 nm. Misfit dislocaties beginnen zich te vormen vanaf een laagdikte van 10 nm vanwege het grote verschil in roosterconstante tussen film en substraat materiaal. De soortelijke weerstand vertoont een sterke toename voor laagdiktes beneden 60 nm, zoals ook voorspeld door theoretische modellen. De Seebeck coefficiënt vertoont echter geen duidelijke dikteafhankelijkheid, in tegenstelling tot theoretische modellen die een sterke afname voorspellen voor zeer dunne lagen. Vanwege het behoud van de Seebeck coefficiënt zijn deze zeer dunne films van Na_xCoO_2 veelbelovend voor gebruik als bouwstenen in multilaag structuren.

De thermo-elektrische eigenschappen van Na_xCoO_2 en $Ca_3Co_4O_9$ dunne films op hoge temperatuur zijn bestudeerd in hoofdstuk 5. Ook wordt de thermische stabiliteit bestudeerd door temperatuusafhankelijke röntgendiffractie metingen. Door het systematisch opwarmen en afkoelen naar steeds toenemende temperaturen en gelijktijdige metingen van de elektrische eigenschappen, zowel tijdens het opwarmen als het afkoelen, is aangetoond dat dergelijke elektrische metingen een gevoelige methode zijn om de thermische stabiliteit te bepalen. In toevoeging hierop is ook de thermische stabiliteit als functie van de partiële zuurstofdruk aangetoond, welke sterk toeneemt in een zuurstofrijke omgeving. Voor deze dunne films met een toegenomen thermische stabiliteit is een significante verbetering van de thermo-elektrische eigenschappen waargenomen op hoge temperatuur vergeleken met bulk monsters.

In het laatste hoofdstuk (hoofdstuk 6) worden multilaag structuren van thermo-elektrische cobaltaten bestudeerd. Het doel van deze multilagen is om de elektrische eigenschappen te behouden en tegelijkertijd de warmtegeleiding te onderdrukken door verstrooiing van fononen aan de grensvlakken. Multilaag structuren van Na_xCoO_2 en isolerende materialen vertonen een verslechtering van de elektrische eigenschappen vanwege de beperkte kristalliniteit in deze multilagen. Deze slechte kristalliniteit wordt veroorzaakt door de lage depositie temperatuur die nodig is vanwege het reactieve natrium in Na_xCoO_2. Daarnaast is ook een nieuwe aanpak geprobeerd waarin de twee thermo-elektrische materialen Na_xCoO_2 en $Ca_3Co_4O_9$ worden gecombineerd in een multilaag structuur zonder gebruik te maken van isolerende materialen. Deze multilagen kunnen gemaakt worden met een hoge mate van kristalliniteit vanwege de vergelijkbare kristalstructuren van deze twee materialen. Door dit behoud van kristalliniteit zijn ook de elektrische eigenschappen behouden in deze multilagen. Hoewel verder onderzoek nodig is om de thermische eigenschappen van dergelijke multilagen te bepalen, vormen de hier beschreven multilagen een veelbelovende nieuwe methode om de thermo-elektrische prestaties van cobaltaten te verbeteren.

List of Publications

P. Brinks, M. Huijben, book chapter in "Epitaxial Growth of Complex Metal Oxides", to be published by Woodhead Publishing

P. Brinks et al., "High-temperature stability and thermoelectric properties of $Ca_3Co_4O_9$ thin films", manuscript in preparation

P. Brinks, G. Rijnders, M. Huijben, "Size effects on thermoelectric behavior of ultra-thin Na_xCoO_2" thin films, manuscript submitted

F. Gunkel, S. Wicklein, S. Hoffmann-Eifert, P. Meuffels, **P. Brinks**, G. Rijnders, M. Huijben, R. Waser, Regina Dittmann, "Transport limits in defect-engineered $LaAlO_3/SrTiO_3$ bilayers", manuscript submitted

P. Brinks, B. Kuiper, E. Breckenfeld, G. Koster, L.W. Martin, G. Rijnders, M. Huijben, "Enhanced thermoelectric power factor of Na_xCoO_2 thin films by structural engineering," *Advanced Energy Materials* **4**, 1301927 (2014)

S.A. Veldhuis, **P. Brinks**, T.M. Stawski, O.F. Göbel, J.E. ten Elshof, "A facile method for the determination of ceramic thin films using X-ray reflectivity," *Journal of Sol-Gel Science and Technology* **71**, 118 (2014)

P. Brinks, H. Heijmerikx, T.A. Hendriks, G. Rijnders, M. Huijben, "Achieving chemical stability in thermoelectric Na_xCoO_2 thin films," *RSC Advances* **2**, 6023 (2013)

K. Wang, T.L.A. Tran, **P. Brinks**, J.G.M. Sanderink, T. Bolhuis, W.G. van der Wiel, M.P. de Jong, "Tunneling anisotropic magnetoresistance in Co/AlOx/Al tunnel junctions with fcc Co (111) electrodes," *Physical Review B* **88**, 05447 (2013)

P.K.J. Wong, T.L.A. Tran, **P. Brinks**, W.G. van der Wiel, M. Huijben, M.P. de Jong, "Highly ordered C_{60} films on epitaxial Fe/Mg(001) surfaces for organic

spintronics," *Organic Electronics* **14**, 451 (2013)

A. George, S. Mathew, R. van Gastel, M. Nijland, K. Gopinadhan, **P. Brinks**, T. Venkatesan, J.E. ten Elshof, "Large area resist-free soft-litographic patterning of graphene," *Small* **9**, 711 (2013)

P. Brinks, W. Siemons, G. Koster, G. Rijnders, M. Huijben, "Anisotropic electrical transport properties of a two-dimensional electron gas at $SrTiO_3$-$LaAlO_3$ interfaces," *Applied Physics Letters* **98**, 052103 (2012)

F. Gunkel, **P. Brinks**, S. Hoffmann-Eifert, R. Dittmann, M. Huijben, J.E. Kleibeuker, G. Koster, G. Rijnders, R. Waser, "Influence of charge compensation mechanisms on the sheet electron density at conducting $LaAlO_3/SrTiO_3$-interfaces," *Applied Physics Letters* **100**, 052103 (2012)

H. Boschker, M. Mathews, **P. Brinks**, E. Houwman, A. Vailionis, G. Koster, D.H.A. Blank, G. Rijnders, "Uniaxial contribution to the magnetic anisotropy of $La_{0.67}Sr_{0.33}MnO_3$ thin films induced by orthorhombic crystal structure," *Journal of Magnetism and Magnetic Materials* **323**, 2632 (2011)

Dankwoord

De afgelopen 4 jaar heb ik met erg veel plezier gewerkt aan mijn promotieonderzoek. Dit proefschrift was nooit tot stand gekomen zonder de hulp en ondersteuning van anderen. Ik wil hierbij dan ook graag iedereen bedanken die dit mede mogelijk heeft gemaakt.

Allereerst zou ik graag mijn begeleiders Guus en Mark willen bedanken voor de mogelijkheid die jullie mij hebben gegeven om dit onderzoek te doen. Guus, ik heb jouw input altijd als nuttig ervaren en de vrijheid die ik kreeg heb ik erg gewaardeerd. Mark, het was leuk om van jou de kans te krijgen om het onderzoek naar thermo-elektrische materialen samen te introduceren binnen IMS. Vanaf het begin heb ik van jou de kans gekregen om mijn resultaten veelvuldig te kunnen presenteren op internationale conferenties, wat ik erg gewaardeerd heb. Je was altijd enthousiast over de nieuwste resultaten en je was altijd beschikbaar om mijn laatste resultaten of problemen te bespreken. Ik heb onze samenwerking altijd als zeer prettig ervaren en jouw enthousiasme en vertrouwen in mij hebben heel motiverend gewerkt. Bedankt voor deze prettige samenwerking!

Door de goede sfeer en gezellige momenten heb ik altijd met veel plezier gewerkt bij IMS. De groepsbesprekingen, koffiepauzes, maar ook uitjes zoals de studiereis naar Oxford waren erg gezellig. Ik wil dan ook alle IMS'ers bedanken voor deze mooie tijd! Voor de vele (soms zinloze) discussies tijdens koffiepauzes, vrimibo's en andere momenten wil ik graag de volgende mensen bedanken: Ruud, Kurt, Rik, Nirupam, Maarten, Tom, Bouwe, Josee, Alim, David, Mark, Guus, Gertjan, Andre, Dave, Sjoerd, Matjaz, Arjen, Hajo, Xin, Antony, Anirban, Evert, Brian, Hans, Petra, Pablo, Werner, Huiyu, Rogier, Wouter, Bernard, Tomasz, Michiel, Peter, Jeroen. In het bijzonder wil ik Henk en Dominic van IMS en Frank en Dick van ICE bedanken voor hun goede technische ondersteuning. Marion en José bedankt voor jullie ondersteuning bij administratieve en financiële zaken. I would also like to thank the people of the MASIF team for their collaboration: Matjaz, Maarten, Alim, Nirupam. We have spent a considerable amount of time in moving the system to the new lab and performing maintenance. Kurt, bedankt voor het overnemen van mijn verantwoordelijkheden voor de XRD, dit leverde vele interessante discussies op.

Ik zou ook graag een aantal mensen bedanken voor een prettige samenwerking. Bouwe, bedankt voor de XPS en XPD metingen die jij voor mij gedaan hebt. Deze hebben een waardevolle bijdrage geleverd voor mijn proefschrift (hoofdstuk 2 en 3) en hebben ook geleid tot een artikel in Advanced Energy Materials. Sjoerd, bedankt voor de TGA metingen en poeder XRD metingen. Dankbaar heb ik gebruik gemaakt van deze resultaten en dit heeft een mooie bijdrage geleverd voor hoofdstuk 5 van dit proefschrift. Eric Breckenfeld and Lane Martin, I would like to thank you for the thermal conductivity measurements, which form a valuable contribution to chapter 3 and led to a nice publication in Advanced Energy Materials. I would also like to thank Nini Pryds and Ngo van Nong for their collaboration on $Ca_3Co_4O_9$. The target material you provided was very useful and made the results in chapter 5 and 6 possible. Verder wil ik de studenten bedanken die ik begeleid heb gedurende de afgelopen 4 jaar. Herman, Ron, Melanie, Chris en Daniel bedankt voor jullie werk. Van de meeste van jullie is een deel van het werk dat jullie gedaan hebben verwerkt in dit proefschrift.

I woulds also like to thank my paranymphs: Alim and Harmen. Alim, we worked together on the MASIF and we also had a lot of enjoyable discussions and conversations. I enjoyed working with you. Harmen, gedurende de afgelopen jaren hebben we samen voor de nodige afleiding van studie en promotie gezorgd. Tijdens onze studietijd hebben we veel achter de snookertafel gestaan wat altijd een prettige manier was om te ontspannen na de colleges of in de lunchpauze. De afgelopen 4 jaar hebben we de snookertafel ingeruild voor de squashbaan en konden we op deze manier goed ontspannen na werktijd. Buiten mijn werk heb ik met veel plezier getennist, met name met Nathan. Bedankt voor de vele geslaagde trainingssessies. Ook wil ik Reinier en Jan Willem bedanken voor de vele avonden en weekenden die vooral gevuld werden met gamen. De vele voetbal- en racespellen waren altijd zeer vermakelijk en vormden een goede afleiding.

Ik wil ook mijn familie bedanken en in het bijzonder mijn ouders, Joke en Henk, en mijn broer, Jan Willem. Ik heb alle mogelijkheden die jullie mij altijd gegeven hebben erg gewaardeerd. Jullie eeuwige interesse in mijn onderzoek en steun heb ik ook erg gewaardeerd. Ook mijn schoonfamilie wil ik bedanken. Tot slot wil ik Hanneke bedanken. Jouw liefde en steun hebben mij erg geholpen en hebben de laatste periode van mijn promotietijd heel bijzonder gemaakt. Samen gaan we nu een nieuwe toekomst tegemoet!

Peter Brinks